

## *Invited Review*

# The Pulsating White Dwarf Stars

G. FONTAINE AND P. BRASSARD

Département de Physique, Université de Montréal, Montréal, Québec H3C 3J7, Canada; fontaine@astro.umontreal.ca, brassard@astro.umontreal.ca

*Received 2008 July 17; accepted 2008 August 25; published 2008 October 1*

**ABSTRACT.** We present a summary of what is currently known about the three distinct families of isolated pulsating white dwarfs. These are the GW Vir stars (He/C/O-atmosphere stars with  $T_{\text{eff}} \approx 120,000$  K), the V777 Her stars (He-atmosphere,  $T_{\text{eff}} \approx 25,000$  K), and the ZZ Ceti stars (H-atmosphere,  $T_{\text{eff}} \approx 12,000$  K), all showing multiperiodic luminosity variations caused by low-order and low-degree  $g$ -mode instabilities. We also provide, in an Appendix, a very brief overview of the newly found evidence in favor of the existence of a fourth category of oscillating white dwarfs bearing strong similarities with these families of pulsators. We begin our survey with a short historical introduction, followed by a general discussion of pulsating white dwarfs as compact pulsators. We then discuss the class properties of these objects, including an updated census. We next focus on the instability domains for each family of pulsators in the  $\log g - T_{\text{eff}}$  diagram, and present their time-averaged properties in more detail. This is followed by a section on excitation physics, i.e., the causes of the pulsational instabilities, with emphasis on the common properties of the different types of pulsator. We then discuss the time-dependent properties of the pulsating white dwarfs featuring, among other things, a brief “picture tour” across the ZZ Ceti instability strip. We next review the methods used to infer or constrain the angular geometry of a pulsation mode in a white dwarf. These include multicolor photometry and time-resolved spectroscopy, the exploitation of the nonlinear features in the observed light curves, and rotational splitting. We also consider basic adiabatic asteroseismology starting with a discussion of the reaction of the period spectrum to variations of model parameters. We next review the various asteroseismological inferences that have so far been claimed for white dwarfs. We also discuss the potential of exploiting the rates of period change. We finally provide some concluding remarks, including a list with several suggestions for future progress in the field.

## 1. INTRODUCTION

Interest in pulsating white dwarfs goes back to at least 1949 when Sauvenier-Goffin (1949) investigated the dynamical stability of degenerate stellar configurations. However, the story really begins with the accidental discovery of rapid luminosity variations in the DA white dwarf HL Tau 76 by Arlo Landolt in 1968 during the course of a photometric program devoted to other scientific goals. Landolt (1968) gathered  $UBV$  light curves of HL Tau 76 and reported on complex multiperiodic luminosity variations with a dominant quasi-period of  $\sim 750$  s and a peak-to-peak amplitude of  $\sim 0.2$  mag (in the  $V$  filter). Following this, surveys were organized by a number of independent groups to search specifically for high-frequency oscillations in white dwarfs on the basis of the then newly developed technique of fast photometry in integrated light. Several luminosity variable DA (H-atmosphere) white dwarfs were soon discovered through such efforts (see, e.g., Fontaine et al. 2001a for a historical account of these early searches), and it became readily apparent that the multiperiodic luminosity variations observed in these isolated, noninteracting stars were caused by  $g$ -mode oscillations (Chanmugan 1972; Warner & Robinson 1972). However, it took the work of John T. McGraw to make

sense of these exciting discoveries. Indeed, in a most remarkable observational Ph.D. thesis, written at the University of Texas at Austin, McGraw (1977) was the first to establish the basic and the unifying properties of the members of a new class of oscillating stars, the pulsating DA—or ZZ Ceti—white dwarfs.<sup>1</sup> A finding of primary importance, McGraw’s (1977) work established that ZZ Ceti stars were all isolated DA white dwarfs tightly regrouped around a color index  $B - V \sim +0.2$  (which corresponds to  $T_{\text{eff}} \sim 12,000$  K).

After McGraw and colleagues had established the fundamental observational properties of the ZZ Ceti stars (and see Robinson 1979 and McGraw 1980 for early reviews), several groups searched for the excitation mechanism that would explain the very existence of these new pulsators. Without contest, the most important advancement in this field came from the

---

<sup>1</sup>On the anecdotal side, it is interesting to point out that ZZ Ceti is the variable star name of Ross 548, the second pulsating DA white dwarf to have been discovered. This finding was made some three years after the variability of HL Tau 76 had been found (Lasker & Hesser 1971). To this day, we have no satisfactory explanation for why the class was named after the second pulsator and not after the prototype HL Tau 76.

outstanding theoretical work of Donald E. Winget, who wrote a prize-winning Ph.D. thesis at the University of Rochester on the topic. Other contemporary and important contributions to the field at the time were those of Dolez & Vauclair (1981), Dziembowski & Koester (1981), and Starrfield et al. (1982). Winget (1981; and see also Winget et al. 1982a) explained quite elegantly and convincingly the class of ZZ Ceti stars as a natural phase in the evolution of DA white dwarfs, a phase during which the hydrogen in the outer envelope—essentially devoid of other elements through gravitational settling—recombines around  $T_{\text{eff}} \sim 12,000$  K, leading to a formidable increase of the envelope opacity which, in turn, strangles the flow of radiation and, ultimately, causes pulsational instabilities against  $g$ -modes. Even though a better understanding of the driving mechanism was offered by Brickhill (1983) shortly after, this basic picture still holds very much true today. It is indeed the partial ionization (recombination) of hydrogen in the envelope of a cooling DA white dwarf that is ultimately responsible for the excitation of low-degree, low-order  $g$ -modes across the ZZ Ceti instability strip.

By direct analogy with the ZZ Ceti stars, Winget (1981) predicted the existence of pulsating DB stars, belonging to those  $\sim 20\%$  of white dwarfs born with no or very little hydrogen in their atmosphere/envelope. Helium, having higher ionization potentials than hydrogen, recombines at higher effective temperatures (around 25,000 K) in a cooling white dwarf, and this also leads to a very large opacity increase potentially able to cause pulsational instabilities as reasoned by Winget. With the help of colleagues (see Winget et al. 1982b), he then set out to search for pulsating DB white dwarfs at the McDonald Observatory 0.9-m telescope in 1982 May. As the fourth target studied during that run, GD 358 (V777 Her) became the first known luminosity variable white dwarf of the DB type. A more extensive theoretical investigation (Winget et al. 1983) subsequently showed that GD 358 indeed had all the expected characteristics of a DB object pulsating in low-degree, low-order  $g$ -modes. The exciting discovery of GD 358 was first reported by Winget & Fontaine (1982) at a pulsation conference held in Boulder (Colorado) just 10 days after their finding at the telescope. As it happened, the conference was held in honor of two pillars of stellar pulsation theory, Paul Ledoux and John P. Cox, and it was more than fitting that the discovery of pulsating DB stars was seen as a tribute to their pioneering work. It took two more years for a second pulsating V777 Her star to be found (Winget et al. 1984).

In the meantime, in 1979, McGraw and collaborators had discovered a unique star named PG 1159–035 showing multi-periodic luminosity variations reminiscent of those seen in medium amplitude ZZ Ceti stars (McGraw et al. 1979). However, there was very little else in common as PG 1159–035 was obviously a much hotter white dwarf than a ZZ Ceti star can be—McGraw et al. estimated its effective temperature as above 50,000 K, at least consistent with the modern value of

140,000 K—and it also showed a unique spectrum that was not understood at all at the time. In fact, PG 1159–035 is the prototype of a spectral class of very hot white dwarfs, fittingly known as the PG 1159 stars, and corresponding to the direct products of the so-called born-again post-asymptotic giant branch (post-AGB) scenario. In this scenario, a violent mixing event is induced by a late helium flash in the post-AGB phase of stellar evolution and produces an envelope devoid of hydrogen and made of a mixture of helium, carbon, and oxygen in very roughly comparable proportions (for more details on this and the class of PG 1159 stars and related objects, please see the excellent review of Werner & Herwig 2006). Although there was initially much debate among some pulsation theorists about the nature of the driving mechanism responsible for the  $g$ -mode oscillations causing the luminosity variations seen in PG 1159–035, there is no doubt today that it is a classic  $\kappa$ -mechanism caused by the cyclic ionization of the K-shell electrons of carbon and oxygen (see Quirion et al. 2007a for a recent account of this). Given that these atomic configurations have much higher ionization potentials than those of hydrogen or helium, it is no surprise then that the GW Vir white dwarfs—the variable star name given to PG 1159–035—pulsate at much higher effective temperatures than their cooler He and H counterparts. The class of GW Vir pulsators was officially born with the discovery of a second luminosity variable belonging to the spectral type PG 1159, K1–16 (Grauer & Bond 1984).

Following the initial efforts of these pioneering years, the study of pulsating white dwarfs has developed most remarkably and has become an essential chapter in asteroseismology, often paving the way for new avenues of research. The field has attracted many capable young researchers and has grown tremendously to the point where it has now become difficult to keep track of all the varied and rich literature that is being produced. Given the space constraints here, it would not be possible to simply list all the papers that have been written on the topic, let alone comment on them. So, this is not, and cannot be, a bibliographical review on pulsating white dwarfs. Instead, our goal is, first, to provide a general overview mostly aimed at nonspecialists and, secondly, to focus on those areas where, in our view, progress is most likely to be made in the coming years. Authors whose work is not cited explicitly here ought not to feel overly troubled by our choices, which remain personal. We also point out that  $g$ -mode pulsations have now been discovered in several accreting white dwarfs in cataclysmic variables following the initial report of van Zyl et al. (2000). The basic theory for this other category of pulsating white dwarfs has been worked out in the enlightening paper of Arras et al. (2006). Given our very limited expertise in that area, and given the fact that the topic deserves a full review of its own, we focus on isolated pulsators in the rest of this paper.

## 2. THE PULSATING WHITE DWARFS AS COMPACT PULSATORS

There are now five known distinct families of compact pulsators defined as those pulsating stars with surface gravities larger than  $10^5 \text{ cm s}^{-2}$ . Figure 1 is a spectroscopic HR diagram showing that portion of the surface gravity–effective temperature plane where they are found. In addition to the three classes of pulsating white dwarfs described previously, two other categories of pulsators were discovered more recently. Both belong to the class of hot B subdwarf (sdB) stars. In all cases, the pulsators that we refer to are isolated stars or components of noninteracting binaries, and their luminosity variations are caused by internal partial ionization mechanisms.

As can be inferred from above, about 80% of the white dwarfs descend from post-AGB remnants that have retained a thin H envelope. The red curve shown in the figure is representative of the evolution of such H-atmosphere white dwarfs. This channel leads to the formation of a first family of compact pulsators, the ZZ Ceti white dwarfs, by the time a star evolves through a narrow range of effective temperature centered around  $T_{\text{eff}} \sim 11,800 \text{ K}$ , in which H recombines in the envelope of the star.

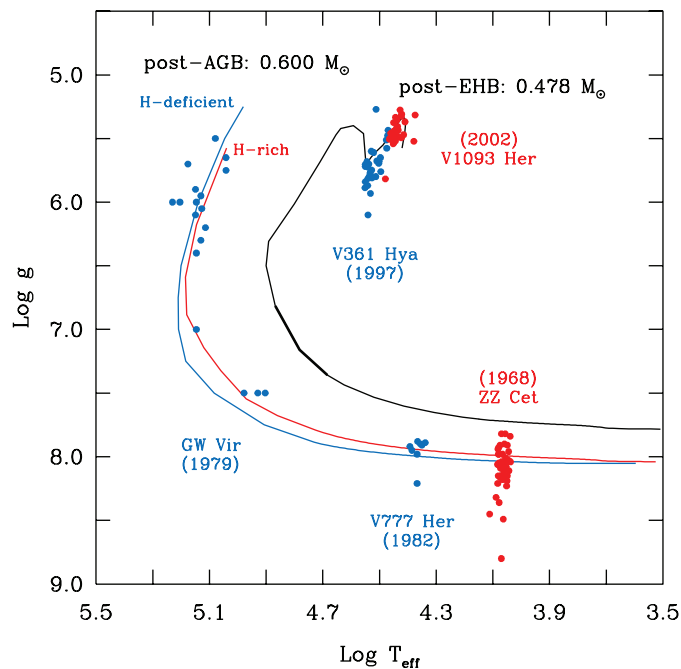


FIG. 1.—Region of the  $\log g - \log T_{\text{eff}}$  plane where the compact pulsators are found. Each of the five distinct families is identified by its official IAU name, and the year of the report of the discovery of the prototype of each class is also indicated. Typical evolutionary tracks are plotted showing (1) the track followed by a  $0.6 M_{\odot}$  post-AGB, H-rich star, which becomes a H-atmosphere white dwarf (red curve), (2) the path followed by a  $0.6 M_{\odot}$  post-AGB, H-deficient star, which becomes a He-atmosphere white dwarf (blue curve), and (3) the path followed by a  $0.478 M_{\odot}$  post-EHB model, which leads to the formation of a low-mass H-atmosphere white dwarf (black curve).

Most of the rest of the white dwarfs instead descend from post-AGB remnants that have managed to get rid of their residual H through the born-again scenario. This second channel gives rise to two other families of compact pulsators: the extremely hot ( $T_{\text{eff}} \sim 120,000 \text{ K}$ ) GW Vir stars, and the much cooler ( $T_{\text{eff}} \sim 25,000 \text{ K}$ ) V777 Her stars. There is a natural evolutionary link between these two types of pulsators along the blue curve shown in Figure 1, and a GW Vir star is bound to pulsate again later in its lifetime, but at that time as a DB white dwarf.

The short-period pulsating sdB stars were discovered some 10 years ago at the South African Astronomical Observatory (Kilkenny et al. 1997). Their existence had been predicted through detailed nonadiabatic calculations carried out by Charpinet et al. (1997a), a feat that was hailed as another small triumph for pulsation theory. These  $p$ -mode pulsators are officially named V361 Hya stars. In the same general area of the  $\log g - \log T_{\text{eff}}$  diagram, but distinctly cooler and less compact, one finds the second family of pulsating sdB stars, the long-period variables (or V1093 Her stars) discovered even more recently by Betsy Green and her collaborators (Green et al. 2003). These are  $g$ -mode oscillators like the pulsating white dwarfs.

The evolution of sdB stars in the diagram is typified by the black curve, which shows the track followed by a  $0.478 M_{\odot}$  post-extended horizontal branch (post-EHB) model. This channel contributes to a small fraction ( $\sim 2\%$ ) of the white dwarf population in the form of low-mass objects. Note that the heavy part of the black track corresponds to a theoretical instability region predicted by the models of Charpinet et al. (1997b). In nature, these would correspond to low-mass DAO white dwarfs—relatively rare objects—undergoing  $g$ -mode oscillations excited through the  $\epsilon$ -mechanism, but this sixth family of compact pulsators, if indeed it exists, has yet to be discovered (and see Handler 1998).

The oscillations of the compact pulsators manifest themselves primarily through multiperiodic luminosity variations. Figure 2 is a montage of representative optical light curves, one each for each type of pulsator, and is meant to illustrate why integrated light photometry has been the tool of choice for studying these stars. It should be pointed out that, residing in the lower portion of the HR diagram, compact pulsators are intrinsically faint, and photon starvation has been a fundamental and inescapable observational constraint in the field. The brightest known pulsating white dwarf is the ZZ Ceti star G226–29 at  $V = 12.24$  but, as it happens, it is also one of the lowest (apparent) amplitude variables in the whole group. It should also be pointed out that each family of compact pulsators has specimens showing a wide variety in the complexity, amplitude, and nonlinear aspect of their light curves (and see § 6 for specific examples). Some caution is to be exercised when enjoying Figure 2: quite different light curves than those displayed there have often been gathered for other members of the various classes of compact pulsators. Note that in the rest of this review, we will concentrate exclusively on the three categories of

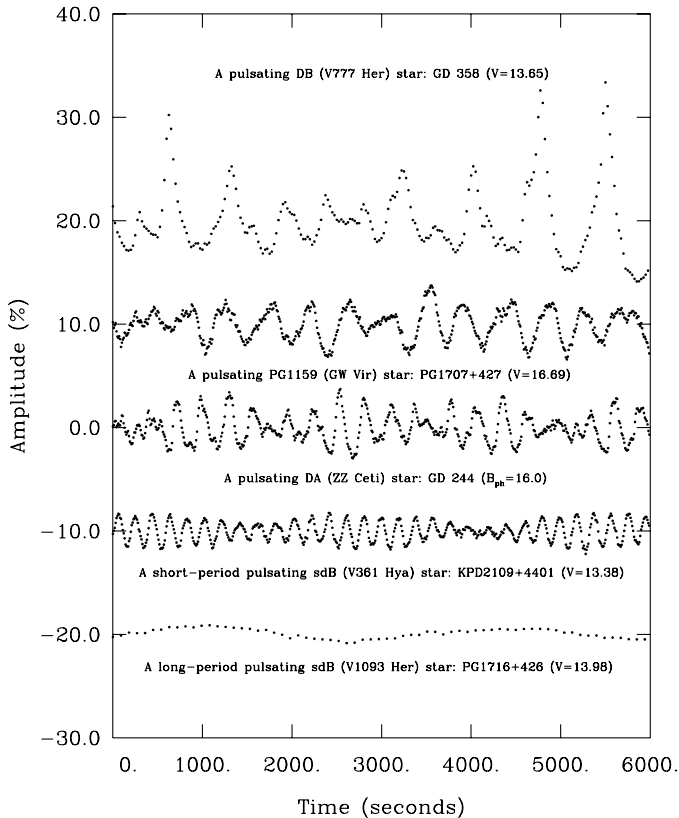


FIG. 2.—Segments of typical optical light curves for compact pulsators. The four upper curves were obtained with LAPOUNE, the Montréal portable three-channel photometer attached to the 3.6-m CFHT telescope. This photometer uses photomultiplier tubes as detectors. No filter was used, so these are integrated “white light” data. In comparison, the lower light curve was obtained by Betsy Green at the Steward Observatory 2.3-m telescope with a CCD detector using a broadband Johnson  $B$  filter in the beam.

pulsating white dwarfs. Interested readers may want to consult Fontaine et al. (2006) for a brief review on the pulsating sdB stars.

We provide, in Figure 3, an unusual look at pulsating white dwarfs as seen through *Far Ultraviolet Spectroscopic Explorer* (*FUSE*). *FUSE* was primarily an orbiting spectrometer sensitive in the FUV spectral range (900–1200 Å), but it also had photometric capabilities in the so-called time tag mode. With the help of *FUSE* scientist Pierre Chayer, we used archived data to construct these light curves. In order to build up the signal-to-noise ratio (S/N), we binned together all the spectral points of each 10 s spectrum into a single FUV “color,” and our results are shown in the figure. We find it rather remarkable that a small 15-cm telescope (the effective diameter of *FUSE*) is able to provide such beautiful light curves for rather faint stars such as PG 1159–035 and EC 20058–5234. But there is a simple explanation: there is quite a bit of flux in the FUV for a hot star such as the DB white dwarf EC 20058–5234 ( $T_{\text{eff}} \sim 28,000$  K) and a lot more still for PG 1159–035 itself

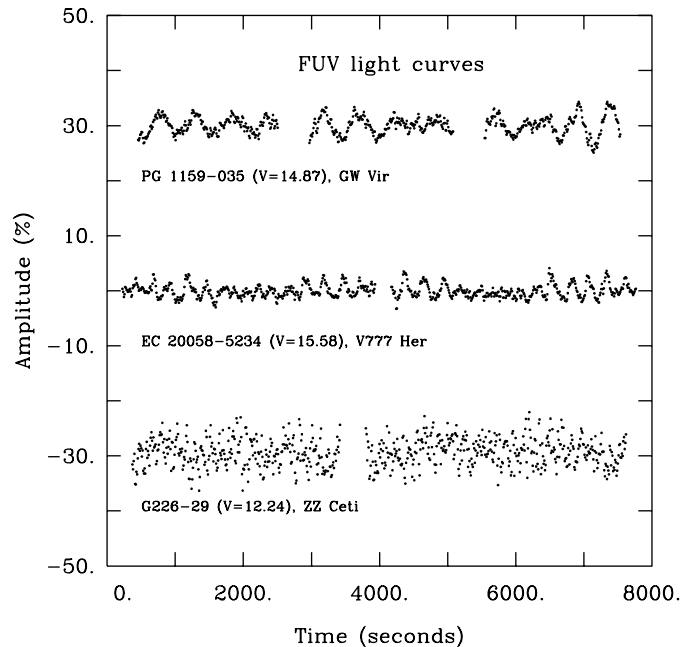


FIG. 3.—FUV light curves for representative members of the three families of pulsating white dwarfs as obtained by *FUSE*. The light curves are expressed in terms of percentage of residual amplitude relative to the mean brightness of the star. Each plotted point represents a sampling time of 10 s. The upper and lower curves have been shifted in the vertical direction away from the zero point for visualization purposes.

at  $T_{\text{eff}} = 140,000$  K. Using the same argument, even though the brightness of G226–29 is significantly higher in the  $V$  band than those of the other two stars, the FUV flux coming from this ZZ Ceti star ( $T_{\text{eff}} = 12,260$  K) has dropped dramatically, and this explains its very noisy FUV light curve.<sup>2</sup> The interest of these FUV light curves goes much beyond simple curiosity and esthetics. And indeed, as we discuss at some length below, the amplitude of a pulsation mode does depend on wavelength, and this bears the signature of, among other things, the degree index  $l$  of the mode. Thus, we draw attention to the fact that the *FUSE* archives offer an interesting, still untapped potential for white dwarf asteroseismology.

An introduction to pulsating white dwarfs would not be complete without mentioning that white dwarfs have a mechanical structure that is fundamentally different from that of normal or giant stars. It is therefore not a good idea to extrapolate pulsation results from the main sequence to the white dwarf regime, for example. In comparison to normal stars, everything is “thin” and “compact” in white dwarfs: they have very thin atmospheres (in fact, the usual plane parallel approximation used to construct model atmospheres is much more justified in white dwarfs than

<sup>2</sup>Even though the pulsational FUV luminosity variations of G226–29 are not at all obvious to the eye in Fig. 3, a standard Fourier analysis of the light curve readily reveals a periodicity at 109 s, the mode already known from optical observations.

in main sequence stars), they have thin superficial convection zones (in the V777 Her and ZZ Ceti phases), and they have thin composition transition zones that define an onion-like compositional structure. While  $g$ -mode propagation is usually confined to the deep interior in normal stars, it extends well into the outer envelope in white dwarfs.

We illustrate this point with the help of Figure 4 showing the profiles of the Brunt-Väisälä frequency (*solid curves*) as well as of the Lamb frequency for modes with  $l = 1$  (*dotted curves*) for four different stellar models. A solar model is used in comparison with typical models of the three kinds of pulsating white dwarfs. As is well known, the condition for local  $g$ -mode propagation is that the square of the frequency of a mode (with  $l = 1$  here),  $\sigma^2$ , has to be less than the smaller of  $N^2$  or  $L_1^2$  at a given depth in a model. Figure 4, then, clearly reveals that  $g$ -mode propagation in the Sun is essentially limited to a region below the extensive outer convection zone, while it extends to much higher levels in white dwarfs. The mechanical properties of white dwarfs are therefore clearly different from those of solar-like stars. The enormous differences in the values of the Brunt-Väisälä and Lamb frequencies shown in Figure 4 also

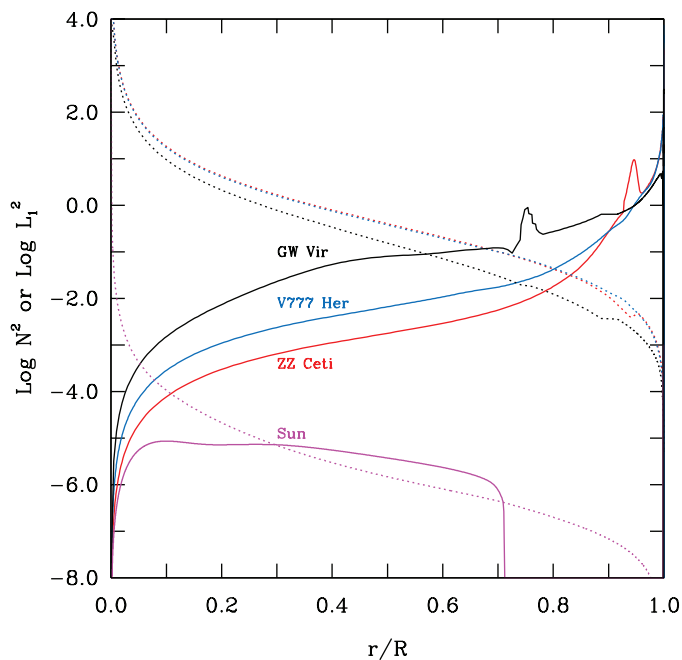


FIG. 4.—Propagation diagram for (1) a solar model (*magenta curves*), (2) a GW Vir star model (*black curves*), (3) a V777 Her star model (*blue curves*), and (4) a ZZ Ceti model (*red curves*). For each model, the profile of the logarithm of the square of the Brunt-Väisälä frequency (*solid curve*) and that of the logarithm of the square of the Lamb frequency for modes with  $l = 1$  (*dotted curve*) are shown as functions of the normalized radius. The well in the Brunt-Väisälä frequency for the solar model corresponds to the outer convection zone, while the peak structure seen in both the GW Vir and the ZZ Ceti curves is associated with a composition transition zone. The three white dwarf models all have a mass of  $M = 0.6 M_{\odot}$ .

indicate that this is again the case for main sequence stars, in general.

A related point concerning the compact nature of white dwarfs is that the period of a mode defined by its radial order index  $k$  and its degree index  $l$  is much smaller than in a normal star. This follows naturally from the propagation diagram shown in Figure 4, but we also wish to provide a more quantitative illustration. For that purpose, we first show in Figure 5 the period spectrum for modes with  $l = 1$  calculated for a standard solar model in the range from 50 to 5500 s. This essentially covers all the ranges of periods observed in the known pulsating white dwarfs. There are 144 modes in that interval for our solar model and, except for the two longest period ones, these are all  $p$ -modes. The circle in the first column of points in Figure 5 identifies the first mode ( $k = 1$ ) of the  $g$ -branch family. It has a period of 3802.6 s.

In comparison, we computed the period spectra of seven evolutionary models appropriate for the GW Vir phase with the aim of illustrating the effects of the end of the contraction phase and the beginning of the cooling phase on the period spectrum. This is well illustrated in Figure 5 where the evolution proceeds from left to right in the central structure containing seven columns. These models actually map the “turning of the bend” in the blue

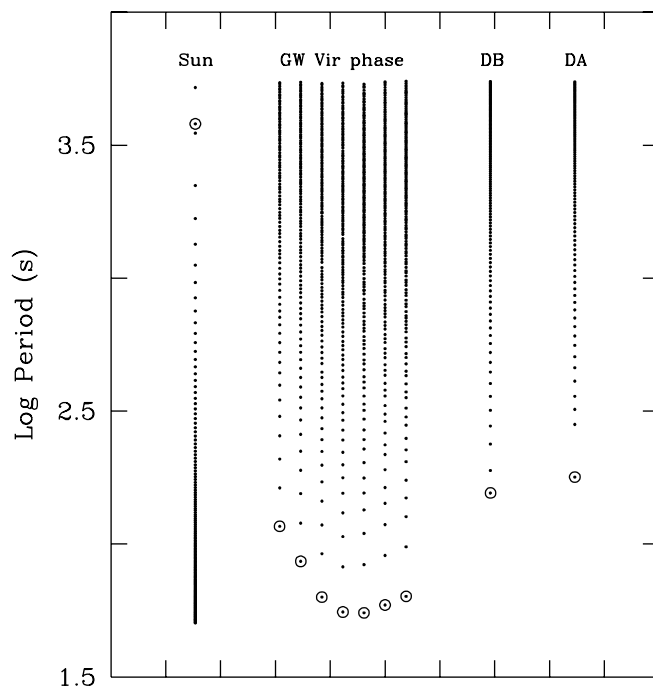


FIG. 5.—Comparison of the period spectra for modes with  $l = 1$  in the period interval 50–5500 s for (1) a solar model (*left column*), (2) seven evolving GW Vir models (*the seven columns bunched together*), (3) a V777 Her model, and (4) a ZZ Ceti model (*right column*). The circle in each column separates the  $g$ -branch above from the  $p$ -branch below and identifies the first overtone ( $k = 1$ ) of the  $g$ -branch. All of the white dwarf models considered have the same total mass of  $0.6 M_{\odot}$ .

evolutionary track shown in Figure 1. In Model 4 from the left, the period of the  $k = 1, l = 1$  mode reaches its minimum value of 55.5 s, way down from its value of 3802.6 s in the solar model. Note that in all models of white dwarfs considered in Figure 5, the longest possible period for a  $p$ -mode (that associated with the  $k = 1$  overtone) is much smaller than the lower limit of 50 s in our search window;  $p$ -modes are therefore absent for the white dwarf models shown in the figure.

As is well known, the contraction phase in a pre-white dwarf ultimately ceases due to the onset of electron degeneracy, which provides the needed internal pressure. After that, the evolution of a white dwarf is governed by cooling, i.e., the loss of thermal energy at a rate depending on the mass, the internal composition, and the composition of the external layers whose opacity controls part of that loss. As illustrated in Figure 4, cooling leads to a general decrease of the Brunt-Väisälä frequency. This is caused by the increase of the overall degeneracy of the evolving model. Given that the period of a  $g$ -mode is approximately inversely proportional to the integral  $\int_0^R |N|/r dr$ ,<sup>3</sup> it follows that white dwarf cooling leads to an increase of the period of a pulsation mode of given  $k$  and  $l$  values. Hence, it is not surprising that the period of the first ( $k = 1$ ) mode of the  $g$ -branch has increased to a value of 155.5 s in the V777 Her model and to 178.5 s in the even cooler ZZ Ceti model. Note that we picked the same mass of  $0.6 M_\odot$  for all the white dwarf models depicted in Figure 5 as there is a strong dependence of the period on the mass.

It is appropriate to point out that the fact that the periods of the  $g$ -modes observed in pulsating white dwarfs are relatively short ought to be considered a good thing. This is because a large number of pulsation cycles can be covered in a single night of observations and, as a consequence, it is easier to assess the multiperiodic character of a given light curve. On the downside, as indicated above, white dwarfs remain intrinsically faint and it is often difficult, observationally speaking, to reach comfortable S/Ns.

Along with its compact nature, the chemical layering of a pulsating white dwarf is another mechanical property that bears a strong imprint on its period spectrum. Even though a typical white dwarf consists of a C/O core containing more than 99% of its mass, the thin He mantle that surrounds the core (containing at most  $<1\%$  of the total mass), and the even thinner H layer that envelops a DA star (containing at most  $<0.01\%$  of the total mass) play a major role in establishing the period distribution. This is because  $g$ -modes in white dwarfs have large amplitudes and propagate easily in these outermost layers. The modes are therefore quite sensitive to the details of the chemical stratification above the core. In fact, the layered structure produces a highly nonuniform period spectrum for a family of  $g$ -modes be-

longing to the same degree index  $l$  but with different values of  $k$  (see, e.g., Figs. 5 and 7 of Brassard et al. 1992c). This is again a good thing because it suggests that chemical layering could potentially be measured accurately through asteroseismological means.

Figure 6 illustrates the chemical profile in a representative model of a ZZ Ceti pulsator. The chemical stratification is shown in terms of the logarithm of the fractional mass depth, a scale used to emphasize the outer layers where  $g$ -modes have large amplitudes in white dwarfs. Note that the atmosphere of a ZZ Ceti star—the only region directly accessible to observations—typically contains less than  $10^{-15}$  of the total mass of the star. In comparison, Figure 7 shows the profile of the square of the Brunt-Väisälä frequency and of the square of the Lamb frequency for dipole modes for that same model. The well in the distribution of the Brunt-Väisälä frequency is due to the presence of a superficial convection zone caused by H partial ionization in the model, and the peaks are clearly associated with the layers where the chemical composition varies. These features are quite significant as they “pinch” the eigenfunctions and produce mode confinement and mode trapping, ultimately leading to a highly nonuniform period distribution (see again Brassard et al. 1992c).

It is important to realize that the  $g$ -modes are more sensitive to the chemical features associated with the H and He outermost layers than to those caused by the nonuniform composition in the C/O core. This is because pulsation modes tend to be formed outside the most degenerate central regions and consequently have very low amplitudes there. To a large extent, and this is particularly true for the most degenerate configuration represented by ZZ Ceti stars, the degenerate interior of a white dwarf is refractory to asteroseismological probing. This poses a

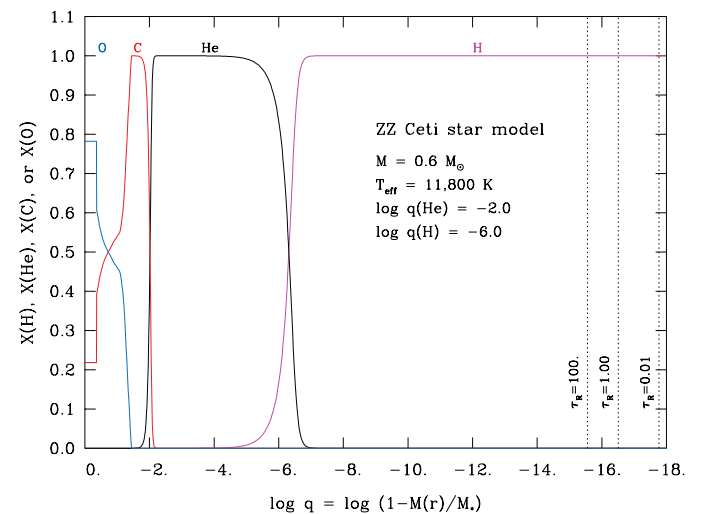


FIG. 6.—Chemical layering in a representative model of a ZZ Ceti pulsator. The location of the atmospheric layers is indicated through the values of the Rosseland optical depth.

<sup>3</sup>This is strictly valid only for purely radiative and chemically homogeneous models in the asymptotic regime of high radial order as demonstrated by Tassoul (1980).

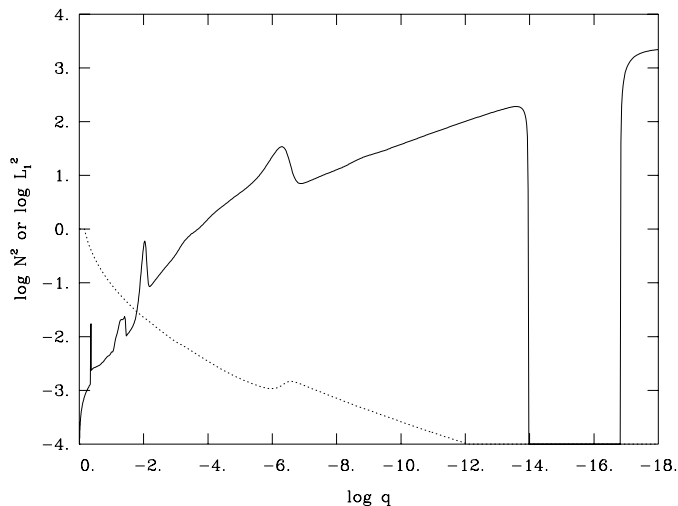


FIG. 7.—Run of the Brunt-Väisälä frequency and of the Lamb frequency (for  $l = 1$  modes) in the representative ZZ Ceti star model.

problem for accurately inferring the structure of the C/O core from period measurements. In addition, the overall degeneracy increases with cooling and the region of mode formation migrates outwards. This implies that mode sensitivity to model parameters changes from the GW Vir phase to the V777 Her and the ZZ Ceti regime. In other words, the type of asteroseismology that is possible for GW Vir stars is not exactly the same as that possible for ZZ Ceti stars, for example.

The top panel in Figure 8 illustrates this notion of changing mode sensitivity along the white dwarf cooling sequence. To avoid the complications caused by chemical layering (mode trapping and mode confinement), complications that would unnecessarily cloud the point that we want to make about mode migration, we considered the evolution of a  $0.6 M_{\odot}$  pure C model. The figure shows the weight function of the lowest-order ( $k = 1$ ) dipole  $g$ -mode in terms of depth, and in terms of different phases of cooling as quantified by the effective temperature. The weight function is normalized so that the area under each curve is the same. The figure clearly reveals the *outward migration* of the region of mode formation with cooling. This implies that the pulsation modes of a white dwarf progressively lose their ability to probe the deep interior (GW Vir regime) and become more sensitive to the details of the outermost layers (ZZ Ceti regime) as cooling proceeds. It is particularly obvious here that the  $k = 1$ ,  $l = 1$   $g$ -mode in the 10,117 K model does not probe the core very well. The same is true, although to a lesser extent, for higher-order modes as illustrated in the bottom panel in Figure 8 for dipole modes with  $k = 1, 5$ , and  $10$ . Hence, it follows that determinations of the exact chemical structure of the C/O core through period-matching exercises remain quite difficult in V777 Her stars, and even more so in ZZ Ceti stars.

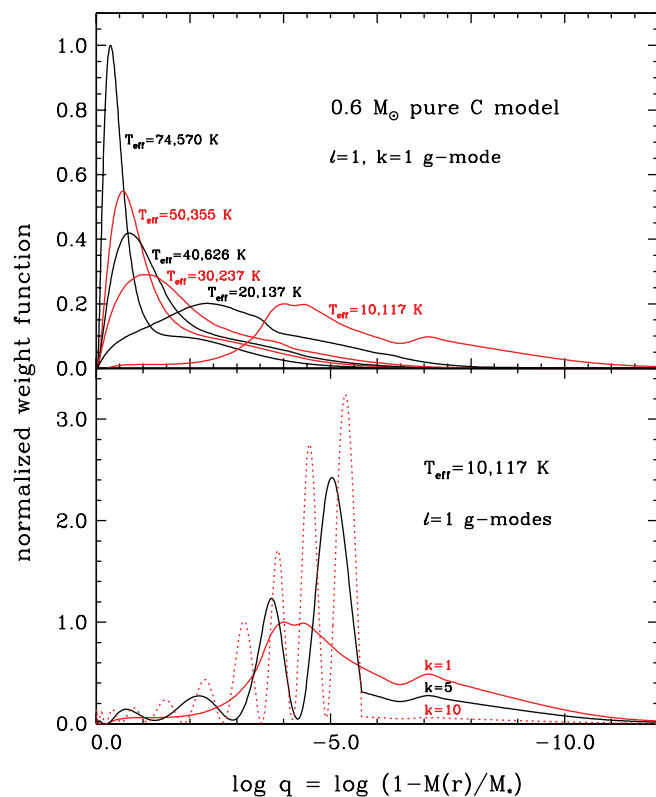


FIG. 8.—*Upper Panel*: Outward migration of the weight function distribution for a cooling white dwarf model. The mode involved is the lowest-order dipole  $g$ -mode. *Lower Panel*: Normalized weight function for the dipole modes with  $k = 1, 5$ , and  $10$  in the coolest stellar structure retained in the evolutionary sequence.

### 3. CLASS PROPERTIES AND CURRENT CENSUS

For the purposes of the present review, we have updated the lists of known pulsating white dwarfs in order to provide that information in a single place. This has proven a bit of work, particularly for the ZZ Ceti stars, because the successive data releases from the Sloan Survey have led to a spectacular increase in the number of known pulsators. For instance, in less than three years, the number of known ZZ Ceti stars has more than doubled. Nevertheless, we made real efforts to see through this maze and we hope that our compilations will be useful to the general reader.

#### 3.1. ZZ Ceti Stars

For the ZZ Ceti stars, we have an ongoing spectroscopic program at the Université de Montréal piloted by our colleague Pierre Bergeron whose aim has been to provide homogeneous and reliable time-averaged atmospheric parameters for those stars. This is of utmost importance for mapping the ZZ Ceti instability strip in the  $\log g - T_{\text{eff}}$  diagram, and also for providing constraints for eventual detailed seismic analyses of individual pulsators. This program started with the study of Bergeron et al.

(1995), who provided the very first homogenous quantitative study of the class properties of the ZZ Ceti stars using optical spectroscopy, optical photometry, and UV spectrophotometry. Bergeron et al. (1995) considered the full sample of 22 ZZ Ceti stars that were known at the time. Among other important results, they were able to “calibrate” the version of the mixing-length theory used to describe convection in the atmospheric layers of these stars by finding out which one provides the best internal consistency between optical measurements, UV observations, parallax determinations, and gravitational redshift measurements (when available). Hence, the so-called  $ML2/\alpha = 0.6$  version of the mixing-length theory has been used ever since by all other modelers in the field and is now considered the standard.

After this was established, Bergeron and colleagues found out that high-S/N optical spectroscopy alone (analyzed with  $ML2/\alpha = 0.6$  synthetic spectra) would provide reliable estimates of the atmospheric parameters of ZZ Ceti stars. Two essential rules were imposed, (1) gathering optical spectra with S/Ns generally above 100 and never below 80, and (2) choosing exposure times to cover several pulsation cycles in order to obtain meaningful time-averaged data. The latter point is particularly important for long-period, large-amplitude pulsators because observing during only part of a cycle can only skew the inferred atmospheric parameters. This spectroscopic program has been very successful and has led to the discovery of many new ZZ Ceti stars. Furthermore, it has provided an ever growing source of time-averaged data with which to discuss the class properties of these stars.

Table 1 gives a list of 48 ZZ Ceti stars analyzed within the framework of this program. It contains all the classic ZZ Ceti stars and most of the brighter ones. The first column gives the WD number of the star if it exists (i.e., if the object is to be found in the White Dwarf Catalog of McCook & Sion 1999), column (2) gives the usual name, and the third column lists the  $V$  magnitude when available (the photographic  $B$  magnitude otherwise). The values of the effective temperature and surface gravity have been taken from Table 1 of Bergeron et al. (2004; 36 stars), from Table 2 of Gianninas et al. (2005; 3 stars), from Table 4 of Gianninas et al. (2006; 3 stars), and from Table 2 of Gianninas et al. (2007; 4 stars). In addition, values for two more objects were kindly communicated to us by Alex Gianninas (personal communication, 2007). Column (6) of Table 1 gives the period or the range of periods observed in the star. In this, we took care not to include periods that would correspond to nonlinear effects such as harmonics or cross frequencies of dominant peaks. Except for G226–29 which, at least to very low detection levels, genuinely shows a single mode at 109 s (it is in fact a triplet when observed at high temporal resolution, a triplet likely to be caused by rotational splitting), the stars listed as showing a single period have simply not been observed at high enough sensitivity and the value of the period relies often on short discovery runs. They are very likely

to reveal themselves as multiperiodic pulsators when observed at higher S/Ns. Finally, column (7) gives reference to the discovery paper.

In addition to the 48 ZZ Ceti pulsators listed in Table 1, Gianninas et al. (2005) have reported the discovery of luminosity variations in three more objects, but those have unreliable atmospheric parameters because the exposure times used in gathering the spectra were too short compared to the main period of a pulsation cycle. These stars were actually observed in spectroscopy before they were known to pulsate. Pending longer spectroscopic measurements, we have refrained from including them in our Table 1. These are MCT 0016–2553 ( $V = 16.10$ ), KUV 03442+0719 ( $V = 16.10$ ), and GD 1212 ( $V = 13.26$ ). Similar new ZZ Ceti stars needing longer spectroscopic observations have been reported by Voss et al. (2006; EC 11266–2217, EC 13429–2342) and Voss et al. (2007; HS 0210+3302, HS 0235+0655, HE 0344–1207, HS 0733+4119, and GD 266).

To this list of 58 (relatively) bright ZZ Ceti stars must be added several discoveries coming out of the SDSS project. Unfortunately, these objects are much fainter on the whole (by 2 to 3 mag), and their atmospheric parameters must be considered a lot less reliable and accurate than the homogeneous bright sample retained in our Table 1. This is not only because the SDSS spectra have much lower S/Ns than the stars in Table 1 but also because the rule about exposing for periods of time longer than several pulsation cycles was not followed by virtue of the SDSS mode of operation. In our survey of the literature, we retained the samples of 35 new ZZ Ceti stars reported by Mukadam et al. (2004; 33 SDSS targets plus HS 0951+1312 and HS 0952+1816), 11 pulsators reported by Mullally et al. (2005; all SDSS stars), 14 SDSS pulsators reported by Kepler et al. (2005a), 11 more reported by Castanheira et al. (2006; 10 SDSS stars plus HE 0031–5525), and finally 7 additional SDSS variables reported by Castanheira et al. (2007). This gives, at the time of writing, a total of 136 known pulsating stars of the ZZ Ceti type.

### 3.2. V777 Her Stars

Following the example set by Bergeron et al. (1995) for the ZZ Ceti stars, a systematic and detailed investigation of the time-averaged class properties of the pulsating DB white dwarfs was carried out by Beauchamp et al. (1999). This was done in the same spirit, emphasizing high-S/N optical spectroscopy and making sure that the integration time for a given spectrum was long enough to cover several pulsation cycles. Prior to that, Beauchamp (1995) had determined that the best parametrization of the mixing-length theory to be used in the construction of DB model atmospheres was the  $ML2/\alpha = 1.25$  version, the one giving the best internal consistency between optical and *IUE*-based effective temperatures. This is the version used by Beauchamp et al. (1999), a paper that has remained the standard reference in the field.

TABLE 1  
THE CURRENT SAMPLE OF KNOWN BRIGHT ZZ CETI STARS WITH HOMOGENEOUS ATMOSPHERIC  
PARAMETERS

WD (1)	Name (2)	$V$ (3)	$T_{\text{eff}}$ (K) (4)	$\log g$ (5)	Period (s) (6)	Reference (7)
0036+312 .....	G132-12	16.20	12,080	7.94	213	zz1
0104-464 .....	BPM 30551	15.26	11,260	8.23	607-840	zz2
0133-116 .....	Ross 548	14.16	11,990	7.98	187-334	zz3
0145-221 .....	MCT 0145-2211	15.4	11,550	8.14	462-823	zz4
0246+326 .....	KUV 02464+3239	15.8	11,290	8.08	832	zz5
0341-459 .....	BPM 31594	15.03	11,540	8.11	177-1147	zz6
0415+271 .....	HL Tau 76	15.20	11,450	7.90	383-1391	zz7
0417+361 .....	G38-29	15.63	11,180	7.91	910-1020	zz8
0455+553 .....	G191-16	15.98	11,420	8.06	519-883	zz9
0507+045.1 .....	HS 0507+0435B	15.36	11,630	8.17	355-743	zz10
0517+307 .....	GD 66	15.56	11,980	8.05	198-303	zz11
0532-560 .....	HE 0532-5605	15.9	11,560	8.49	586-689	zz4
0836+404 .....	KUV 08368+4026	16.54	11,500	8.07	495-618	zz12
0858+363 .....	GD 99	14.55	11,830	8.09	105-1151	zz13
0921+354 .....	G117-B15A	15.54	11,630	7.98	215-304	zz14
1039+412 .....	PB 520	15.9(B)	11,550	8.09	837-856	zz15
1116+026 .....	GD 133	14.57	12,090	8.06	116-147	zz16
1137+423 .....	KUV 11370+4222	16.56	11,890	8.06	257-463	zz12
1149+057 .....	PG 1149+057	15.1(B)	11,210	8.19	1024	zz17
1150-153 .....	EC 11507-1519	16.00	12,030	7.98	250	zz1
1159+803 .....	G255-2	16.0	11,440	8.17	569-985	zz18
1236-495 .....	BPM 37093	13.96	11,750	8.80	512-635	zz19
... ..	HS 1249+0426	15.8(B)	12,040	8.15	289	zz17
1258+013 .....	HE 1258+0123	16.26	11,410	8.04	439-1092	zz20
1307+354 .....	GD 154	15.33	11,180	8.15	1084-1191	zz21
1349+552 .....	LP 133-144	16.0(B)	12,010	7.93	209-327	zz20
1350+656 .....	G238-53	15.5	11,880	7.91	122-258	zz22
1401-147 .....	EC 14012-1446	15.5	11,900	8.16	399-937	zz23
1422+095 .....	GD 165	14.32	11,980	8.06	114-250	zz24
1425-811 .....	L19-2	13.75	12,100	8.21	113-350	zz25
1429-037 .....	HE 1429-0343	15.8(B)	11,370	8.08	450-1085	zz15
... ..	HS 1531+7436	16.2(B)	12,920	8.45	113	zz17
1541+650 .....	PG 1541+651	15.7(B)	11,640	8.18	467-757	zz26
1559+369 .....	Ross 808	14.36	11,160	8.04	769-1250	zz13
... ..	HS 1625+1231	16.1(B)	11,730	8.15	385-863	zz17
1647+591 .....	G226-29	12.24	12,260	8.32	109	zz27
1714-547 .....	BPM 24754	15.55	11,070	8.03	978-1176	zz28
... ..	HS 1824+6000	15.7(B)	11,380	7.82	294-384	zz17
1855+338 .....	G207-9	14.64	11,960	8.36	259-557	zz29
1935+276 .....	G185-32	12.98	12,120	8.06	142-652	zz9
1950+250 .....	GD 385	15.13	11,720	8.04	128-256	zz30
2148+539 .....	G232-38	16.40	11,350	8.01	742-1147	zz31
2148-291 .....	MCT 2148-2911	16.10	11,740	7.82	261	zz1
2254+126 .....	GD 244	16.0(B)	11,680	8.08	203-307	zz5
2303+242 .....	PG 2303+243	15.50	11,480	8.09	571-901	zz32
2326+049 .....	G29-38	13.03	11,820	8.15	110-1016	zz33
2347+128 .....	G30-20	16.05	11,070	7.96	1068	zz34
2348-244 .....	EC 23487-2424	15.33	11,520	8.10	805-993	zz35

One difficulty in the interpretation of optical spectra of DB white dwarfs is that there is a sensitivity to small traces of H which might be present in the otherwise He-dominated atmospheres (see Beauchamp et al. 1999 for a detailed discussion). These traces are generally invisible in the optical domain,

but may be detected in the UV if such measurements are available. Because of this, Beauchamp et al. (1999) provided two sets of atmospheric parameter solutions for pulsating DB white dwarfs, one assuming no H whatsoever, and another assuming a trace of H just below the detection limit in the optical. For our

present needs, we retained the no H solutions, but we invite the reader to consult Table 1 of Beauchamp et al. (1999) for the other possibilities.

Table 2 then gives the list of known V777 Her pulsators with homogeneous and reliable atmospheric parameter determinations (with the proviso that traces of H may perturb these values). The format is the same as that of Table 1 for the ZZ Ceti stars. To this sample of 8 stars must be added EC 20058-5234 (Koen et al. 1995), also discussed in Beauchamp et al. (1999), but it has uncertain atmospheric parameters and, therefore, was not retained in our list. It is this object that was observed by *FUSE* and for which we produced the FUV light curve shown in Figure 3. In addition to those, welcome new members of the class were reported recently by Nitta et al. (2007), who discovered eight faint pulsating DB white dwarfs out of the SDSS project. This brings the total of known pulsating V777 Her stars to 17.

### 3.3. GW Vir Stars

What we know today of the class properties of the GW Vir pulsators, and more generally of the hot white dwarfs, is very largely due to the work of Klaus Werner and his coworkers (see, e.g., Werner & Herwig 2006 for a recent review of their work). Although there is no convection in the atmospheres of these very hot objects, their analysis is seriously complicated by the fact that the LTE approximation fails miserably, which necessitates very sophisticated and detailed model atmosphere and synthetic spectra computations. This is not only a science, but also an art in itself. Moreover, contrary to ZZ Ceti stars or V777 Her pulsators which have, respectively, essentially pure H or pure He atmospheres, GW Vir stars have atmospheric chemical compositions that vary from one object to another. This necessitates the time-consuming task of determining the chemical composition on an individual basis, and Werner and company have done this using all possible spectral windows, from the optical domain, to the UV, the FUV, the EUV, and even the X-ray ranges when appropriate.

Table 3 gives the list of all 18 GW Vir stars currently known. The format is the same as above. Note that we have provided fictitious WD numbers for objects whose names do not convey any information about their positions in the sky and which do not belong to the McCook & Sion (1999) catalog. Except for NGC 2371 (see Herald & Bianchi 2004), the values of the effective temperature and the surface gravity are the homogeneous determinations coming out of the Werner group. They were taken from Tables 1 and 2 of Werner & Herwig (2006), where the reader will also find the details of the atmospheric chemical composition of each star. These are mixtures dominated by He, C, and O in widely varying proportions from star to star and also containing a number of trace elements, again in varied proportions. Note that Werner & Herwig (2006) have explicitly stressed that their determinations of the atmospheric parameters of seven objects must be considered preliminary. These stars are: NGC 2867, NGC 5189, Abell 43, K1-16, NGC 6905, NGC 7094, and HS 2324+3944.

For completeness we point out that our list of 18 GW Vir stars includes 12 stars formally belonging to the PG 1159 spectral class, five belonging to the Wolf-Rayet Central Stars of Planetary Nebula ([WCE]) type (NGC 1501, NGC 2867, Sanduleak 3, NGC 5189, and NGC 6905), and one belonging to the so-called [WC]-PG1159 transition spectral type (NGC 2371). We raise this issue because, until quite recently, it had been usual to consider only the pulsating PG 1159 stars to belong to the GW Vir family. As mentioned in the Introduction, GW Vir is the variable star name of the prototype of the PG 1159 spectroscopic class, PG 1159-035 itself. Some authors have given the name DOV to the high-gravity ( $\log g \geq 7.0$ ) GW Vir stars, and PNNV to the low-gravity ( $\log g < 7.0$ ) ones, thus suggesting implicitly some distinct physical characteristics for the two categories. As discussed in Quirion et al. (2007a), there are serious problems with this nomenclature, along with the fact that the driving mechanism is the same in both cases (which implies that the division into low-gravity and high-gravity pulsators is completely unjustified). No GW Vir star belongs to the DO spectral type, thus disqualifying the name DOV for this category of pulsating stars. Furthermore,

TABLE 2  
THE CURRENT SAMPLE OF KNOWN BRIGHT V777 HER STARS WITH HOMOGENEOUS ATMOSPHERIC PARAMETERS

WD	Name	$V$	$T_{\text{eff}}$ (K)	$\log g$	Period (s)	Reference	
0513+260	.....	KUV 0513+2605	16.70	26,300	8.19	350-900	vh1
0954+342	.....	CBS 114	17.2(B)	26,200	8.00	230-670	vh2
1115+158	.....	PG 1115+158	16.1(B)	25,300	7.89	831-1072	vh3
1351+489	.....	PG 1351+489	16.4(B)	26,100	7.89	333-490	vh3
1456+103	.....	PG 1456+103	15.9(B)	22,400	7.91	423-854	vh4
1645+325	.....	GD 358	13.65	24,900	7.91	423-810	vh5
1654+160	.....	PG 1654+160	16.2(B)	27,800	8.00	149-851	vh6
2246+120	.....	PG 2246+120	16.73	27,200	7.89	256-329	vh7

the name PNNV, for Planetary Nebula Nucleus Variable, seems odd when we consider that not all of the so-called PNNVs have planetary nebulae, while some high-gravity GW Vir stars, classified as DOVs, are surrounded by such planetary nebulae. This is enough to also disqualify the name PNNV. Instead, Quirion et al. (2007a) have proposed that the denomination GW Vir be used for all H-deficient post-AGB stars showing GW Vir-like pulsations, that is, every star in the high-gravity, high-temperature region of the  $\log g - T_{\text{eff}}$  diagram showing nonradial  $g$ -mode oscillations due to the  $\kappa$ -mechanism associated with the partial ionization of carbon and/or oxygen.

#### 4. THE INSTABILITY STRIPS

We provided, in Figure 1, a bird’s eye view of the instability domains for the five families of compact pulsators in the surface gravity-effective temperature diagram. We now turn to more detailed discussions of the instability strips of pulsating white dwarfs by zooming in on each appropriate region of that diagram. Such discussions become meaningful because we have at our disposal reliable and homogeneous time-averaged atmospheric parameters as listed in our Tables 1, 2, and 3.

##### 4.1. ZZ Ceti Stars

Figure 9 shows the part of the  $\log g - T_{\text{eff}}$  plane where the ZZ Ceti stars are found. The locations of each of the 48 objects listed in Table 1 are indicated by filled circles. In comparison, the open circles give the locations of stars that have been found not to vary (with typical upper limits on the integrated light amplitude of about 1 millimag in the period range 20–2000 s). Most of these constant stars have been monitored several times,

especially those near the pulsators. While the determination of the location and extent of the empirical ZZ Ceti instability strip in the  $\log g - T_{\text{eff}}$  diagram is being perfected through an ongoing program (see Gianninas et al. 2007 for the latest progress report), Figure 9, as it stands, is already entirely consistent with the idea of a pure strip, a suggestion first articulated by Fontaine et al. (1982). A pure instability strip implies that all DA white dwarfs, with no exception, are to become ZZ Ceti pulsators as they cool across the strip. This, in turn, means that ZZ Ceti asteroseismology could be used as a probing tool for inferring the basic structural properties of the DA white dwarfs as a class, a most interesting prospect from a stellar evolution point of view. In contrast, a strip showing a mixed population of constant and variable stars would imply the existence of an extra parameter to discriminate between pulsators and nonpulsators. Currently, theory has no provision for such a “missing” parameter based on plausible physics, although bold theorists could probably find one or two. In any case, the available evidence, as seen in Figure 9, is overwhelmingly in favor of a pure strip.

For the record, we have to mention that, over the last 20 years, there have been many different claims that the ZZ Ceti instability strip contains a mixed population of variable and nonvariable stars. In every single instance, our colleague Pierre Bergeron examined the case closely by gathering himself a higher S/N spectrum according to the two rules mentioned above and by carefully modeling it following the same homogeneous approach he has always used. It was an uphill battle, but, in every instance, he was able to convincingly move the “offending” constant stars out of the empirical instability strip. Most recently, there has been an attempt to use part of the SDSS sample of ZZ Ceti stars to rediscuss this issue. To know more about this,

TABLE 3  
THE CURRENT SAMPLE OF KNOWN GW VIR STARS

WD	Name	$V$	$T_{\text{eff}}$ (K)	$\log g$	Period (s)	Reference
0044–121	NGC 246	11.74	150,000	5.7	1464–1842	gw1
0122+200	PG 0122+200	16.1( <i>B</i> )	80,000	7.5	336–612	gw2
(0402+608)	NGC 1501	14.39	134,000	6.0	1154–5235	gw1
(0722+296)	NGC 2371	14.85	135,000	6.3	923–1825	gw1
(0920–581)	NGC 2867	16.6( <i>B</i> )	141,000	6.0	769	gw1
1003–441	Longmore 4	16.6	120,000	5.5	831–2325	gw3
1159–034	PG 1159–035	14.87	140,000	7.0	339–982	gw4
(1201+296)	Sanduleak 3	15.98	140,000	6.0	929–2183	gw5
(1330–657)	NGC 5189	14.1( <i>B</i> )	135,000	6.0	690	gw1
1428–125	HE 1429–1209	15.98	160,000	6.0	919	gw6
1707+427	PG 1707+427	16.7	85,000	7.5	336–942	gw7
1751+106	Abell 43	14.75	110,000	5.7	2380–6075	gw8
(1821+643)	K1–16	15.04	140,000	6.4	1500–1700	gw9
(2020+199)	NGC 6905	15.7	141,000	6.0	710–912	gw1
2131+066	PG 2131+066	16.6	95,000	7.5	339–508	gw10
2134+125	NGC 7094	13.68	110,000	5.7	2000–5000	gw11
2215+339	RXJ2117.1+3412	13.16	170,000	6.0	694–1530	gw12
2324+397	HS 2324+3944	14.6( <i>B</i> )	130,000	6.2	2005–2569	gw13

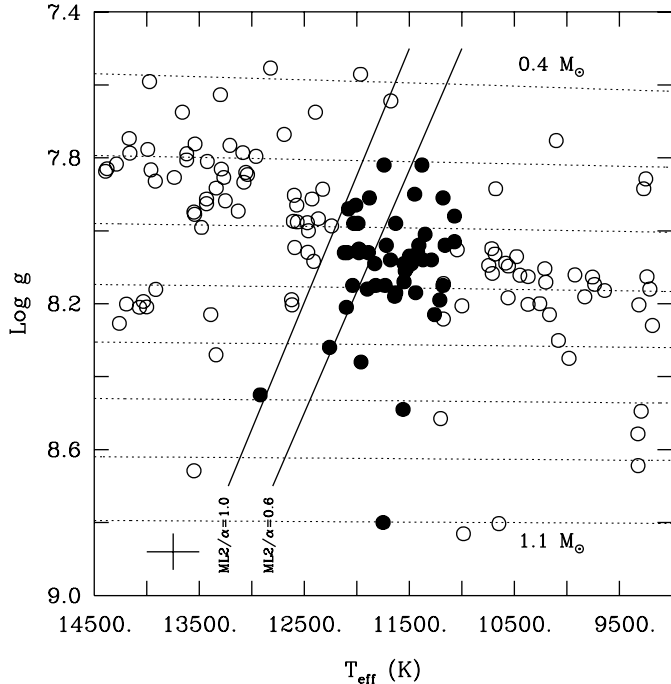


FIG. 9.—Instability domain in the  $\log g - T_{\text{eff}}$  diagram for the ZZ Ceti stars. The positions of the pulsators are indicated by the filled circles, while those of the nonvariable stars are given by the open circles. The error cross in the lower left part of the figure gives the typical uncertainties on the atmospheric parameters. The dotted curves illustrate evolutionary tracks for H-atmosphere white dwarfs of different masses, from  $0.4 M_{\odot}$  above to  $1.1 M_{\odot}$  below in steps of  $0.1 M_{\odot}$ . The thin solid curve on the left (right) gives the location of the theoretical blue edge assuming a convective efficiency given by the so-called ML  $2/\alpha = 1.0$  (ML  $2/\alpha = 0.6$ ) version of the mixing-length theory used in the construction of the equilibrium models employed in the nonadiabatic calculations.

the interested reader should read § 3 of Gianninas et al. (2005). The bottom line is that the rough atmospheric parameters derived from the SDSS stars are not suitable for a serious discussion of the instability strip.

The data plotted in Figure 9 indicate not only that the empirical strip is pure, but also that there is a surface gravity-effective temperature correlation in the sense that the blue edge of the strip occurs at lower effective temperatures for lower surface gravity stars. This trend was already observed in the initial sample of 22 ZZ Ceti stars investigated by Bergeron et al. (1995). The same is also true of the empirical red edge, and there is even an indication that the slope of the red edge is more pronounced than that of the blue edge (see Fig. 2 of Gianninas et al. 2007). While there is an obvious need to build up statistics to better pin down the locations of the empirical boundaries of the strip (and this is exactly what we are pursuing in our ongoing spectroscopic and photometric programs in Montréal), it has been known for some time that these are the trends expected from theory, at least for the blue edge.

The most recent detailed investigations of the theoretical blue edge for ZZ Ceti stars is the study of Brassard & Fontaine

(1999). We have reproduced some of their results in Figure 9. These calculations were obtained through full nonadiabatic calculations of complete stellar models under the assumption that the outer convection zone (due to H recombination) reacts instantaneously to the perturbations caused by the oscillatory motions in the star. This is appropriate because, as first pointed out by Brickhill (1983), the convective turnover timescale is about 2 to 3 orders of magnitude smaller than the measured pulsation periods of ZZ Ceti stars near the blue edge. This is exactly the opposite of the frozen convection hypothesis used in all of the early nonadiabatic investigations of pulsating DA and DB white dwarfs. As indicated in Figure 9, the results do depend on the assumed version of the mixing-length theory used in the construction of the equilibrium stellar models. These should not be confused with the model atmospheres and the synthetic spectra computed by Bergeron et al. (1995) whereby a calibration of the mixing-length theory, the ML  $2/\alpha = 0.6$  parametrization, was achieved as mentioned above. That calibration, we recall, only applies in the atmospheric layers, in regions where the observable flux comes from.

In comparison, the theoretical blue edge is most sensitive to the physical conditions found at the *base* of the convection zone (see the next section), well below the atmospheric layers. In fact, the location of the theoretical blue edge is a measure of the depth of the base of the convection zone, and the edge can be pushed to higher effective temperatures by increasing the assumed convective efficiency (which produces a more extensive convection zone). Of course, this game of shifting the theoretical blue edge to higher temperatures by increasing the convective efficiency has its limits when the latter reaches the adiabatic regime (see, in particular, Fig. 9 of Tassoul et al. 1990 for an enlightening view of this).

As found originally by Bergeron et al. (1995), and as can be appreciated in Figure 9, it appears that a higher efficiency (the ML  $2/\alpha = 1.0$  flavor) than the one used in the atmospheric analyses (the ML  $2/\alpha = 0.6$  version) has to be invoked to account for the empirical blue edge. (In fact, this more efficient version provides a rather good match to the current empirical blue edge.) This implies that convection in the atmospheric layers of a ZZ Ceti star is less efficient than in the deeper envelope. Quite interestingly, this is essentially what was found by Ludwig et al. (1994) in their numerical simulations of convective energy transport at the surface of a ZZ Ceti model. They found that the temperature profile of their test model resulting from their 2D hydrodynamic calculations could not be reproduced with a single value of the  $\alpha$  parameter (the ratio of the mixing length to the local pressure scale height). Instead, they determined that their temperature distribution was best represented by mixing-length models with  $\alpha$  increasing toward the interior. This interesting finding deserves further investigations in the future. In particular, model atmospheres with a depth-variable  $\alpha$  should be attempted in order to verify if an

internal consistency between the atmospheric studies and the nonadiabatic calculations can be reached.

In concluding this subsection, we note that Brassard & Fontaine (1999) did not find a credible red edge in their calculations and, therefore, we did not plot any such edge in Figure 9. This concurs with the independent results of Wu & Goldreich (1999) who also found the theoretical red edge to be rather elusive. These authors provide possible explanations for this state of affairs, but we would like to point out on our own that the instantaneous convective flux adjustment approximation may no longer be valid near the red edge. A better model of the interaction convection-pulsations may be needed. This problem of the red edge remains a nice challenge to pulsation theorists and should be reinvestigated in more detail than has been done heretofore.

#### 4.2. V777 Her Stars

To a large extent, the pulsating DB white dwarfs have remained the poor relatives of the ZZ Ceti stars and comparatively few papers have been devoted to them. They are as intrinsically interesting to study as their cooler H counterparts and their asteroseismological potential is comparable, but the first one was found some 14 years after the discovery of the first ZZ Ceti pulsator and they remain much less numerous (17 known versus 136 ZZ Ceti stars). The reason for this is twofold. First, the DB stars constitute a relatively small fraction of the total white dwarf population compared to the DA white dwarfs. Second, because of the cooling properties of these stars (their cooling slows down with decreasing luminosity, at least in the range of interest here), the number of DB white dwarfs per unit volume that may pulsate with  $T_{\text{eff}} \sim 25,000$  K is significantly smaller than the number of DA white dwarfs per unit volume with  $T_{\text{eff}} \sim 12,000$  K. Hence, it should not be surprising that the number of known V777 Her stars will remain lower than the number of ZZ Ceti stars. Furthermore, it should not be surprising either to realize from Table 2 that only one known pulsating DB star, GD 358, is relatively bright at  $V = 13.65$ . The others have remained difficult to study with small telescopes, even in integrated light.

This being said, much of what we wrote in the previous subsection on ZZ Ceti pulsators can be directly applied to V777 Her stars because their underlying physics is expected to be very similar. In particular, the location and extent of the instability strip for V777 Her stars is also governed by the behavior of the superficial convection zone that develops with cooling, the main difference being that it is now due to the recombination of He instead of H. However, one added difficulty in the mapping of the empirical instability strip for these stars is that, as mentioned above, the inferred parameters coming out of quantitative spectroscopic analyses are sensitive to the possible presence of small traces of H that generally remain spectroscopically invisible in the optical domain. This is because H is much more opaque than He under the physical conditions en-

countered in V777 Her atmospheres. Hence, in the absence of UV observations or very high S/N optical observations that could reveal the presence of these traces of hydrogen, the determination of their atmospheric parameters suffers from this additional uncertainty.

Figure 10 summarizes the situation. We plotted the positions of the 8 V777 Her stars listed in Table 2 and of 9 nonvariable stars. Following the work of Beauchamp et al. (1999), we indicated two possible atmospheric solutions for those stars for which we have no knowledge of the possible presence of small traces of H. The solution on the left is an extreme, and corresponds to the pure He case (this is the case retained in Table 2 for the pulsators). The solution on the right is also an extreme and corresponds to the maximum possible amount of H that would lie just below detection level. The exact amount varies from one star to another (see Beauchamp et al. 1999) and is found in the range of number abundance ratio  $N(\text{H})/N(\text{He})$  from  $10^{-5}$  to  $10^{-3}$ . Presumably the true solution in each case is

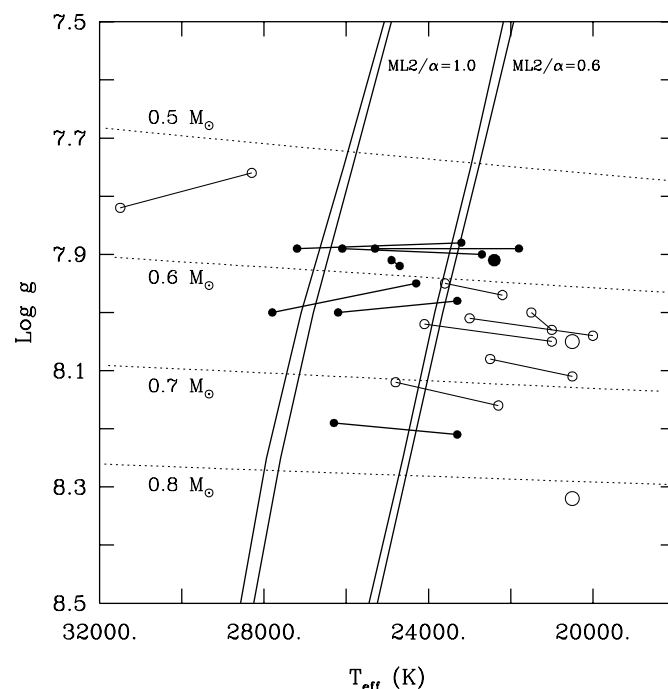


FIG. 10.—Instability domain for the V777 Her stars. The positions of the pulsators are indicated by small filled circles while those of the nonvariable stars by small open circles. Two solutions are given for those objects with unknown H contents: the left position corresponds to zero H, and the right position to the maximum possible amount just below the detection limit. The true values of the atmospheric parameters are presumably within these two limits. Those 3 objects with *known* H/He atmospheric abundances are indicated by larger symbols. The solid curves represent theoretical blue edges, sensitive to the assumed efficiency of convection and also, but to a lesser degree, to small traces of H in the envelope. The curve on the left in a given double convection structure gives the theoretical blue edge when there is no H, the one on the right gives the equivalent when there is a representative trace of invisible H. The dotted curves illustrate evolutionary tracks for He-atmosphere white dwarfs of different masses.

sandwiched between these two extremes. Note that there are three stars in Figure 10 (one pulsator and two nonvariables) for which the  $N(\text{H})/N(\text{He})$  ratio has been measured, in which case there is a unique solution (given by the larger symbols).

Our current view of the empirical V777 Her instability strip is clearly limited by small-number statistics. More importantly, this view is unfortunately clouded by the uncertainties on the time-averaged atmospheric parameters produced by the potential presence of spectroscopically invisible (in the optical domain) traces of hydrogen. This situation could be improved in the future if someone were to go beyond the investigations of Beauchamp et al. (1999) and concentrate on the determination of the atmospheric H abundance in as many pulsating and nonvariable DB stars as possible. This could be achieved through very high S/N ratio optical spectroscopy or, more readily, with the *Hubble Space Telescope (HST)* if the instrument Space Telescope Imaging Spectrograph (STIS) were to be repaired. We note that the empirical boundaries of the V777 Her strip will always retain a significant degree of intrinsic “fuzziness” because the H content in the atmosphere of a DB white dwarf seems to vary from one object to another by some 2 to 3 orders of magnitude and more, as inferred from the detailed atmospheric analyses of the three stars illustrated in Figure 10 and many other targets. This is in contrast to the empirical ZZ Ceti instability strip, which should show relatively sharp boundaries in the  $\log g - T_{\text{eff}}$  diagram. Making allowance for this fuzziness at the boundaries, the data shown in Figure 10 are consistent with the idea of a pure strip, but a whole lot of work on the observational side (including new discoveries) will be needed to establish that on a firm basis.

To provide a measure of comparison with theory, we added in Figure 10 theoretical blue edges (*solid curves*) computed for two different parametrizations of the mixing-length theory. In each case, we also illustrated the effects of including small traces of H in the envelopes of our equilibrium stellar models. Hence, for each flavor of the assumed convective efficiency, the double curves correspond, respectively, to the case of pure He (*on the left*), and to the case of a trace  $N(\text{H})/N(\text{He}) = 10^{-4}$  (*on the right*). The effects of adding H in the envelopes of DB models are thus to push the blue edge to lower effective temperatures, but the change remains relatively small in magnitude. Note that, contrary to the theoretical blue edges computed for ZZ Ceti stars and shown in Figure 9, the present calculations are cruder because they are based on the assumption of the frozen convection approximation. These computations are quite sufficient for our present purposes, however. In addition, our theoretical red edges are not realistic (they are too cool) and have not been retained in the figure. It is clear that the underlying physics responsible for the existence and actual location of the red edge is very similar to that operating in ZZ Ceti stars. Once we have a physically convincing explanation for the red edge of the ZZ Ceti strip or that of the V777 Her strip, whichever comes

first, it should be a simple matter to directly transpose the results to the other type of pulsator.

### 4.3. GW Vir Stars

As already obvious from Figure 1, the pulsating white dwarfs of the GW Vir type occupy a much wider domain in the  $\log g - T_{\text{eff}}$  plane than V777 Her or ZZ Ceti stars do. A closer look at that domain is provided by Figure 11, which gives a current view of the instability region. The positions of the 18 known GW Vir pulsators listed in Table 3 have been plotted along with those of 20 other stars monitored for luminosity variations but found not to vary. The objects that are known central stars of planetary nebulae (CSPN) are identified in the figure. Some of these CSPN pulsate, others do not, showing that the presence or absence of a nebula is immaterial to the excitation mechanism.

Perhaps the most striking characteristic of the GW Vir instability domain is that it features a mixed population of variable and nonvariable stars with similar values of  $\log g$  and  $T_{\text{eff}}$ , in stark contrast with the pure ZZ Ceti instability strip, for example. Until recently, the existence of this mixed population was considered as a real challenge to nonadiabatic pulsation theory. This long-standing puzzle was solved only a few years ago

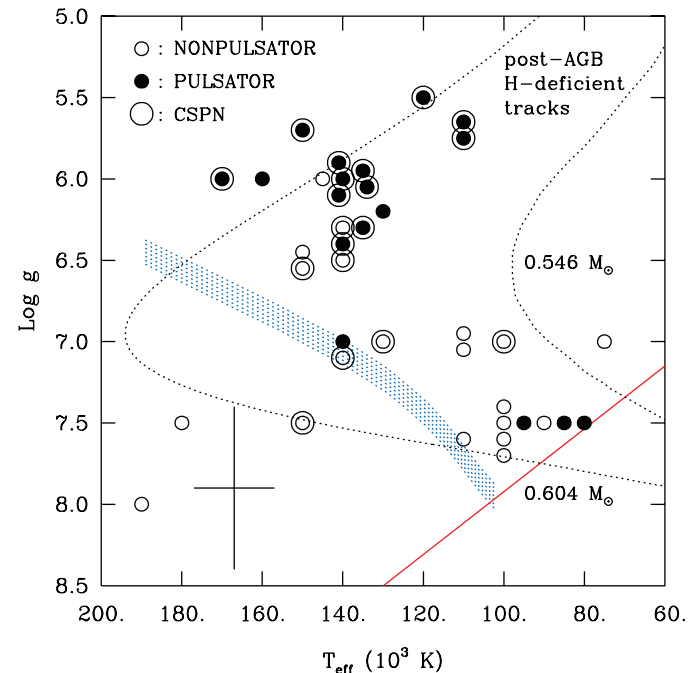


FIG. 11.—Instability domain for the GW Vir stars. The known pulsators are indicated by small filled circles, and the nonvariable stars by small open circles. The CSPN among those objects are identified by the larger open circles. The cross illustrates typical uncertainties on the atmospheric parameters. The dotted curves are the evolutionary tracks of two representative post-AGB, H-deficient models that differ in their total mass. The theoretical blue edge is drawn fuzzy to signal its dependence on the atmospheric chemical composition. The theoretical red edge obtained from a specific wind mass loss law is also indicated.

through the calculations of Quirion et al. (2004), who demonstrated that it could naturally be understood in terms of a spread in chemical composition from one star to another, a composition dominated by He, C, and O in various proportions. In particular, only the stars with the most carbon and oxygen (depending on their values of  $\log g$  and  $T_{\text{eff}}$ ) can pulsate. This breakthrough was made possible thanks to the work of the Werner group—and also to important progress on the front of opacity calculations—which has been providing reliable atmospheric parameters for these objects over the years. This allowed Quirion et al. (2004) to compute, on a star-to-star basis, the stability of individual specialized models.

Because the composition of the atmosphere/envelope of a PG 1159 or [WCE] star does vary from object to object, this implies that the pulsational blue edge cannot be sharply defined in the  $\log g - T_{\text{eff}}$  plane but must be the superposition of several blue edges, one each for each possible chemical composition (and see Quirion et al. 2007a for more details). It is thus in this spirit that we have drawn a fuzzy blue edge in Figure 11. This fuzzy blue edge is appropriate for dipole ( $l = 1$ ) modes and is derived from detailed nonadiabatic calculations.

For its part, the high-gravity empirical red edge is currently defined by PG 0122+200 with an effective temperature of 80,000 K. While the red edges of the ZZ Ceti and V777 Her strips are most likely to depend on convection-pulsation interactions, convection is a nonfactor in the driving of  $g$ -modes in GW Vir objects as the envelopes of these very hot stars are essentially radiative throughout. As discussed in § 5, the excitation mechanism at work in GW Vir pulsators is a standard  $\kappa$ -mechanism occurring in a mixture of He, C, and O. Interestingly enough, though, if one keeps a typical GW Vir envelope composition, one can find unstable models much cooler than the current empirical red edge, indicating that there is something else at work.

That something else is directly related to the very nature of GW Vir stars. Indeed, it is currently thought that H-deficient, post-AGB stars are born with a large variety of He/C/O mixtures in their envelopes, depending on complicated details of their individual formation (see, e.g., Herwig et al. 1999 or Córscico & Althaus 2006). It is also known that a wind threads the envelope of such a star, thus ensuring the homogeneity of its chemical composition. There is, in fact, overwhelming evidence in favor of important residual mass loss in H-deficient, post-AGB stars as discussed in Koesterke & Werner (1998) and Koesterke et al. (1998), and summarized by Werner (2001). Such a wind plays a key role by slowing down the separation of He, C, and O in a PG 1159 star and thus preventing the quick settling of the latter two key elements below the driving region in a pulsating star. Otherwise, in its absence, diffusion would be able to very quickly turn the envelope of a GW Vir star into a He-dominated region, with no possibility for pulsational driving. In fact, the PG 1159 spectral type simply would not exist without the slowing effect of a wind. Ultimately, it is the competition between

the wind and gravitational settling of C and O that produces the high-gravity red edge of the GW Vir instability strip and turns a PG 1159 star into a DO white dwarf at that boundary.

Evolutionary calculations of PG 1159 star models taking into account diffusion and mass loss were recently performed by Quirion et al. (2007b) in order to simulate this scenario. The red edge plotted in Figure 11 comes from some of their sequences. In that case, the mass loss rate (assumed proportional to some power of the luminosity and calibrated on the observed winds reported by Koesterke and Werner) was adjusted so that the theoretical red edge would just match the empirical red edge.<sup>4</sup> Related results, but based on a different mass loss law, are also shown in Figure 12, where the red dots give the predicted spectrum of excited dipole modes in the post-PG 1159 phase of the evolution of a  $0.6 M_{\odot}$  model with a fixed envelope composition defined by  $X(\text{He}) = 0.38$ ,  $X(\text{C}) = 0.40$ ,  $X(\text{O}) = 0.20$ , and  $Z = 0.02$ , a typical PG 1159 atmospheric composition. Such cool He/C/O-atmosphere white dwarfs do not exist, but if they did, they would show pulsational instabilities all the way from the PG 1159 phase down to almost 30,000 K in effective temperature. In comparison, the more physical model in which diffusion and mass loss were turned on—otherwise similar to the first one in terms of its parameters—leads to the period spectrum given by the black dots. There is a natural red edge around 75,000 K due to the settling of C and O below the driving region and, with time, the buildup of an essentially pure He envelope. When this almost pure He envelope model reaches V777 Her conditions; i.e., when He starts to recombine in the outer layers in the cooler phases of the evolution,  $g$ -modes again become excited and we can neatly observe another phase of instability in the figure. This is a nice illustration of our comment in § 2 to the effect that a GW Vir star is likely to pulsate again later in its evolution, this time as a DB white dwarf.

We conclude this subsection by briefly going back to Figure 11 to point out that the distribution of observational points plotted there is quite consistent with the locations of both our theoretical blue and red edges. In particular, no pulsating stars should be observed in the lower left corner of the diagram, and although this is small-number statistics, at least the four objects in that region do not pulsate, as expected. We also draw attention to the two evolutionary tracks that we added in the figure. The stellar model with a mass of  $0.546 M_{\odot}$  stays inside the instability domain during its excursion “around the bend” in its evolution and, therefore, shows a single phase of instability as a GW Vir pulsator. In comparison, the  $0.604 M_{\odot}$  model wanders outside the instability domain during its evolution

<sup>4</sup>We point out that the low-gravity red edge, where the stars enter the diagram in Fig. 11 at low effective temperatures and low gravities, has been investigated theoretically by Córscico et al. (2006) among many other things. As for the blue edge, it is composition dependent.

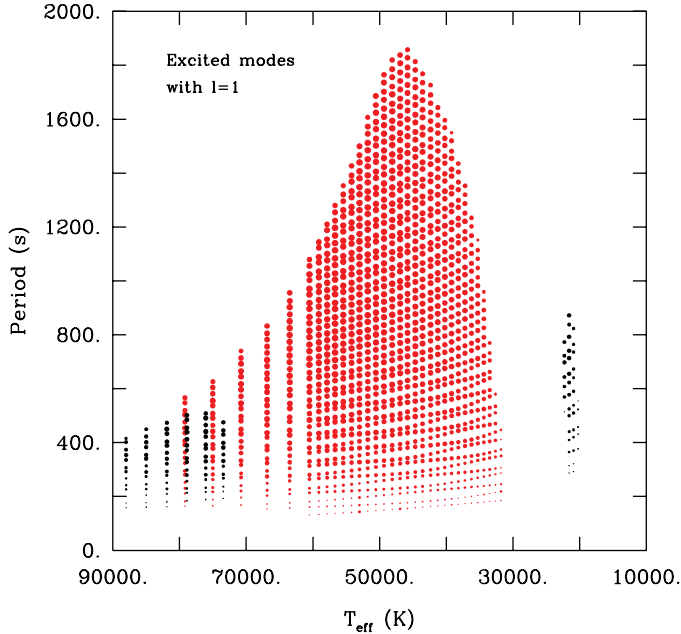


FIG. 12.—Period spectra of excited dipole modes in two post-PG 1159 evolutionary models. The red dots refer to a model with a fixed envelope chemical composition specified by  $X(\text{He}) = 0.38$ ,  $X(\text{C}) = 0.40$ ,  $X(\text{O}) = 0.20$ , and  $Z = 0.02$ . The black dots refer to a similar  $0.6 M_{\odot}$  model defined by the same initial conditions but for which diffusion and mass loss have been turned on in the calculations. In the latter sequence, a GW Vir red edge is naturally found around  $T_{\text{eff}} = 75,000$  K, and a V777 Her instability phase is also recovered near the end of the evolution. Each dot gives the period of a mode, and its size represents a logarithmic measure of the modulus of the imaginary part  $\sigma_I$  of the complex eigenfrequency. The bigger the dot, the more unstable the mode.

and it thus features two distinct instability phases as a GW Vir pulsator during its lifetime.

## 5. EXCITATION PHYSICS

The ultimate cause of the pulsational instabilities observed in the three distinct categories of pulsating white dwarfs is the same: *partial ionization of the main envelope constituents*. Indeed, the K-shell electrons of carbon and oxygen ionize and then recombine during the excursion “around the bend” in the GW Vir phase of the evolution of a H-deficient, post-AGB star, helium recombines in the strictly cooling phase of a He-atmosphere white dwarf corresponding to the V777 Her regime, and so does hydrogen in the even cooler phase of a H-atmosphere star corresponding to the ZZ Ceti regime. In each case, partial ionization leads to a very important increase of the envelope opacity, and this tends to choke the outgoing energy flux. In the case of V777 Her models, and even more so in ZZ Ceti models, the opacity bump becomes so large that a superficial convection zone develops as a result of the buildup of a superadiabatic temperature gradient, and this significantly affects the mechanics of the actual process responsible for the

excitation of pulsation modes. Convective energy transport must then be taken into account in addition to the usual radiative channel.

Figure 13 illustrates the details of the driving/damping region in a representative model of a GW Vir pulsator. In this diagram, the abscissa corresponds to the logarithm of the fractional mass above the depth of interest, the same as used in our Figures 6, 7, and 8 above. On this scale, the center of the star would be at a  $\log q$  value of 0.0. However, because all of the “action” in terms of driving/damping is going on only in the outer envelope of the model, we have chosen to emphasize only that part of the star in our plot.<sup>5</sup> The first vertical dotted red line when moving into the star from the right gives the location of the photosphere (corresponding to optical depth  $\tau_R = 2/3$ ), and the second dotted red line indicates the position of the base of the atmosphere ( $\tau_R = 100$ ). The dotted curve shows the profile of the Rosseland opacity—to be read on the right-hand ordinate axis—as a function of depth. One can notice two maxima in the opacity profile: the larger one nearer to the surface is the usual “Z-bump,” while the deeper one corresponds to the partial ionization of the K-shell electrons in carbon and oxygen. Note that the *envelope* chemical composition of this model is uniform and made of a mixture of He, C, and O in proportions typical of those observed in the atmospheres of real PG 1159 pulsators ( $X(\text{He}) = 0.38$ ,  $X(\text{C}) = 0.40$ ,  $X(\text{O}) = 0.20$ ,  $Z = 0.02$ ).

Of the many  $g$ -modes found excited in this model, we have singled out a representative one with indices  $k = 7$  and  $l = 1$ . It has a period of 296.6 s. For this particular mode, the solid curve shows the arbitrarily normalized integrand  $dW/d \log q$  of the so-called work integral. A negative value of this quantity at a given depth means that the mode is locally damped. Conversely, a positive value implies that the mode is locally driven. The dashed curve is related and illustrates the running work integral  $W$ , from left to right, i.e., from the center toward the surface of the model. This quantity is also arbitrarily normalized. A final positive value of the work integral at the surface—as is the case illustrated here—means that the mode is globally excited and is potentially observable. Conversely, a negative value of the work integral at the surface would imply that the mode is globally damped and should not be seen.

The plot clearly shows that maximum driving corresponds to the opacity bump associated with the partial ionization of the K-shell electrons in C and O. Of prime interest, the work integral curves bear the telltale signature of a classic  $\kappa$ -mechanism. The first correct identification of this process in GW Vir star models was made by the Los Alamos group in the early

<sup>5</sup> Most pulsation theorists working on normal or giant stars prefer to use a temperature axis as the abscissa in such a diagram because they can readily recognize “canonical” ionization temperatures associated with specific elements. This is not a good idea for white dwarf models because the ionization temperatures are completely skewed in the highly nonideal, dense plasma environments found in their interiors.

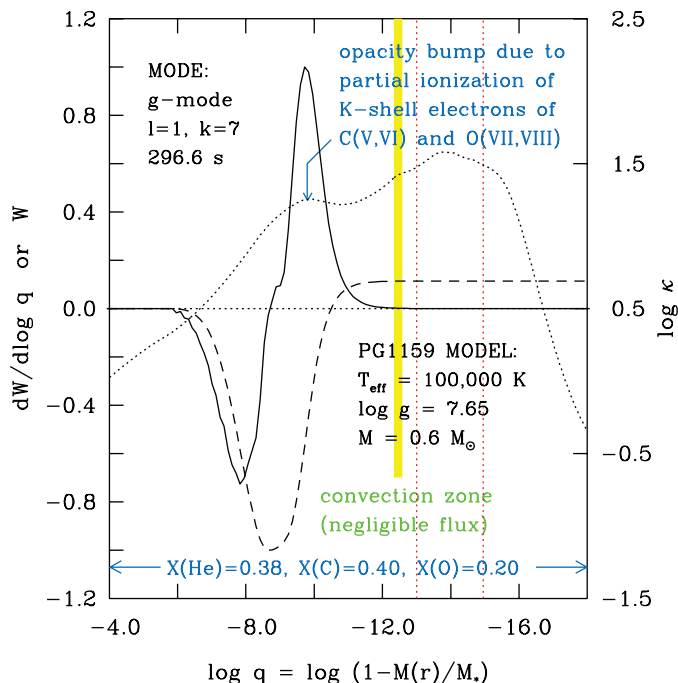


FIG. 13.—Details of the driving/damping process for a typical  $g$ -mode excited in a representative model of a GW Vir star. The solid curve shows the integrand of the work integral of the mode as a function of fractional mass depth. The dashed curve shows the running work integral, from left to right, toward the surface of the model. The dotted curve gives the profile of the Rosseland opacity, to be read on the right-hand ordinate axis. The vertical dotted red line on the left (right) gives the location of the base of the atmosphere at optical depth  $\tau_R = 100$  (of the photosphere at  $\tau_R = 2/3$ ). The narrow yellow stripe indicates the location of a thin inefficient subphotospheric convection zone.

1980s (Starrfield et al. 1983, 1984, 1985), but difficulties persisted. It took the important work of Saio (1996) and Gautschy (1997), both based on modern opacity calculations, to get a clearer picture of the basic excitation physics in these stars (and see Quirion et al. 2004 for the detailed story). Note that there is no contribution to the driving/damping process coming from the region associated with the higher maximum in the opacity profile in Figure 13, simply because it is located in the atmospheric layers where there is practically no inertia.

Another point of interest is that the narrow yellow stripe gives the location and extent of a thin subphotospheric convection zone in this particular model of a GW Vir star. Note that this convection zone is quite inefficient and carries essentially no flux, less than 0.001% at maximum. Note further that it does not overlap with the region of significant driving/damping, and so it practically does not affect the pulsation properties of the model. This can be generalized to other GW Vir models, and it can be deduced that convection/pulsation interactions are negligible in this type of pulsating white dwarfs.

The story is different for the pulsating DB white dwarfs as illustrated in Figure 14. This figure has the same format as the previous one, except for the addition of the profile of the ratio of

the convective to the total flux,  $F_c/F_t$  (dotted green curve). This now refers to a representative V777 Her model, and we again picked the  $g$ -mode with  $k = 7$  and  $l = 1$ , which is again excited in this model.

Here, the envelope is constituted of pure He, and one can observe a large opacity peak caused by the partial ionization of He I near the photosphere and, more importantly, that of He II in the deeper layers where the opacity reaches a maximum around  $\log q \sim -12.7$ . The two partial ionization zones of helium are practically fused together in this 25,000 K DB white dwarf model because of pressure effects. This leads to the formation of a significant convection zone extending from above the photosphere well into the driving/damping region below. Quite importantly, this convection zone carries up to 98% of the total flux at maximum efficiency.

One can notice from the figure that maximum driving does not occur at the depth where the opacity reaches its maximum value, but somewhat below. In addition, driving ( $dW/d\log q > 0$ ) is concentrated in a broad region near the base of the convection zone, a region in which the fraction of the flux carried by convection varies from zero at the base to its maximum value near the top of that region. Contrary to GW Vir pulsators then, convection has a significant role to play in the pulsation of DB white dwarfs. Its presence in the driving region implies that it is not the classic  $\kappa$ -mechanism that is at work in these stars because that mechanism only op-

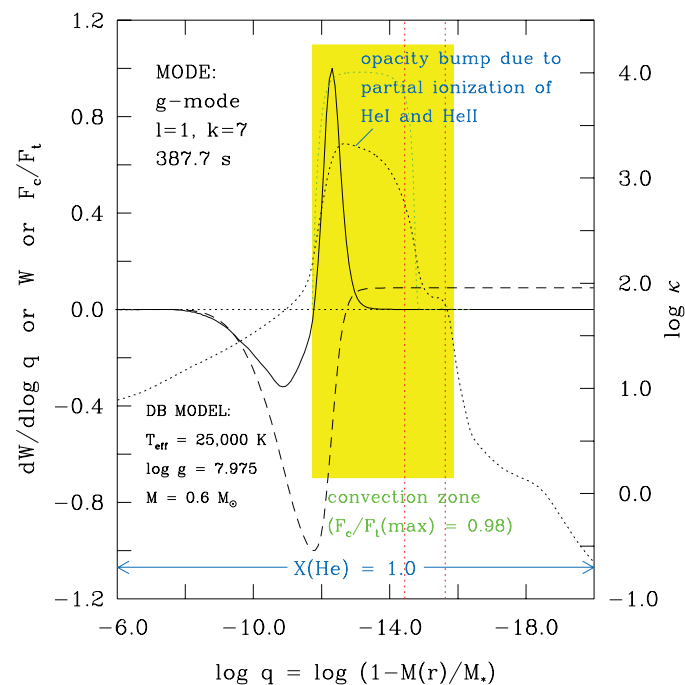


FIG. 14.—Similar to Fig. 13, but for a representative model of a V777 Her star. The superficial convection zone is here much more extensive, and there is the added dotted green curve that shows the profile of the ratio of the convective to the total flux.

erates in a purely radiative environment.

A very similar situation is encountered in ZZ Ceti stars, but the physical conditions are even more extreme in these cooler objects than in V777 Her pulsators. This is illustrated in Figure 15, which now refers to the case of a typical model of a pulsating DA white dwarf. Taking into account the different scale used for the opacity axis as compared to the previous figure for example, one can notice the huge opacity peak in the pure H envelope of this model. This bump is due to the partial ionization of neutral hydrogen. And notice the gradual increase of the opacity maximum from Figure 13 to Figure 15.

The convection zone associated with this opacity feature extends all the way from the photosphere to the base of the driving region. It is more important than in the DB model in the sense that up to 99.9% of the total flux can be carried convectively in this zone. The driving region is again concentrated at the base of the convection zone, but in a narrower domain than in the DB case. Moreover, maximum driving is clearly more separated from maximum opacity than in the previous case. We can see, from both Figures 14 and 15, that pulsation driving in V777 Her and ZZ Ceti stars is intimately associated with the physical conditions near the base of the superficial convection zone.

This particular situation was fully appreciated in the earliest investigations of the ZZ Ceti star excitation mechanism carried out by Dolez & Vauclair (1981), Dziembowski & Koester (1981), Winget (1981), Winget et al. (1982a), and Starrfield et al. (1982), but some unfortunate choices were made in the *naming*

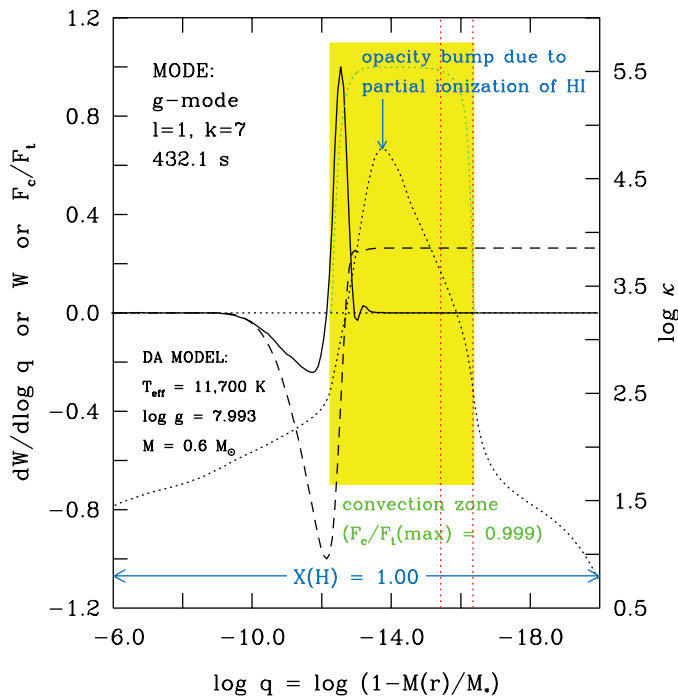


FIG. 15.—Similar to Fig. 14, but for a representative model of a ZZ Ceti star.

of the exact process at work in the numerical calculations. Terms such as “ $\kappa$ -mechanism,” “generalized  $\kappa$ -mechanism,” and “partial ionization mechanism” were used and led to unnecessary confusion. To complicate things, and for the lack of a better general recipe, all of these earlier calculations were made within the framework of the frozen convection approximation, which consists in neglecting the perturbations of the convective flux. It was shown somewhat later by Pesnell (1987) that, under this assumption, the driving found in the numerical calculations could be physically explained in terms of a process that he named “convective blocking.”

In the meantime, Brickhill (1983) realized that a better approach would be to assume that the convective flux responds instantaneously to pulsations—the exact opposite of the frozen convection approximation—because, as he pointed out, the turnover timescale in the convection zone of a ZZ Ceti star is usually much smaller than the pulsation periods of interest. He went on to develop a numerical model based on this assumption of instantaneous convective response, which allowed him to explore many interesting aspects of ZZ Ceti star physics (Brickhill 1990, 1991a, 1991b). Among others, Brickhill computed a theoretical instability strip based on this notion of instantaneous reaction. His important contributions were not immediately recognized. We owe him the basic physical explanation for pulsational excitation in ZZ Ceti (and V777 Her) stars, a process known as “convective driving.”

On the numerical front, and to our knowledge, Brassard & Fontaine (1997) were the first to implement this concept of instantaneous convection reaction into a complete nonadiabatic pulsation code in a white dwarf context. They were able to improve on the determination of the theoretical blue edge for the ZZ Ceti stars, but the red edge still was not satisfactory. Further comparisons carried out by Brassard & Fontaine (1999) between the predictions of calculations based on the two different extreme hypotheses indicate that, for the blue edge, the results of the earliest numerical calculations were not that far off. In this connection, we do not agree with Wu & Goldreich (1999), who have in our view too summarily dismissed the results of all of the numerical calculations that were carried out before they presented their semi-analytical approach. We concur with them, however, that the red edge problem is still very much a challenge.

This short discussion of the excitation physics of pulsating white dwarfs would not be complete without mentioning that low-order  $p$ -modes, including radial modes, are expected to be excited in some DB and some DA white dwarfs. We recall that the period of the fundamental ( $k = 0$ ) radial mode in a typical white dwarf is of the order of 10 s, and this drops to 1 s for the tenth overtone. Early indications that low-order  $p$ -modes could be driven in white dwarfs go back to the calculations of Saio et al. (1983). These authors found a blue edge for the putative  $p$ -mode pulsators that was slightly hotter than the blue edge for the standard  $g$ -mode pulsators in DA white

dwarf models. Hence, searches were carried out in known ZZ Ceti stars close to the blue edge or in constant DA white dwarfs also close to the blue edge but on the hot side, to no avail. Short-period  $p$ -mode pulsations have yet to be found in white dwarfs (and see the report of Silvotti et al. 2007 for the last attempt to uncover such pulsations using the Very Large Telescope [VLT]).

It is not clear at this stage if these pulsations will ever be found even if they exist. We do expect these pulsational instabilities to be present because the same mechanism that drives low-order  $g$ -modes in white dwarfs ought also to do the same for low-order  $p$ -modes. However, there could be an important visibility effect if, indeed, these modes are excited as expected from theory. We may speculate, for instance, that pulsational energy is spread among tens of closely spaced modes in frequency space, none of them having sufficient amplitude to be detected. Alternatively, it may be that the pulsational energy available is simply not sufficient to lift material to an observable amplitude in the radial direction during a  $p$ -mode pulsation cycle because of the very high surface gravity involved ( $\log g \sim 8$ , typically). In comparison, the  $g$ -modes excited in pulsating white dwarfs feature much larger horizontal motions than radial displacements. In fact, at a distance and in a very good approximation, the  $g$ -modes in white dwarfs can be seen as simple temperature waves at the surface of an otherwise spherically symmetric star that does not change its shape or volume (and see § 7). Hence, relatively little work is done to displace material against the gravitational field during the pulsation cycle of a  $g$ -mode in a white dwarf, contrary to what is needed to drive a  $p$ -mode to a sufficiently large amplitude. These considerations are only speculations, of course; the absence of  $p$ -mode pulsators among white dwarfs remains a very interesting puzzle.

## 6. PROPERTIES OF THE PULSATIONS

The most basic quantities that can be extracted from light curves of pulsating stars are the periods that can be derived from standard periodogram and Fourier technique analyses of these curves. The periods provide the essential ingredients with which to carry out a classical asteroseismological investigation in which the observed periods are best matched to the periods computed from stellar models in the hope of isolating an optimal and convincing stellar structure that approaches the real star. The light curves, however, contain a lot more information beyond the periods, and analyses of the amplitudes, phases, and nonlinearities of the various pulsation modes present in the curves can also be extremely rewarding. Among other things, constraints on the angular geometry of a given pulsation mode may be obtained from such exercises, and this can be used to test seismic models. Furthermore, the light curves may show trends with location in a given instability strip which, in turn, can be extremely valuable input for nonadiabatic asteroseismology. The latter, for example, should be able to reproduce the range of periods excited in a given pulsating star.

Pulsating white dwarfs show a very rich and wide variety of light curves, from very simple sinusoidal-shaped light pulses to extremely complicated and highly nonlinear curves that may or may not be stable with time. It is often said that a picture is worth a thousand words, and so we decided to show a few “pictures” of light curves. Given that ZZ Ceti stars are the most numerous white dwarf pulsators and have been studied, most extensively, and given that we ourselves gathered several ZZ Ceti light curves over the years, it follows that they are the logical candidates to show in this gallery. In Figure 16, we indicated the path followed in an exploration of the ZZ Ceti instability strip. Each dot represents the location of a particular ZZ Ceti star in the  $\log g - T_{\text{eff}}$  diagram, which, in turn, is also identified in the figure. The values of  $\log g$  and  $T_{\text{eff}}$  come from Table 1, except for the last three stars for which we have only provisional estimates. Note that we also plotted the empirical blue and red edges of the strip as determined by Gianninas et al. (2007). Hence, the exploration starts with an excursion along the blue edge from high to low gravities, then turns around, comes down and up again, going across the midsection of the strip, and finally ends with a look along the red edge.

Figure 17 shows the light curves of the first eight “stations” along our path, from top to bottom. The data shown here and in the other figures were obtained by us using our photometer

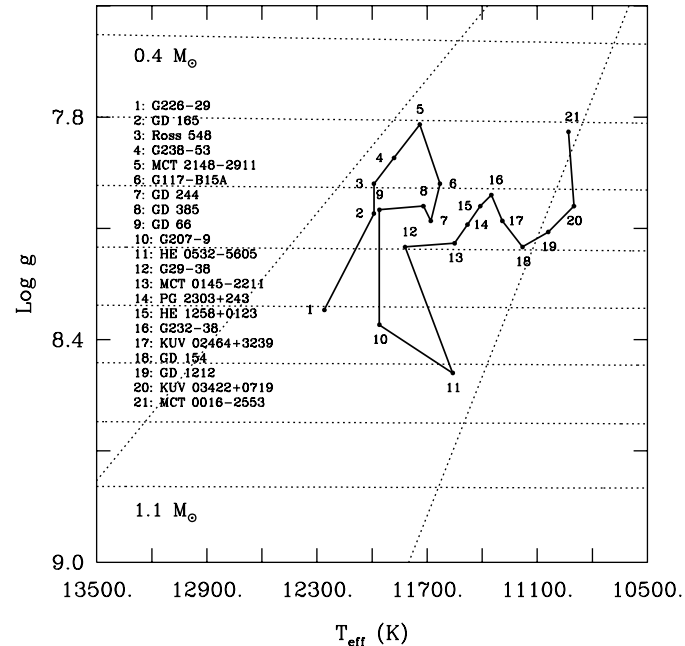


FIG. 16.—Path followed in our exploration of the ZZ Ceti instability strip in the  $\log g - T_{\text{eff}}$  plane. Each stop identifies a star for which we show a light curve and a Fourier transform of that light curve in the following figures. The nearly horizontal dotted curves illustrate evolutionary tracks for H-atmosphere white dwarfs of different masses, from  $0.4 M_{\odot}$  above to  $1.1 M_{\odot}$  below in steps of  $0.1 M_{\odot}$ . The two diagonal dotted lines are the empirical blue and red boundaries of the instability domain as obtained by Gianninas et al. (2007).

LAPOUNE. In most cases, we used the 3.6-m Canada-France-Hawaii Telescope (CFHT) telescope, but in a few instances the observations were gathered at the Steward Observatory 2.3-m telescope. These are therefore homogeneous integrated white light observations. There are two exceptions, however: HE 0532–5605 (star no. 11) and HE 1258+0123 (star no. 15) were observed by Malvina Billères using the SUSI2 CCD detector attached to the 3.6-m New Technology Telescope (NTT) in La Silla. No filter was put in the beam.

The light curve shown at the top of Figure 17, that of G226–29, is the simplest of all of the known pulsating white dwarfs. It is essentially sinusoidal in appearance and is characterized by a very low peak-to-peak amplitude. The other curves are distinctly multiperiodic, and show beating between various harmonic oscillations present in them. The amplitudes tend to remain low along the blue edge, but there is a tendency for the lower-gravity objects to show larger amplitudes and longer quasi-periods. When moving toward the middle of the strip, one cannot help but notice an obvious increase in the peak-to-peak amplitudes. Nonlinearities also start to creep in and, upon reaching star number 12 (G29–38) in Figure 18, the light curve is highly distorted in shape. We note the puzzling case of star number 2 (GD 165) and star number 9 (GD 66) which, despite their nearly identical values of  $\log g$  and  $T_{\text{eff}}$  according to Table 1, show rather different light curves in their amplitudes and dominant periods. We come back to this case below. The light curves reach their largest peak-to-peak amplitudes in the cooler mid-section of the strip as shown in Figures 18 and 19 (star nos. 12 through 17). The largest pulses observed tend to show a faster

rise followed by a slower decline, a characteristic noted long ago, by McGraw (1977) in particular. Then, in Figure 20, we find an interesting trend as the light curves of the stars at the red edge tend to become simpler again and are dominated by a single period, while the amplitude goes down. It is as if the pulsations are literally “dying” in front of our eyes. This behavior certainly has strong ties to the physics of the red edge. All along our path, the figures clearly show that the quasi-periods increase with decreasing effective temperature.

Figures 21, 22, and 23 show a montage of the Fourier transforms of the 21 light curves shown previously. It is most unfortunate that the temporal resolution is not uniform here. In many instances, the light curves are only short discovery runs gathered outside main observing programs. They certainly are sufficient to establish the variability (see, e.g., the very short light curve for KUV 02464+3239 at the bottom of Fig. 19), but the associated Fourier transforms are badly underresolved in those cases. Despite this limitation, the mosaic of Fourier transform presented in Figures 21 through 23 clearly shows the migration toward the longer periods when moving from the blue to the red edge. It also shows the increasing complexity of the light curves which tend to contain more and more harmonic oscillations down into the cooler half of the ZZ Ceti instability strip. Nonlinear peaks due to harmonic and cross-frequencies also appear (GD 154 is an obvious example of this). Finally, near the red edge, things apparently become simpler again.

It is possible to illustrate more quantitatively how the spectrum of observed periods in ZZ Ceti stars behaves as a function of location in the instability strip. To do that, we used the data of

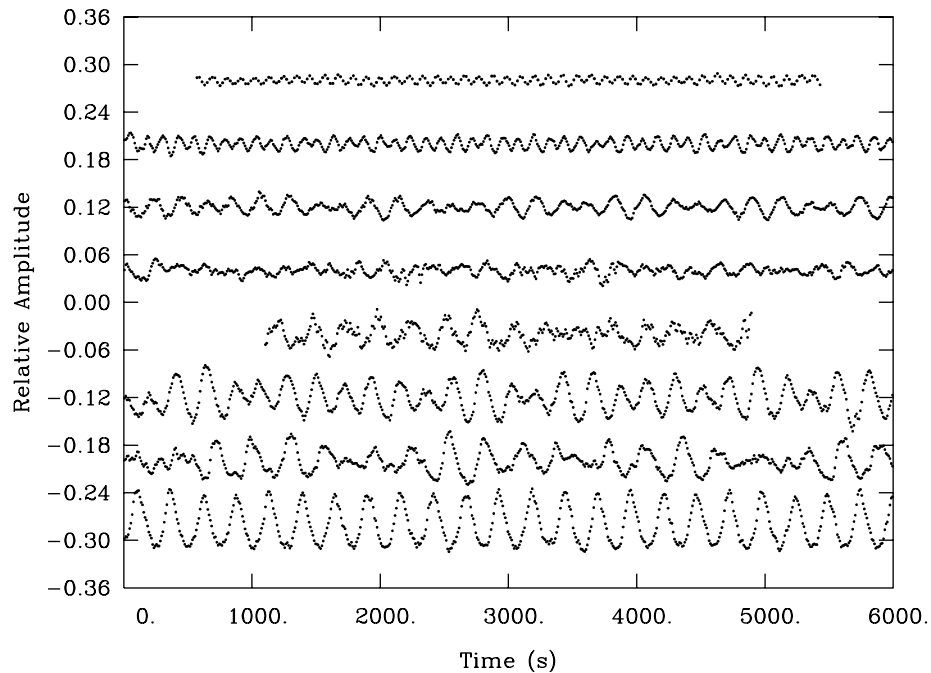


FIG. 17.—Segments of the optical light curves of the ZZ Ceti stars identified in Fig. 16. From top to bottom: star no. 1 (G226–29) to star no. 8 (GD 385).

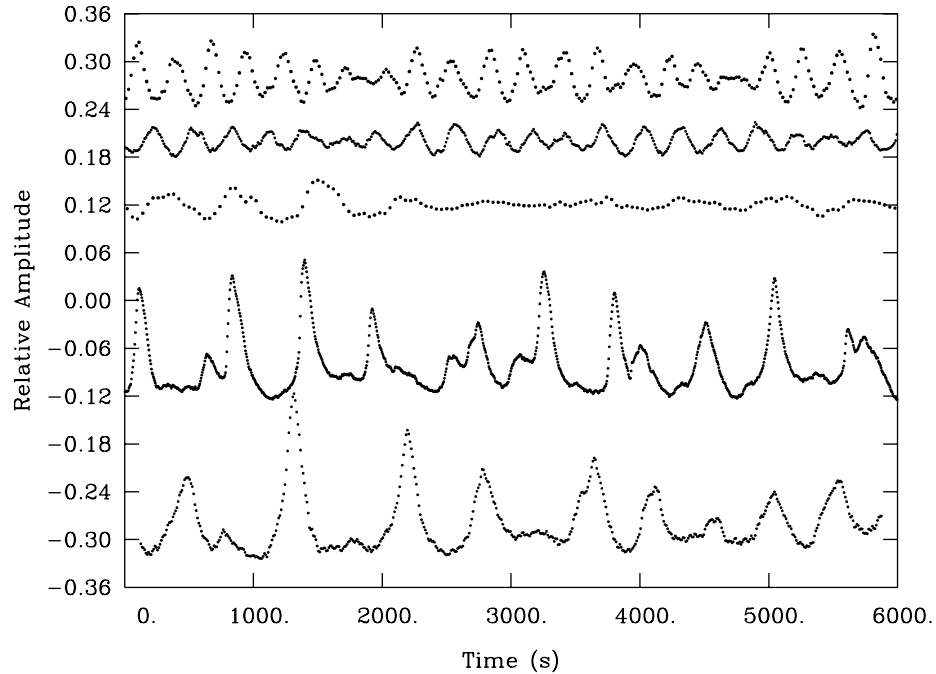


FIG. 18.—Segments of the optical light curves of the ZZ Ceti stars identified in Fig. 16. From top to bottom: star no. 9 (GD 66) to star no. 13 (MCT 0145–2211).

Table 1 to construct Figure 24, which again shows the locations of the known pulsators in the  $\log g - T_{\text{eff}}$  diagram, but, this time, an open circle is used as a measure of “the” typical period for each object. To derive that typical period, we simply took the

middle value of the range of periods given in Table 1 for those stars for which multiple modes have been reported, or the single tabulated value for those stars not yet well observed. Of course, other more involved recipes could have been employed, such as

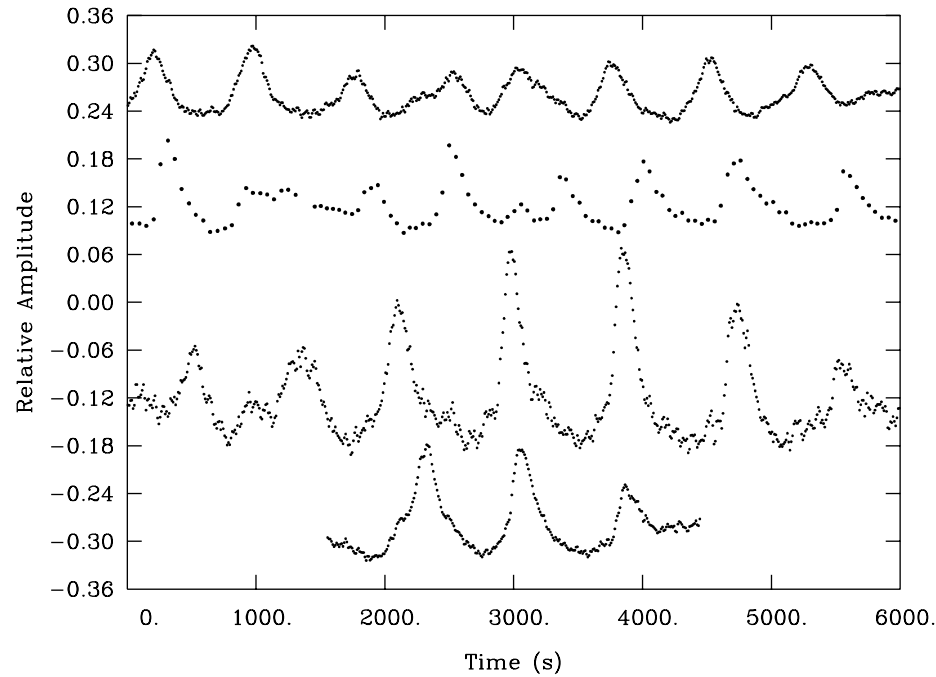


FIG. 19.—Segments of the optical light curves of the ZZ Ceti stars identified in Fig. 16. From top to bottom: star no. 14 (PG 2303+243) to star no. 17 (KUV 02464 +3239).

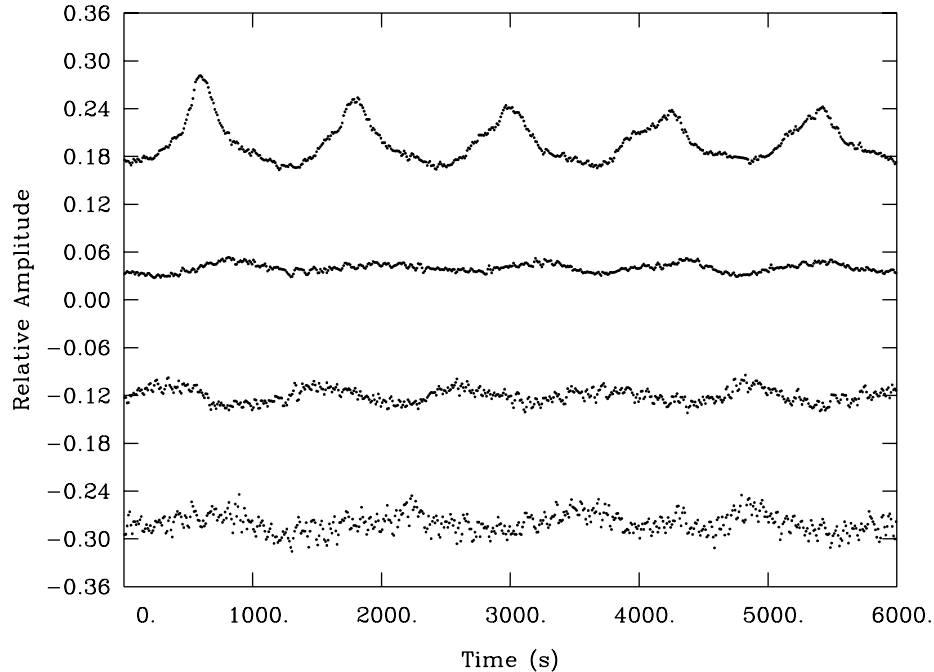


FIG. 20.—Segments of the optical light curves of the ZZ Ceti stars identified in Fig. 16. From top to bottom: star no. 18 (GD 154) to star no. 21 (MCT 016–2553).

using only the period of the largest amplitude mode in each star or, better still, computing the amplitude-weighted mean period. However, given that the period data are not uniform and that some stars have been studied at much higher sensitivity than others while several more have only been looked at during short discovery runs until now, it was deemed sufficient for our illustrative purposes to adopt the simpler choice of the average period. Note that, along with the 48 stars listed in Table 1, we have added three more objects for which we only have provisional estimates of their atmospheric parameters in Figure 24. These are MCT 0016–2553, KUV 03442+0719, and GD 1212, important objects because they are located at the red edge (we showed their light curves in Fig. 20). The two circles outside the formal empirical red edge in Figure 24 belong to two of these stars; they should not be seen as necessarily lying “outside” the strip as currently drawn. Longer spectroscopic observations covering several pulsation cycles are likely to bring them back within the formal strip.

In Figure 24, the *size* of a circle gives a logarithmic measure of the average period reported for each ZZ Ceti star (51 objects in all). The smallest circle corresponds to the single period of 109 s observed in G226–29, and the largest one to the dominant period of 1385 s reported in KUV 03442+0719. Keeping in mind the nonuniformity of the period data and, also, the possibility for true exceptions, Figure 24 very clearly confirms that there is a period-temperature trend in the sense that cooler objects tend to show longer periods than their hotter counterparts. This is not a new result by any means—this point was first made by Winget & Fontaine (1982) many years ago on the basis of a

sample of 12 stars. Since then, there have been many reports reinforcing this conclusion (see Mukadam et al. 2006 for a recent example). So, no surprise here, but Figure 24 presents the clearest view of this correlation using the most reliable atmospheric parameter determinations currently available.

Quite interestingly, Figure 24 also reveals another trend, never noted before to our knowledge, and that is the fact that higher gravity ZZ Ceti stars tend to show shorter excited periods. Although never mentioned before at the empirical level, this new result is also not surprising, given that more massive ZZ Ceti stars have shorter periods by virtue of their mechanical structure. We refer the reader to the very detailed discussion of the adiabatic properties of pulsating DA white dwarfs presented by Brassard et al. (1992c), which describes the sensitivity of the periods to parameters such as effective temperature, mass (or surface gravity), envelope layering, thickness of the composition transition zones, and convective efficiency. We mention this because there have been some attempts recently to use the periods of ZZ Ceti stars as “thermometers,” i.e., as independent indicators of the effective temperature (see, e.g., Mukadam et al. 2006). What Figure 24 shows is that such an approach is bound to fail because, very clearly, this game must be played in two dimensions at the very least. Periods *do* depend on surface gravity, not only on effective temperature in the ZZ Ceti strip.

The example of GD 165 and GD 66 as two spectroscopic twins (they practically have the same values of  $\log g$  and  $T_{\text{eff}}$  according to Table 1) having quite different pulsation properties is a reminder that the game, in fact, can be played in more dimensions still. GD 165 has observed periods between 114 and 250 s

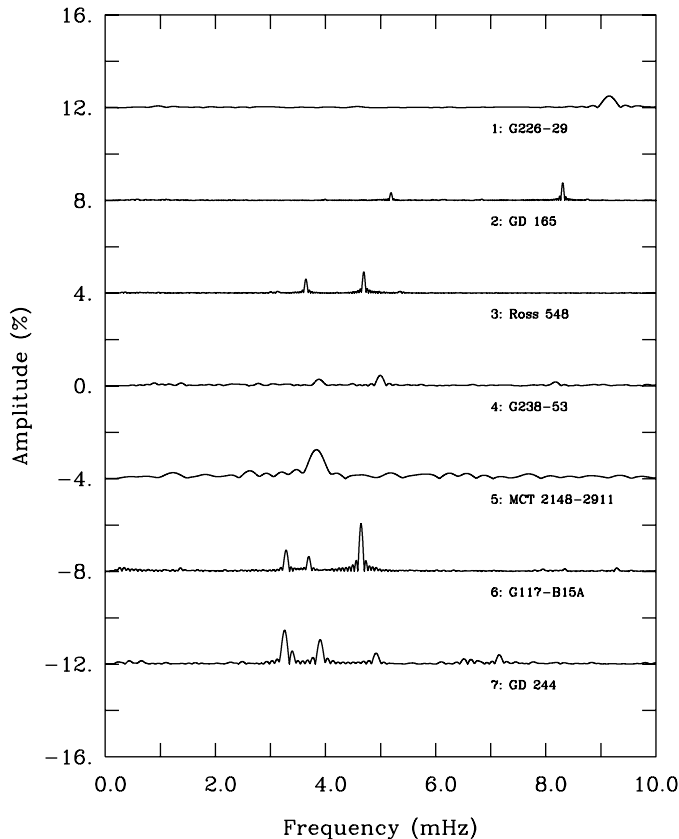


FIG. 21.—Fourier transforms of the optical light curves of the ZZ Ceti stars identified in Fig. 16. From top to bottom: star no. 1 (G226–29) to star no. 7 (GD 244).

and its light curve is distinctly different (see the second curve from the top in Fig. 17) from that of GD 66 (the top curve in Fig. 18). The latter has periods observed in the range 198 to 303 s. By fixing the values of  $\log g$  and  $T_{\text{eff}}$  at their spectroscopic estimates, it is possible, in fact, to find models of GD 165 and GD 66 that can account for the different observed periods by varying the H/He envelope layering from one model to the other.

We must point out here that part of the differences observed in the pulsation characteristics of GD 165 and GD 66 could certainly be due to differences in atmospheric parameters. The latter, according to Bergeron et al. (1995), are known to within  $\Delta T_{\text{eff}} = \pm 350$  K and  $\Delta \log g = \pm 0.05$  dex, due primarily to flux calibration uncertainties. Hence, we cannot exclude that GD 66 could be cooler than GD 165 by a few hundred degrees, for example. Nevertheless, envelope layering is an additional parameter that strongly affects the periods of ZZ Ceti models, and this should not be forgotten. Hence, it is very dangerous to interpret changes of periods across the ZZ Ceti instability strip from one star to another as a sole indication of effective temperature.

We carried out a similar exercise for the V777 Her stars on the basis of the data given in Table 2. There, one can see that

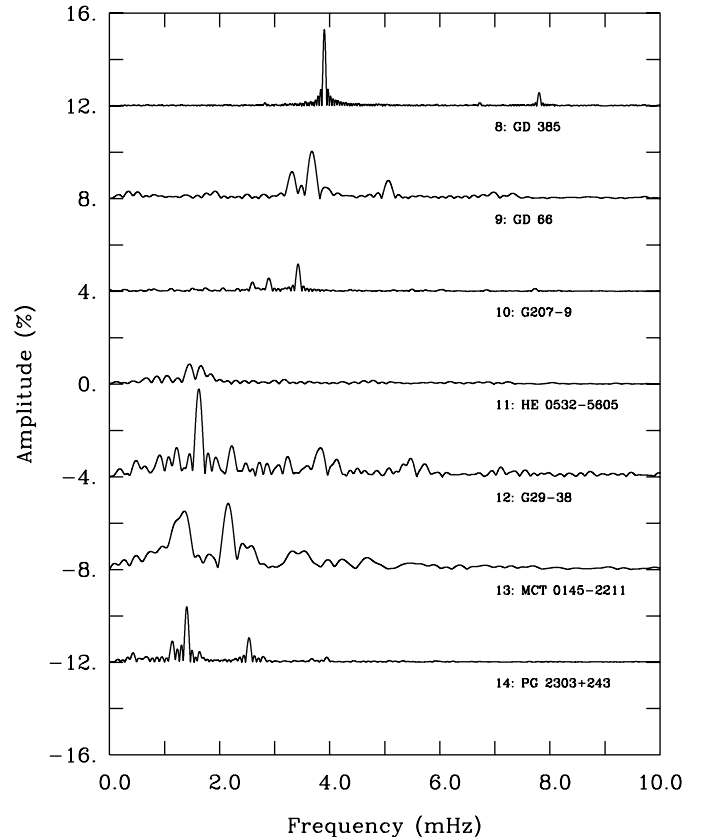


FIG. 22.—Fourier transforms of the optical light curves of the ZZ Ceti stars identified in Fig. 16. From top to bottom: star no. 8 (GD 385) to star no. 14 (PG 2303+243).

periods are found in the range from 149 to 1072 s in pulsating DB white dwarfs. In order to boost our statistics a little, we also added EC 20058-5234, the star with very large uncertainties in its atmospheric parameters to our sample. It pulsates in the range of periods from 111 to 351 s. Unfortunately, but not surprisingly in the light of what we wrote above, the results of this experiment are not conclusive, as shown in Figure 25. We do not see any obvious correlation between the sizes of the open circles and the effective temperature or surface gravity. Beyond the fact that there are only a few stars to build a case on, we are defeated by the uncertainties in the atmospheric parameters associated with the possible presence of small traces of hydrogen in the surface layers of these stars. As indicated above, it is possible that the boundaries of the V777 Her instability domain are intrinsically fuzzy.

In the case of the GW Vir pulsators, trends such as those observed in ZZ Ceti stars cannot be put in evidence because the picture is dominated by the important variations of the envelope chemical composition from star to star. However, thanks to Quirion et al. (2004, 2005) who computed an individual model for each star of interest with its own composition, it is possible to compare the ranges of observed periods with

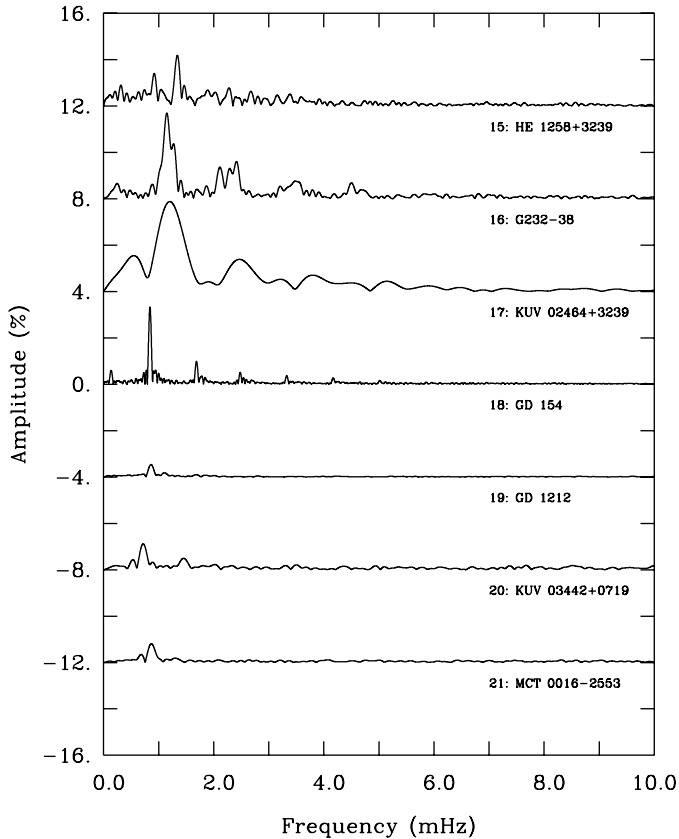


FIG. 23.—Fourier transforms of the optical light curves of the ZZ Ceti stars identified in Fig. 16. From top to bottom: star no. 15 (HE 1258+3239) to star no. 21 (MCT 016–2553).

the ranges expected from nonadiabatic pulsation theory. This is summarized in Figure 26 where we assembled the results for 10 stars for which this exercise has been possible so far. In this figure, the red dots give the locations of these stars in the  $\log g - T_{\text{eff}}$  diagram, and the red lines extending downward measure the range of predicted periods for modes with  $l = 1$ . The scale of these ranges is calibrated for the star HS 2324+3944 for which the predicted unstable modes fall in the interval of periods from 1355 to 3013 s. In comparison, the blue line segments give the ranges of observed periods as reported in Table 3. For instance, for HS 2324+3944, we read an interval of between 2005 and 2569 s, and this also appears in Figure 26.

In an ideal situation, the red line segment should completely overlap with the blue line segment, meaning that the theoretically predicted range of unstable periods should be larger than the range observed since many modes are probably missed because of amplitude effects. In addition, there could be observed modes with a degree index  $l = 2$ , in which case the blue line segments would be slightly shifted in the vertical direction as compared to dipole ( $l = 1$ ) modes. Taking that into account,

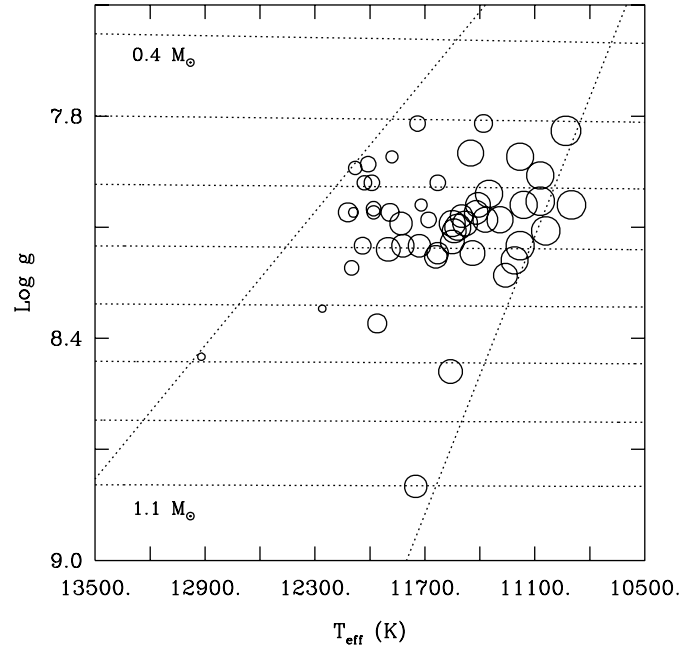


FIG. 24.—Correlation between excited period and effective temperature or surface gravity for ZZ Ceti pulsators. The locations of 51 stars are specified by open circles whose sizes give a logarithmic measure of the representative period for each star. The nearly horizontal dotted curves illustrate evolutionary tracks for H-atmosphere white dwarfs of different masses, from  $0.4 M_{\odot}$  above to  $1.1 M_{\odot}$  below in steps of  $0.1 M_{\odot}$ . The two diagonal dotted lines are the empirical blue and red boundaries of the instability domain as obtained by Gianninas et al. (2007).

the general agreement between theory and observations is quite satisfactory. There are two cases where the match is not very good, the two stars in the upper left part of the diagram (RXJ2117.1+3412 and NGC 246), and this implies some inadequacies in the modeling of these low-gravity, very hot stars. On the whole, however, nonadiabatic theory passes the test with distinction.

Compared to V777 Her and ZZ Ceti stars, the range of periods of interest in GW Vir pulsators is much larger, but this simply reflects the wide range of surface gravity (nearly 2 orders of magnitude) found in these stars. Abell 43, for example, with  $\log g = 5.7$  and  $T_{\text{eff}} = 110,000$  K, is a star that is still contracting and getting hotter on the low-gravity branch of its evolutionary track. It features a range of observed periods between 2380 and 6075 s corresponding to medium-order  $g$ -modes in what could be called a “pre-white dwarf.” In comparison, PG 0122+200 with  $\log g = 7.5$  and  $T_{\text{eff}} = 80,000$  K currently defines the empirical high-gravity red edge. That star, definitely in its final cooling phase, is slowly exiting from the GW Vir instability domain and is expected to turn into a He-atmosphere DO white dwarf. It shows a range of observed periods between 336 and 612 s corresponding to low-order  $g$ -modes as appropriate for a compact star.

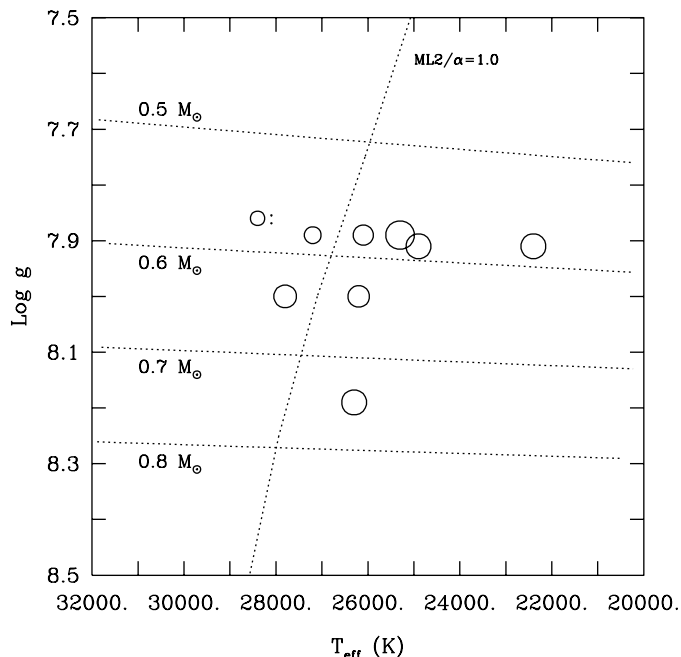


FIG. 25.—Attempt to find a correlation between excited period and effective temperature or surface gravity in V777 Her pulsators. The locations of nine stars are specified by open circles whose sizes give a logarithmic measure of the representative period for each star. The dotted curve labeled  $ML2/\alpha = 1.0$  shows the theoretical blue edge based on stellar models with no H in their atmospheres. The other dotted curves illustrate evolutionary tracks for He-atmosphere white dwarfs of different masses.

## 7. PARTIAL MODE IDENTIFICATION AND ANGULAR GEOMETRY

There are a number of known ways in asteroseismology to measure or directly infer the angular geometry of a pulsation mode defined by its degree index  $l$ , its azimuthal order  $m$ , and its inclination angle  $i$  with respect to the line of sight. When this information becomes available, and this is particularly true for the degree index  $l$ , invaluable constraints can be used to test seismic models. In turn, those can be changed or improved until a satisfactory match is reached between the observed and predicted periods, while being consistent with such constraints. These methods can be readily applied to white dwarfs, at least in principle, but those have their own peculiarities and simulation codes must be adapted accordingly. Moreover, it should be kept in mind that, by virtue of their intrinsic faintness, it may be difficult, observationally speaking, to use these techniques for pulsating white dwarfs.

The first method is well known and consists in exploiting the wavelength dependence of the amplitude of a pulsation mode that bears, among other things, the signature of the angular geometry of the mode. Observations of the photosphere through multicolor photometry or, better still, time-resolved spectroscopy, may become very useful tools. The second method, potentially very interesting but hardly used so far for white dwarfs,

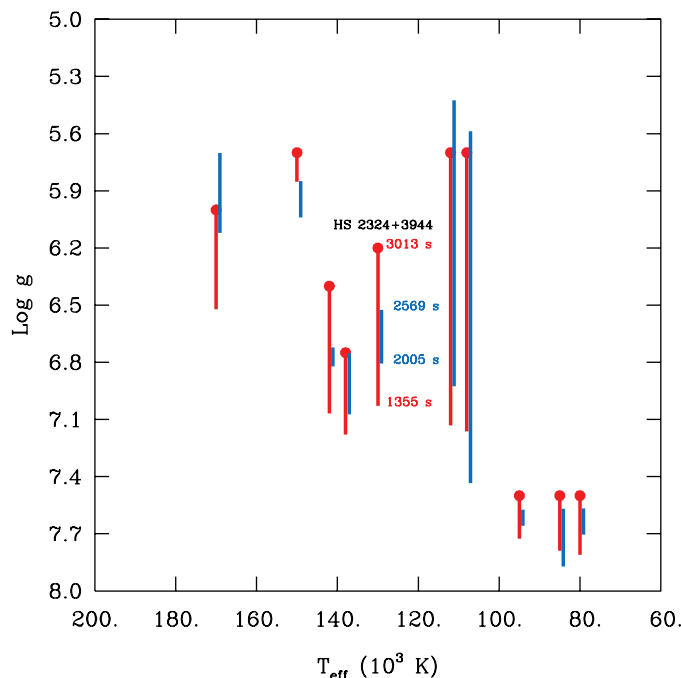


FIG. 26.—Comparison of the predicted period ranges (*red line segments*) with the observed period ranges (*blue line segments*) for 10 stars from Table 3. These are PG 0122+200, PG 1159–035, PG 1707+427, RXJ 2117.1+3412, PG 2131+066, HS 2324+3944, Abell 43, K1–16, NGC 246, and NGC 7094. The positions of these stars in the  $\log g - T_{\text{eff}}$  plane are given by the red dots.

exploits the ratios of the amplitudes of pulsation modes to the amplitudes of their harmonics and cross-frequencies in the Fourier domain. These amplitude ratios also bear the signature of the angular geometry of pulsation modes. A third approach is the classic phenomenon of rotational splitting which may allow the identification of the indices  $l$  and  $m$ . We review briefly these three methods in what follows. In a nutshell, the  $g$ -modes observed in pulsating white dwarfs and for which such techniques have been successfully applied so far belong to degree indices  $l = 1$  and 2.

### 7.1. Multicolor Photometry and Time-Resolved Spectroscopy

The first formalism with which to analyze the results of multicolor photometry for white dwarfs was developed by Robinson et al. (1982) in a very important paper. They argued that luminosity variations are completely dominated by temperature perturbations in pulsating white dwarfs. This was followed many years later by Brassard et al. (1995) who built upon that formalism. They introduced the use of detailed specialized model atmospheres (instead of using published tables of limb-darkening coefficients), and showed how to compute not only the first-order perturbation to the emergent flux, but also the higher-order terms. That last step proved essential in the analyses of the nonlinearities often observed in the light curves of pulsating white dwarfs (see below).

More recently, Randall et al. (2005) adapted the approaches developed by Cugier & Daszyńska (2001) and Townsend (2002) for main sequence pulsators to analyze multicolor photometry of pulsating sdB stars of the two kinds described briefly in § 2 above. The method allows the computation of the first-order perturbation to the flux. The authors were able to connect their formalism with the first-order calculations of Brassard et al. (1995) when pushed into the regime appropriate for white dwarfs. Taking into account the perturbations of not only the temperature, but also of the radius (important in main sequence stars and in  $p$ -mode sdB pulsators of the V361 Hya type) and of the local gravity (small but significant in main sequence stars and essentially negligible in V361 Hya stars) in the atmospheric layers, Randall et al. (2005) were able to quantitatively confirm the prediction of Robinson et al. (1982) that temperature effects completely dominate in pulsating white dwarfs.<sup>6</sup> This implies an absence of phase shifts between the light curves of different colors. (Note that the usual practice in white dwarf asteroseismology of using “white light” integrated photometry is well justified in this context because one aims primarily at maximizing the sensitivity of the light curves in order to extract as many pulsation modes as possible and determine their periods. As is well known, the periods are the most basic input quantities used in asteroseismological exercises. Of course, by carrying out integrated light photometry, one loses the spectral information about the modal angular geometry.) In addition, Randall et al. (2005) were able to alleviate the worry expressed by Robinson et al. (1982) about the legitimacy of using the adiabatic relationship between the temperature perturbation  $\delta T/T^0$  and the radius perturbation  $\delta r/r^0$  in their discussion of color variations in white dwarfs. Indeed, it turns out that, when the brightness variations are completely dominated by temperature effects, the ratio of the amplitudes of a pulsation mode in two different wavebands becomes independent of nonadiabatic effects in the linear regime. This does not imply that the atmospheric layers of a white dwarf are adiabatic by any means (such layers, as is well known, are *always* highly nonadiabatic), but, to first order in the perturbation of the emergent flux, the amplitude at all wavelengths depends in the same way on nonadiabatic effects. Moreover, the dominance of temperature effects for the  $g$ -modes observed in pulsating white dwarfs also implies that the amplitude ratio is independent of the period of the mode in question. The latter then depends only on the degree index  $l$  of the mode, as well as on the atmospheric parameters of the star, including, in the case of DA and DB stars, the choice of the mixing-length parametrization.

The color-amplitude technique is usually applied to broadband photometry, but we find it instructive to examine the behavior of the key monochromatic quantities. We begin with the unperturbed emergent Eddington flux, which is shown in the top

panel of Figure 27 for a representative model of a ZZ Ceti star with  $T_{\text{eff}} = 12,000$  K,  $\log g = 8.0$ , and computed with the ML  $2/\alpha = 0.6$  version of the mixing-length theory. As is typical for a 12,000 K DA white dwarf, the Eddington flux is characterized by the presence of very broad hydrogen Balmer lines in the optical domain. The features in the FUV are satellite structures due to quasi-molecular absorption in the red wing of an even broader Lyman  $\alpha$  line (see Allard et al. 1994). For comparison, the middle panel illustrates the predicted first-order perturbation to the emergent Eddington flux,  $H_\nu^1$ , assuming a  $g$ -mode with three values of the degree index from  $l = 1$  (*top curve*) to  $l = 3$  (*bottom curve*). Note that here,  $H_\nu^1$  is divided by the unknown factor  $\epsilon_r \bar{Y}_l^m(i)$  in the notation of Randall et al. (2005). In this product,  $\epsilon_r$  represents the dimensionless amplitude (modulus) of the complex radial eigenfunction describing the radius perturbation, and  $\bar{Y}_l^m(i)$  is the viewing aspect depending on the indices  $l$ ,  $m$ , as well as the inclination angle  $i$ . It is evident that the pulsational amplitude rapidly decreases with increasing  $l$ , which is a direct manifestation of the well-known geometric cancellation effects associated with an increasing number of nodal lines crisscrossing the visible disk. By dividing the curves by the unperturbed flux  $H_\nu^0$ , one obtains the *relative* monochromatic amplitude of the assumed mode (again to within the unknown parameter  $\epsilon_r \bar{Y}_l^m(i)$ ), as indicated in the bottom panel of the figure. It is the latter quantity that forms the basis of the color-amplitude technique, which relies on comparing the relative amplitude at two wavelengths in order to eliminate the unknown factor.

The result of such an operation is illustrated in Figure 28, where we have divided the relative monochromatic amplitude curves for each  $l$  by the corresponding relative amplitude at an (arbitrary) frequency point in the continuum with  $\lambda = 2000$  Å. We can easily observe that the signatures of the  $l = 1$  and  $l = 2$  modes are rather similar, particularly in the optical domain. This implies that very high S/N observations are required if the color-amplitude technique is to be applied successfully to pulsating white dwarfs in the optical domain, especially for discriminating between dipole and quadrupole modes. In comparison, modes with  $l = 3$  appear to be easily recognizable from their  $l = 1$  and 2 cousins. The figure also reveals that the discriminatory power of the method is much better in the UV/FUV than in the optical as there are significant differences between predicted amplitudes in that regime. However, one should keep in mind that there is very little flux in this spectral range for a ZZ Ceti star (see, e.g., the top panel of Fig. 27), so the gain in discriminatory power is weighted down by the available flux. The prospects are much better, of course, when observing V777 Her and GW Vir stars in the UV/FUV because they have much larger fluxes in that spectral range.

Some of the earliest multicolor photometry observations to have been carried out for pulsating white dwarfs are those of Keith Horne who looked at the relatively bright ( $V = 13.03$ ) large-amplitude ZZ Ceti star G29–38 in 1979 October. Prior

<sup>6</sup>This statement is strictly valid in the continuum only; it does not hold true in the cores of spectral lines, for example.

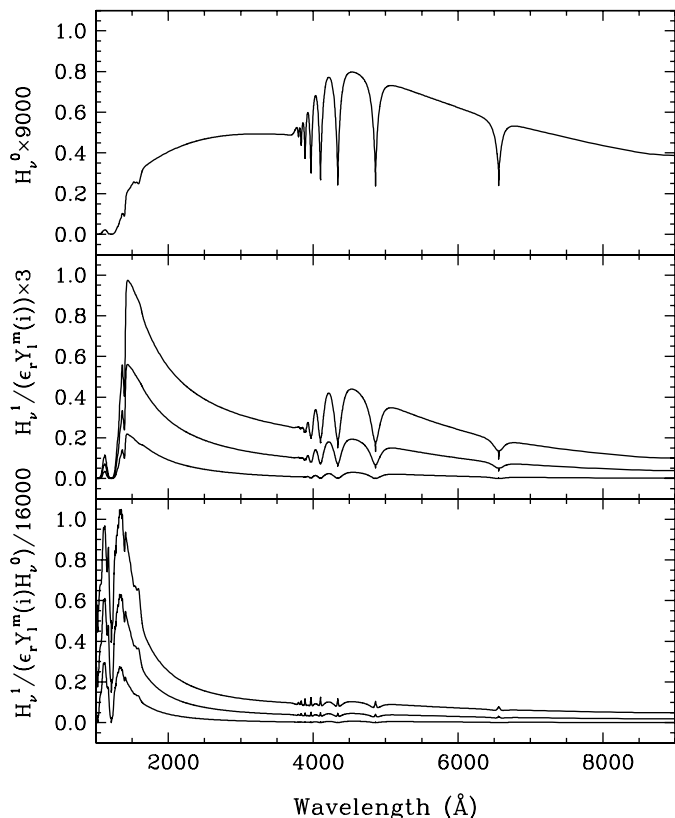


FIG. 27.—Behavior of some key monochromatic quantities for a representative ZZ Ceti star model atmosphere. The atmosphere has  $\log g = 8.0$  and  $T_{\text{eff}} = 12,000$  K, and  $ML2/\alpha = 0.6$  convective efficiency. *Top panel:* Unperturbed emergent Eddington flux. *Middle panel:* First-order perturbation to the flux caused by a  $g$ -mode pulsation; from top to bottom, each curve is characterized by a value of the degree index  $l = 1, 2,$  and  $3$ . *Bottom panel:* Similar to the middle panel, but illustrating the *relative* amplitude of the perturbation.

to that, McGraw (1979) had also gathered Strömgren multicolor light curves for G29–38, as well as for HL Tau 76, another large-amplitude pulsator. Unfortunately, the S/N obtained by McGraw (1979) in his observations turned out to be inadequate for quantitative modeling (he used the 2.1-m Struve telescope at McDonald Observatory in Texas). Horne, however, used the Palomar 5.0-m telescope (the second-largest optical telescope at the time) equipped with the wonderful Multi Channel Spectrophotometer instrument (MCSP) designed by Bev Oke. That instrument, in operation for two full decades, was able to provide simultaneous photometry in up to 32 distinct wavelength channels. In Horne’s observations, a total of 436 spectra were gathered over a period of about 5200 s. Useful data were obtained in 23 channels corresponding to rectangular bandpasses with widths of 160 Å in the blue part of the optical spectrum and 320 Å in the red.

Although of exceptional quality at the time (and still better than some recent observations), that data set was never fully

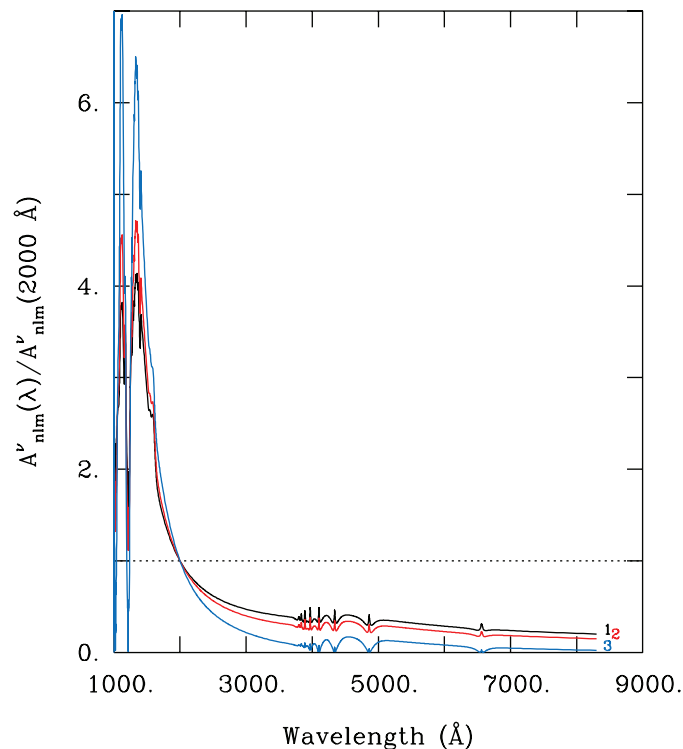


FIG. 28.—Monochromatic amplitude ratios with respect to an arbitrary spectral point at 2000 Å. This again refers to our representative ZZ Ceti star model and for a  $g$ -mode with a degree index  $l = 1$  (black curve), 2 (red curve), and 3 (blue curve).

exploited for a number of reasons. Be that as it may, we were given the data by Keith Horne a long time ago for quantitative analysis. We thought therefore that it would be appropriate, in the context of this review, to discuss some of these older observations as an example of a successful determination of the  $l$  index of a pulsation mode in a white dwarf through an application of the color-amplitude method. In particular, we focused on the pulsation with the largest amplitude in Horne’s G29–38 data, a mode with a period of 605 s (with a fairly large uncertainty of more than 1% because of the poor temporal resolution of this short run). We computed the expected amplitude ratios using a model atmosphere tailored to G29–38, i.e., using  $T_{\text{eff}} = 11,820$  K and  $\log g = 8.15$  as indicated in Table 1, and also assuming the standard atmospheric convection calibration of  $ML2/\alpha = 0.6$ .

Our results are summarized in Figure 29 which, first of all, shows the observed color-amplitude distribution for this mode on a relative scale. In comparison, the solid curves illustrate the predicted distributions if the 605 s mode has a value of  $l = 1, 2, 3,$  or  $4$ . What we do in this comparison is to best fit in a  $\chi^2$  sense the *shape* of the observed color-amplitude distribution with the theoretical distribution of amplitude ratios for a given value of  $l$  (obtained after convolving the monochromatic amplitudes with the response of the MCSP instrument in the 23 useful channels).

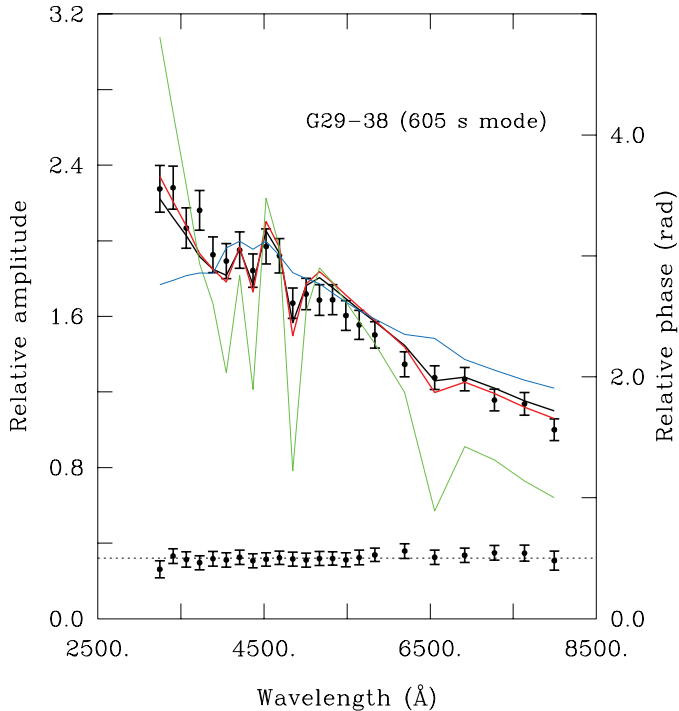


FIG. 29.—Mode discrimination in the ZZ Ceti star G29–38 using multicolor photometry. The color-amplitude distribution for the dominant pulsation mode (605 s) present that night was measured with the MCSP instrument attached to the Palomar Observatory 5.0-m telescope and is given here by the 23 data points with error bars. The solid curves give the model predictions for the same 23 channels assuming that the 605 s mode has a degree index of  $l = 1$  (black curve),  $l = 2$  (red curve),  $l = 3$  (green curve), or  $l = 4$  (blue curve). The observations are clearly compatible with the possibilities that  $l = 1$  or 2. The values of  $l = 3$  and 4 can be ruled out. Also shown are the phases of the 23 light curves with respect to some arbitrary zero point. As expected from theory, the data are consistent with the idea that there are no phase differences between the various colors.

Clearly, Figure 29 shows that the possibilities  $l = 3$  and 4 do not provide acceptable fits to the data. In contrast, the figure also reveals that the 605 s mode is either a dipole or a quadrupole mode. In fact, the formal  $\chi^2$  fit is better for the  $l = 1$  solution, but the available S/N does not allow us to completely rule out the  $l = 2$  solution at this stage. Still, Figure 29 illustrates marvelously, we think, how multicolor photometry can be used to constrain the  $l$  index in pulsating white dwarfs. It also demonstrates that, as expected for  $g$ -modes in white dwarfs, there are no phase shifts between colors.

To our knowledge, the first successful *published* determination of the  $l$  index of a pulsation mode in a white dwarf using the color-amplitude method is that of Robinson et al. (1995) who presented and analyzed a most interesting set of measurements using, in part, two UV filters inside the long-gone fast photometer on board *HST*.<sup>7</sup> Robinson et al. (1995) measured the am-

plitudes of the dominant pulsation mode (215.2 s) in the ZZ Ceti star G117-B15A not only in two UV bandpasses but also on the ground through Johnson-Cousins *UBVR* filters. Although these two sets of observations were not contemporary in time, G117-B15A is one of those “simple” ZZ Ceti stars showing very stable pulsation properties as functions of time. It was, in fact, because of the stability of the amplitudes of its three known pulsation modes that G117-B15A was chosen as a target, and not due to its brightness ( $V = 15.54$ ). Using these six-color data, Robinson et al. (1995) determined that the 215.2 s mode observed in G117-B15A is most likely a dipole mode.

This identification was confirmed by Fontaine et al. (1996), who independently reanalyzed the same data set. However, these authors went considerably further than Robinson et al. (1995) could, by investigating the sensitivity of the predicted pulsation amplitudes to the convective efficiency used in the model atmosphere calculations. To this end, they used three grids of model atmospheres based on the  $ML2/\alpha = 1.0$ ,  $ML2/\alpha = 0.6$ , and  $ML1/\alpha = 1.0$  parametrization of the mixing-length theory. Fontaine et al. (1996) found, as did Robinson et al. (1995), that the observations are best explained if  $l = 1$ . However, for each version of the mixing-length theory and for an assumed value of the degree index  $l$ , no unique best-fitting model was found but, instead, a full *family* of solutions emerged in the  $\log g - T_{\text{eff}}$  plane. Examples of models providing comparable quality fits and belonging to a same family are given in Figure 30. The figure shows, for instance, that a  $ML2/\alpha = 1.0$ ,  $l = 1$  model with  $T_{\text{eff}} = 10,950$  K and  $\log g = 7.5$  is as good as a cousin model with  $T_{\text{eff}} = 11,750$  K and  $\log g = 8.5$  at explaining the amplitude data. Fontaine et al. (1996) could not fully discriminate between the various versions of the mixing-length theory on the basis of the pulsation data alone, but they invoked the constraints derived in the completely independent analysis of the time-averaged optical and ultraviolet spectra of G117-B15A carried out by Bergeron et al. (1995). In the end, they found a model of G117-B15A with  $T_{\text{eff}} \approx 11,500$  K,  $\log g \approx 8.0$ , and  $ML2/\alpha = 0.6$  convection to be consistent with both the observed pulsation amplitudes and the time-averaged spectroscopic observations (see Table 1). This notion of *families* of solutions should be kept in mind when applying the color-amplitude method to pulsating white dwarfs.

Although the combination of UV and optical color data (as in the example just discussed) is ideal for maximizing the chances of mode discrimination in pulsating white dwarfs, very few experiments could be carried out in practice because of limited access to the UV facilities and difficulties in organizing, in an ideal situation, overlapping observations with ground-based telescopes. In particular, it has proven very difficult to get the long runs necessary to reach a good temporal resolution and high S/N on the UV/FUV facilities. For instance, this is what

<sup>7</sup> Incidentally, it is a real shame that this instrument was sacrificed when a correcting lens was added to *HST*. Probably unknown to the younger generation,

the whole field of observational asteroseismology suffered a huge setback then, the consequences of which have not been fully appreciated yet.

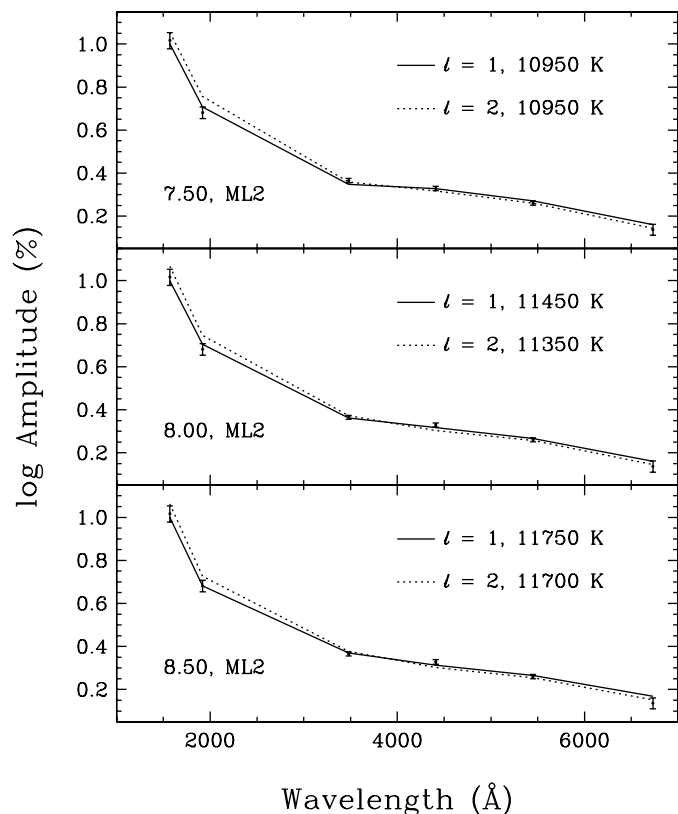


FIG. 30.—Comparison of the observed pulsation amplitudes of the 215.2 s mode in G117-B15A (points with the  $1\sigma$  error bars) with the predicted amplitudes (solid curves) in the six bandpasses of interest for three models ( $\log g = 7.5, 8.0, 8.5$ ) belonging to the family of best-fitting ML2/ $\alpha = 1.0$  models under the assumption that  $l = 1$ . A similar comparison with models belonging to the family of optimal ML2/ $\alpha = 1.0$  models under the assumption that  $l = 2$  is provided by the dotted curves.

limits the usefulness of the currently available *FUSE* data on pulsating white dwarfs, although these data remain largely untapped as indicated above and could still prove their worth. Furthermore, as is described in the interesting paper of Kepler et al. (2000), observations gathered on space-borne detectors not specifically designed for fast photometry or time-resolved spectroscopy are difficult to analyze because these data have their own idiosyncrasies associated with calibration problems and other difficulties. Kepler et al. (2000) have used the Faint Object Spectrograph on board *HST* to obtain low-resolution time-resolved spectroscopic observations of the ZZ Ceti stars G226–29 ( $V = 12.24$ ) and G185–32 ( $V = 12.98$ ) as well as the V777 Her star PG1351+489 ( $B_{ph} = 16.4$ ). They concluded that the pulsation modes they detected were dipole modes in all likelihood, but they also pointed out several problems in the comparison between observed and predicted amplitudes likely to be associated with the data reduction procedure.

The problem is illustrated in Figure 31 where we compared the UV amplitude distribution of the dominant component of a

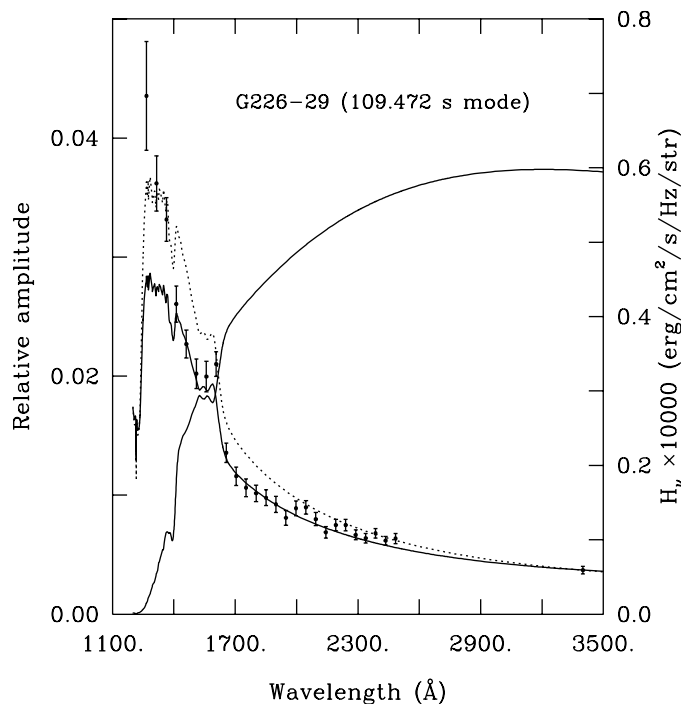


FIG. 31.—Identification of the  $l$  index of the 109.472 s pulsation mode observed in the ZZ Ceti star G226–29 on the basis of the color-amplitude method as applied in the UV spectral domain. The observational data have been taken from Table 2 of Kepler et al. (2000) who used the FOS on board *HST* to gather low-resolution time-resolved UV spectroscopy. In comparison, the predictions of our model of G226–29 give the amplitude distributions illustrated by the solid curve for  $l = 1$  and by the dotted curve for the possibility  $l = 2$ . The three distributions have been normalized at 3400 Å. The other solid curve, to be read on the right-hand axis, shows the emergent unperturbed flux. Note the dramatic fall of the flux when reaching the shortest wavelengths.

(presumably) rotationally split frequency triplet in the ZZ Ceti star G226–29 as obtained by Kepler et al. (2000) with the predictions of one of our models tailored after that star, i.e., built with the specifications of Table 1 ( $T_{\text{eff}} = 12,260$  K,  $\log g = 8.32$ , ML2/ $\alpha = 0.6$  convection). Note that we made no effort to optimize the fits in any way because we simply wanted to make a point. Hence, we simply normalized the data as well as the two theoretical amplitude curves for  $l = 1$  and  $l = 2$  at the single spectral point with  $\lambda = 3400$  Å. It can be seen from the figure that the observed amplitude distribution best matches the  $l = 1$  curve over most of the spectral range of interest, except for the three “bluest” points which would rather better match the  $l = 2$  distribution in that spectral region. Given the plummeting behavior of the flux in that region (also plotted in the figure), we strongly suspect that the uncertainties on the amplitudes of these three spectral points have been largely underestimated. While we concur with Kepler et al. (2000) that the 109.472 s mode observed in G226–29 is indeed a  $l = 1$  mode, the main point of this discussion has been to underline some of the difficulties inherent to observations gathered from UV/FUV facilities as applied to the color-amplitude method. In

this context, we also draw attention to the work of Dreizler et al. (2005) and Stahn et al. (2005) who used *STIS/HST* time-resolved spectroscopy to study the main pulsation mode at 516 s in PG 1159–035.

Despite these difficulties, we feel that the potential of multicolor photometry has barely been tapped for pulsating white dwarfs. We believe that even optical observations alone could be useful provided they reach sufficiently high S/Ns. This is currently possible on 4-m class telescopes, as has been recently demonstrated by Fontaine et al. (2008b) for the  $V = 12.1$  pulsating sdB star Bal 090100001. To explore this possibility in more detail for pulsating white dwarfs, we carried out an experimental run with our photometer LAPOUNE attached to the CFHT monitoring the ZZ Ceti star G117-B15A. Despite its relative faintness, we were able to obtain excellent  $U$ ,  $B$ , and  $V$  light curves as can be judged from Figure 32. To accompany this diagram, Figure 33 shows the Fourier transforms of these light curves gathered over a single night. In both figures, but particularly in the Fourier domain, a decrease of the amplitudes of the three detectable modes with increasing effective wavelength is clearly observable. We have gathered similar-quality data for several consecutive nights, but have not found the time yet to properly evaluate and model these data. We are very confident, however, that at least partial mode identification will come out of this venture.

Curiously, despite the relative faintness of pulsating white dwarfs, it would appear that there have been a few more at-

tempts to exploit low- and medium-resolution time-resolved spectroscopy than multicolor photometry so far for these stars. Nevertheless, such attempts have remained few and far between as the observational difficulty of obtaining a high enough sensitivity has dominated the scene. We have singled out the work of Clemens et al. (2000) as an outstanding example of a successful exercise in the field. These authors were able to gather a remarkable data set on the relatively bright high-amplitude ZZ Ceti star G29–38, consisting of about 4.5 h of medium-resolution ( $\sim 7 \text{ \AA}$ ) optical spectroscopy with an effective time sampling of 24 s at the 10-m Keck II telescope on Mauna Kea. We draw the attention of the reader to Figures 4 and 5 of Clemens et al. (2000), where the wavelength dependence of the amplitude and phase of six distinct pulsation modes are presented. On the basis both of these observed distributions and of detailed modeling, Clemens et al. (2000) were able to identify the degree index  $l$  of these six pulsation modes (five are dipole modes and one is a quadrupole mode).

Beyond these identifications, Clemens et al. (2000) also discussed the spectral signature of surface motions detected for the first time in a pulsating white dwarf as reported by themselves in an accompanying paper (van Kerkwijk et al. 2000). Motions with projected velocities up to  $5 \text{ km s}^{-1}$  were discovered. These motions correspond to the integrated projection along the line of sight of the essentially horizontal displacements during a  $g$ -mode cycle in a white dwarf as one integrates from the center toward the limb over the visible disk. Obviously, the main

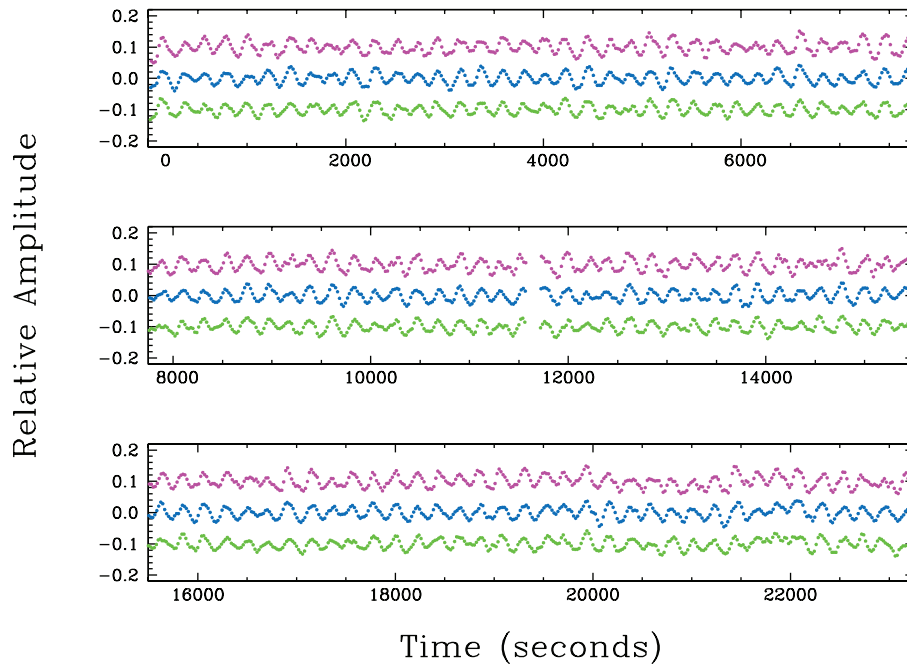


FIG. 32.—Imbricated  $U$ ,  $B$ , and  $V$  light curves, from top to bottom, of the pulsating ZZ Ceti star G117-B15A as obtained by us, using the LAPOUNE/CFHT combination. Each plotted point corresponds to an effective sampling time of 20 s. The excellent quality of these light curves underscores the potential of optical multicolor photometry for identifying the  $l$  index of pulsation modes.

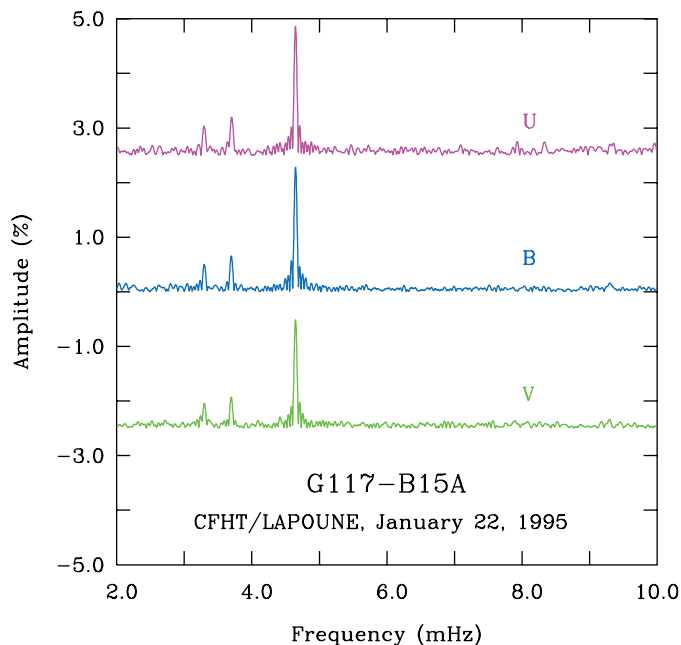


FIG. 33.—Fourier transforms of the single night light curves shown in Fig. 32. There are three major peaks in the transforms corresponding to distinct pulsation modes with periods of 304.1, 270.5, and 215.2 s. The amplitude of each of these modes clearly decreases with increasing effective wavelength of the bandpass.

contributions to the measured surface motions must come from regions near the limb. These motions are detected in the cores of spectral lines where, contrary to the continuum, the flux perturbation is not completely dominated by temperature effects. This very nice development allows one to probe deeper into the physics of  $g$ -mode pulsations in white dwarfs.

To illustrate the basic principles uncovered in the Clemens et al. (2000) study, we have modeled the normalized amplitude of a pulsation mode relative to the unperturbed flux across the  $H\beta$  line assuming an effective resolution of 1 Å. In this process, we used the atmospheric parameters appropriate for G29–38 (see Table 1). In the absence of surface motions, i.e., if we assume that the flux variation depends *only* on the perturbations of the temperature in the atmospheric layers, we get the profile given by the dotted black curve in Figure 34 if the mode has a degree index  $l = 1$ , or that given by the dotted red curve if the mode has  $l = 2$ . Also, there is no phase shift across the line. Note that the dotted curves in Figure 34 are equivalent to those shown in Figure 28 above, except that the (arbitrary) normalization point here is taken at 5110 Å for obvious convenience instead of 2000 Å as above.

If we now add surface motions measured by the parameter  $a_v$  defined in Clemens et al. (2000) and assume, for illustration purposes, a value of  $10 \text{ km s}^{-1}$  for that parameter, we now obtain the solid curves in Figure 34. It can be seen that the surface motions leave a clear signature in the line core and also significantly enhance the slight blue-red asymmetry observed on each side of the line core in the absence of motions. In addition, sig-

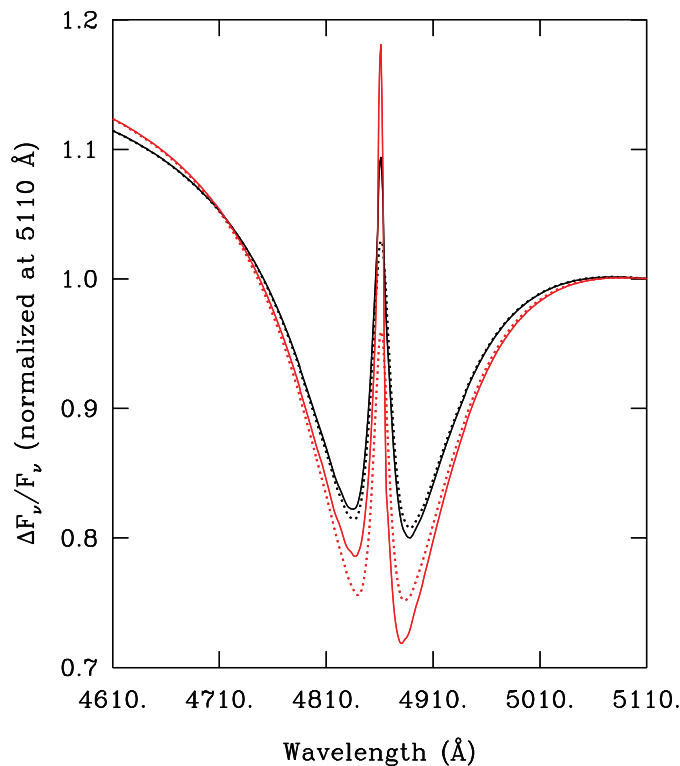


FIG. 34.—Predicted normalized amplitude of a  $g$ -mode across the  $H\beta$  line in a model of the ZZ Ceti star G29–38 assuming a degree index  $l = 1$  (black curves) or  $l = 2$  (red curves). The dotted curves refer to the case where the brightness variations are assumed to be due to temperature effects only, while the solid curves show the results when a velocity field characterized by the parameter  $a_v = 10 \text{ km s}^{-1}$  is included in the modeling of the line. The spectral resolution in the computations is 1 Å. The relative mode amplitude is normalized at 5110 Å.

nificant phase shifts, including a spectacular  $180^\circ$  reversal at the line center are now predicted. This is illustrated in Figure 35 for the model with  $l = 1$  and the other with  $l = 2$ . Such phase differences are sufficiently large to be detected as already shown by Clemens et al. (2000).

The use of high S/N, low- or medium-resolution optical spectroscopy can therefore be a very useful tool for white dwarf asteroseismology as eloquently established by Clemens et al. (2000). For the moment, however, it has been limited to the few brightest members of the class (see, e.g., Thompson 2004).

## 7.2. Exploitation of the Nonlinearities in the Light Curves

There is another way of extracting information about the angular geometry of a pulsation mode, and that is to compare the amplitudes of modes with those of their harmonics and cross-frequency combinations in the Fourier domain. The advantage of this approach for pulsating white dwarfs is that it can be carried out with “white light” data (hence with the optimal sensitivity). Furthermore, there are many pulsating white dwarfs showing nonlinear peaks in the Fourier domain. In fact, probably all of them would do so if observed at sufficiently high

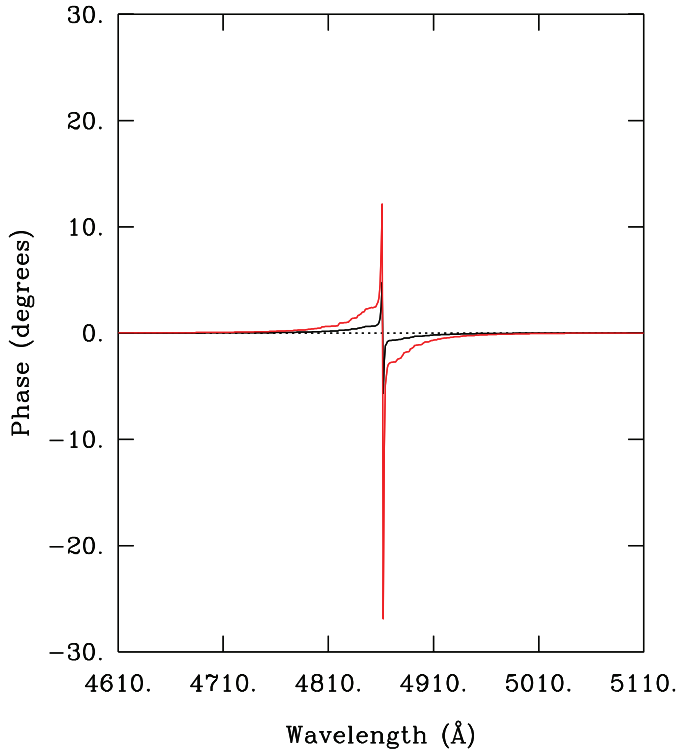


FIG. 35.—Similar to Fig. 34, but showing the relative phase across the  $H\beta$  line. No phase shifts are predicted for the case with no velocity field (*dotted horizontal line*), while there is a different signature for a mode with  $l = 1$  (*solid black curve*) or one with  $l = 2$  (*solid red curve*). The reversal in the line center is remarkable.

sensitivity. The use of that approach, however, requires detailed modeling of nonlinear effects.

Our group was the first to quantitatively explore this avenue in a white dwarf context and we presented a model that nicely explained the presence of eight nonlinear peaks—harmonics and cross-frequencies of three basic modes—in the light curve of the ZZ Ceti star G117-B15A as uncovered in very high S/N observations gathered at the CFHT (Brassard et al. 1993; Fontaine & Brassard 1994a). The basic theory behind this was exposed in details in Brassard et al. (1995). Their fundamental assumption is that a  $g$ -mode in a pulsating white dwarf could be seen, in a first approximation, as a pure temperature wave with a sinusoidal temporal dependence. This harmonic time dependence was referred to as the “first linearization” in the approach of Brassard et al. (1995). The authors then argued that the usual linearization of the resulting perturbed flux in the standard linear approach (they named that the “second linearization”) was unnecessary and counterproductive because information that may be useful is lost in the process, namely the nonlinear response of the flux to a temperature perturbation. It is indeed well known by those who build model atmospheres that the response of the emergent flux is highly nonlinear following a variation of the temperature over the atmospheric layers. Hence by correctly treating the energy transfer problem,

Brassard et al. (1995) were able to produce emergent fluxes containing nonlinear effects.

We point out that the presence of these nonlinear effects does not require the existence of an atmospheric convection zone such as those present in pulsating DA and DB white dwarfs, for example. Of course, convective energy transport does affect the resulting nonlinearities when involved, but it is not an essential ingredient in the approach of Brassard et al. (1995). What this approach implies is that there must be minimal nonlinear effects due exclusively to the energy transfer process in the atmospheric layers of a pulsating star, irrespective of the presence of a convection zone or not in the atmosphere. And indeed, there are well-documented cases of harmonics and cross-frequency oscillations observed in the light curves of pulsating stars such as GW Vir white dwarfs, pulsating sdB stars of the V361 Hya and V1093 Her types, as well as other oscillating stars that have radiative atmospheres/envelopes.

For illustration purposes, we computed time-dependent energy distributions for a representative model of a pulsating DA white dwarf undergoing a single  $g$ -mode pulsation following the method of Brassard et al. (1995). The model was built using the parameters  $T_{\text{eff}} = 11,800$  K,  $\log g = 8.0$ , and  $ML2/\alpha = 0.6$  convection. The pulsation mode (temperature wave) was assumed to have an intrinsic dimensionless amplitude of  $\epsilon_T = 0.3$ , not necessarily a “small” perturbation but useful for the present demonstration. It was also assumed to have angular indices  $l = 1$  and  $m = 0$ , and to be seen under an inclination angle of  $i = 1$  radian.

The results of our calculations are summarized in Figure 36 where the solid curves show the instantaneous emergent flux for six distinct phases equally spaced in time during a pulsation cycle. In comparison, the dotted curve shows the unperturbed flux. It should be obvious from the figure that the excursions about the unperturbed flux are not symmetric as they would be in the strictly linear approach in which the flux variation is reduced to the first-order correction. In that case, for a given wavelength, the flux variation would amount to a strictly sinusoidal oscillation about the unperturbed value: the flux perturbation at a given wavelength would show the same amplitude in a high-luminosity phase as in its low-luminosity counterpart. This is not the case in the present simulations, and nonlinear deviations—magnified here by our use of a relatively large value of  $\epsilon_T = 0.3$ —can be clearly seen. We note that attempts to fit these instantaneous energy distributions with standard, unperturbed synthetic spectra would only lead to fictitious “measurements” of variations in  $T_{\text{eff}}$  and  $\log g$ . In particular, by construction, the surface gravity is strictly constant during a pulsation cycle modeled after a pure temperature wave. We also note that the results illustrated in the figure are independent of the period of the  $g$ -mode.

If the basic assumption that  $g$ -modes can be described by sinusoidal temperature waves is justified (at least in a first approximation), then it should be possible (1) to quantitatively

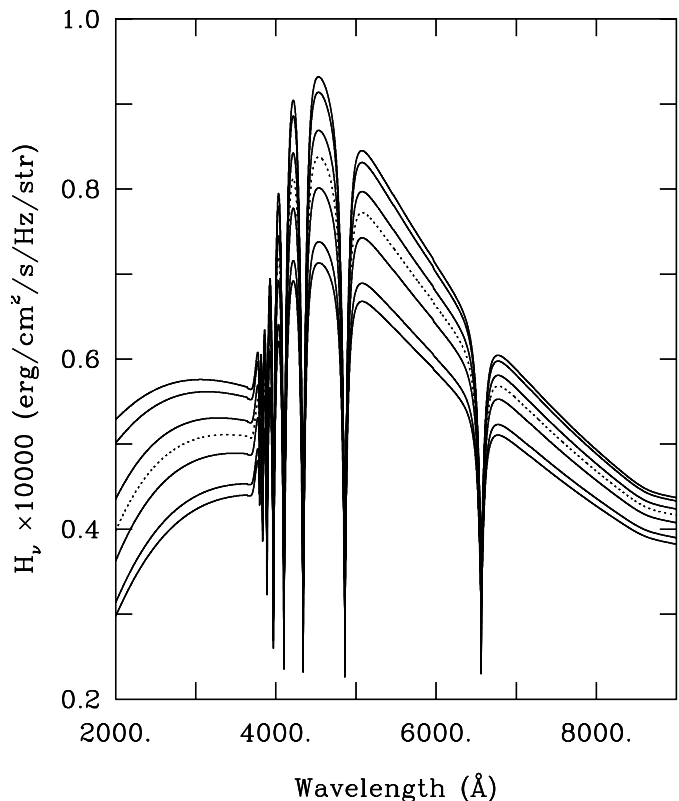


FIG. 36.—Computed instantaneous energy distributions for a typical DA white dwarf model ( $T_{\text{eff}} = 11,800$  K,  $\log g = 8.0$ ,  $\text{ML2}/\alpha = 0.6$  convection) undergoing a single  $g$ -mode pulsation. The solid curves represent six different phases equally spaced in time and covering a full pulsation cycle. The dotted curve shows the unperturbed emergent flux. The mode is modeled in terms of a pure temperature wave with an intrinsic amplitude of  $\epsilon_T = 0.3$ . The angular geometry of the mode is specified by  $l = 1$ ,  $m = 0$ , and  $i = 1$  radian.

explain the presence of nonlinear features in the observed light curves, and (2) to turn the table around and use the amplitudes of the nonlinear oscillations relative to those of their parent oscillations to infer the angular geometry of these modes, as well as their intrinsic amplitudes. This is precisely what Brassard et al. (1993) and Fontaine & Brassard (1994a) set out to do in the case of the ZZ Ceti star G117-B15A for which high sensitivity LAPOUNE/CFHT white light photometry had revealed the presence of at least eight nonlinear harmonic oscillations in addition to three basic modes.

Figure 37 summarizes their results. It shows the Fourier amplitude spectrum of the light curve of G117-B15A obtained at the CFHT. In addition to the largest frequency peaks  $f_1$  (215.2 s),  $f_2$  (270.5 s), and  $f_3$  (304.1 s) corresponding to independent pulsation modes, the Fourier spectrum also reveals the presence of at least eight nonlinear peaks. Two of these peaks are the first and second harmonics of  $f_1$ , while the six others are cross-frequencies of second and third order, again involving the dominant mode  $f_1$ . Plotted upside down is the Fourier spectrum of a synthetic light curve computed for

G117-B15A on the basis of only three input modes ( $f_1$ ,  $f_2$ , and  $f_3$ ) using the Brassard et al. (1995) approach. That synthetic light curve was sampled in the exact same way as the CFHT observations. The angular indices  $l$  and  $m$  of each of the three basic modes, their intrinsic amplitudes  $\epsilon_{T1}$ ,  $\epsilon_{T2}$ , and  $\epsilon_{T3}$ , and the inclination axis  $i$  were varied until a satisfactory agreement (as shown here) was reached between the “observed” Fourier spectrum and the “synthetic” one. We note that the agreement between theory and observations is indeed most remarkable, which bodes in favor of the Brassard et al. (1995) approach.

The most interesting outcome of this exercise has been the determination of the angular geometry of each of the three modes detected in G117-B15A, as well as the first measurements of their intrinsic amplitudes. Since the work of Brassard et al. (1993) and Fontaine & Brassard (1994a), progress has been made with the calibration of the mixing-length theory proposed by Bergeron et al. (1995) for the atmospheric layers, the  $\text{ML2}/\alpha = 0.6$  parametrization, and the values of the inferred parameters have thus been updated. The key results are (1) the three pulsation modes have the same set of angular indices, i.e.,  $l = 1$  and  $m = 0$ ,<sup>8</sup> (2) their intrinsic amplitudes are  $\epsilon_{T1} = 0.107$ ,  $\epsilon_{T2} = 0.030$ , and  $\epsilon_{T3} = 0.043$ , and (3) the inclination angle  $i$  between the pulsation axis and the line of sight is  $69.9^\circ$ .

We note that, to date, this remains the only example of a pulsating white dwarf for which the observed nonlinear structure has been accounted for quantitatively. That structure is solely due to distortions in the light curve caused by the nonlinear response of the emergent flux to a temperature perturbation. We stress that there are *several* other pulsating white dwarfs for which this technique could and should be applied. This is particularly true of all low-amplitude pulsators for which the approximation of a sinusoidal temporal dependence for the temperature wave is most likely to be justified. This includes a good 15 ZZ Ceti stars found in the hotter third of the instability strip. For more details on this technique, we recommend the paper of Fontaine & Brassard (1994a), which has a high pedagogical value.

When it comes to large-amplitude pulsators with their distinctive nonsinusoidal pulse shapes, other nonlinear effects come into the picture. And indeed, the nonlinear response of the flux to a simple sinusoidal temperature perturbation is insufficient, by itself, to produce those highly distorted pulse shapes. This simply implies that the *assumption* of sinusoidal temperature waves breaks down in these high-amplitude variables. However, in perturbation theory, the true temperature distribution can still be modeled in terms of a sinusoidal law, to which one adds perturbations expressed by its successive harmonics. Hence, given a recipe for computing the nonsinusoidal

<sup>8</sup> Note that the identification of  $f_1$  as a dipole mode is consistent with the analyses of Robinson et al. (1995) and Fontaine et al. (1996) using multicolor photometry.

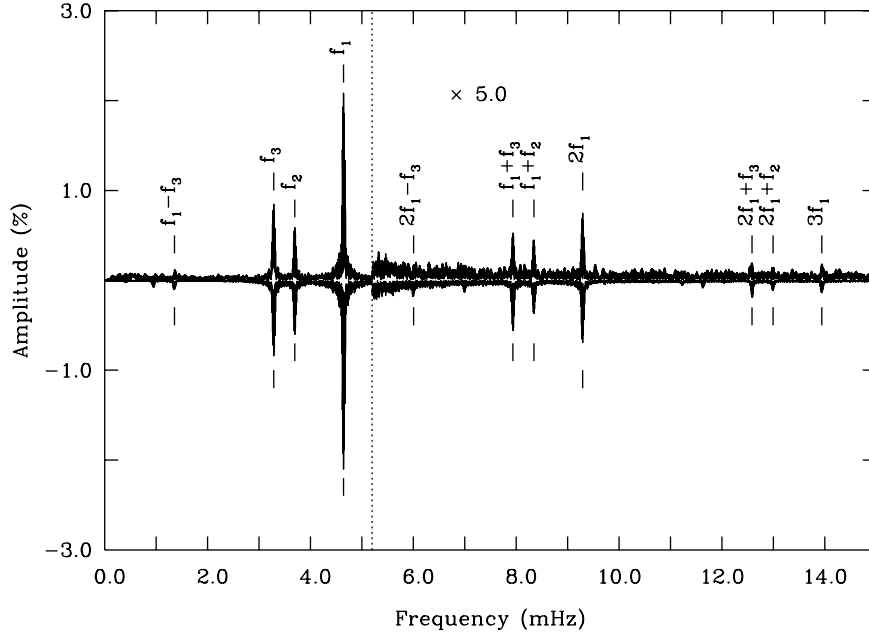


FIG. 37.—Fourier amplitude spectrum of the light curve of G117-B15A gathered in white light photometry using the LAPOUNE/CFHT combination over four consecutive nights. Three independent modes are detected as well as eight nonlinear peaks. Note that the nonlinear feature at  $2f_1 - f_3$  lies in the “wing” of the main mode; its presence makes no doubt after removing the  $f_1$  peak through prewhitening. Plotted upside down is the Fourier spectrum of a synthetic light curve computed for G117-B15A on the basis of only three input modes ( $f_1$ ,  $f_2$ , and  $f_3$ ) using the Brassard et al. (1995) approach. For better visualization, the amplitude scale has been multiplied by a factor of 5 for frequencies larger than 5.2 mHz.

temperature distribution, the same tools developed by Brassard et al. (1995) can readily be applied to produce realistic light curves for high-amplitude pulsators, including nonsinusoidal pulse shapes.

We illustrate this by using the example of the large-amplitude ZZ Ceti star GD 154 for which we have obtained high sensitivity white light observations at the CFHT. A segment of its light curve is depicted in Figure 20 (*top curve*). A total of 18.6 h of high-quality data were obtained over four consecutive nights. The light curve is dominated by a pulsation mode with a period of 1186.03 s. That mode is accompanied by at least its first five harmonics in the Fourier domain, which are easily detectable. By folding the light curves over the period of 1186.03 s, we get the pulse shape illustrated in Figure 38. It is given by the dots which also define the phase bins. Note that the folding technique hugely increases the S/N and that the formal uncertainties on the amplitude points are only about twice the size of a dot. The 1186.03 s mode in GD 154 has a pulse shape that shows a characteristic rapid rise followed by a slower decline as observed in many other large-amplitude pulsating white dwarfs. Note also the peak-to-peak amplitude, which is large by ZZ Ceti standards.

In the current absence of a credible physical prescription to predict the nonsinusoidal temperature distribution of the 1186.03 s mode observed in GD 154 (this is an area of research that we hope will be developed in the future), we decided to “model” it by using the apparent amplitudes and relative phases

of the mode and its first five harmonics. These quantities were obtained by fitting the observed light curves using a standard least-squares technique. Hence, the time dependence of the temperature wave that we used to describe the 1186.03 s mode is simply the superposition of the main sinusoidal variation and of five harmonics with relative amplitudes and phases fixed by the observational data.

Since, to first order, there is a degeneracy between the effects of changing the intrinsic amplitude and those of varying the inclination angle on the pulse shape (many modes must be analyzed simultaneously to derive independent values of  $\epsilon_T$  and  $i$ , such as in the case of G117-B15A discussed just above, for example), we thought that it would be sufficient here, in this demonstration, to fix the value of  $\epsilon_T$  at some appropriate value and vary  $i$ . In this way, we are able to reproduce the pulse shape if the mode has indices  $l = 1$  and  $m = 0$  and if the inclination angle  $i$  is near  $30^\circ$ . Note that we do *not* pretend that the real inclination angle of GD 154 is  $i \approx 30^\circ$ . In addition, the choice of angular indices is not arbitrary here, but has been inspired from the work of Pfeiffer et al. (1996). Our results are shown in Figure 38 where the dotted curves depict the predicted pulse shape as a function of the inclination angle for a fixed intrinsic amplitude. The predicted apparent amplitude is largest when  $i = 0^\circ$  and zero when  $i = 90^\circ$ , as appropriate for a nonradial mode with indices  $l = 1$  and  $m = 0$ .

Our purpose in the last demonstration was to show that we can, on the basis of the Brassard et al. (1995) method, explain

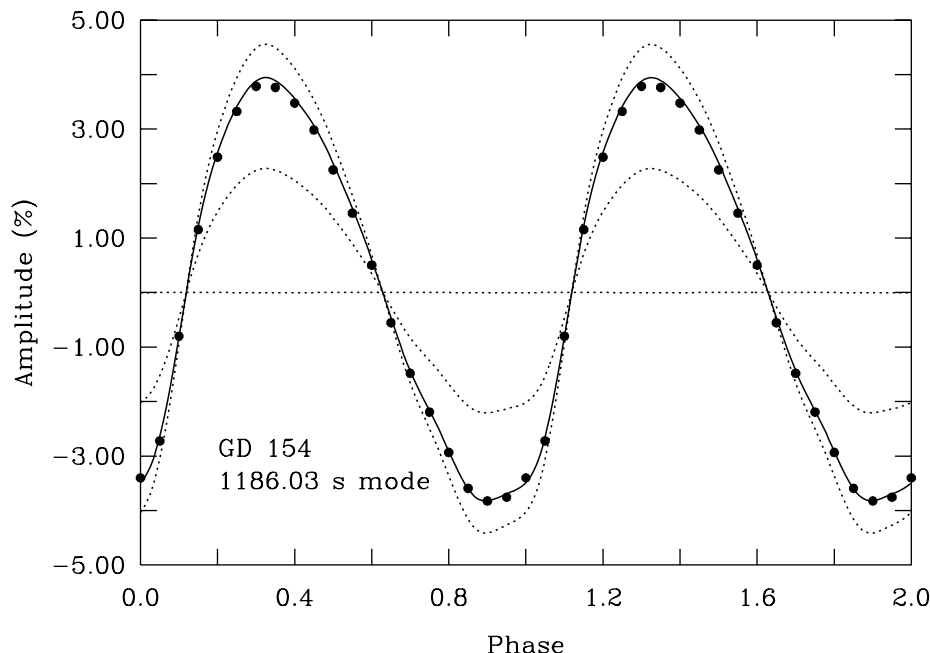


FIG. 38.—Pulse shape of the dominant pulsation mode observed in the light curve of the ZZ Ceti star GD 154 (*dots*), and models assuming various inclination angles, from 0 (largest predicted amplitude), 30°, 60°, and 90° (zero amplitude) as given by the dotted curves. The models also assume a mode with angular indices  $l = 1$  and  $m = 0$ . The inferred inclination angle is close to 30°.

the nonlinear pulse shape of modes observed in large-amplitude pulsators. As in the case of the nonlinear structure modeled above for G117-B15A, there is no need to explicitly invoke the presence of a convection zone. As far as the energy transfer process across the atmospheric layers is concerned, the effects of the convection zone are built-in within that method. As mentioned above, there are many types of pulsating stars with no envelope convection zone and yet showing nonlinear structure in their light curves. The example of the pulsating sdB star PG 1605+072 (see, e.g., Figs. 9 and 10 of Fontaine & Chayer 2006) is a spectacular reminder that highly nonlinear pulse shapes do not have to be associated with a superficial convection zone. Our insistence on this point may surprise the general reader, but we felt that this issue must be addressed because there are currently many in the specialized community who seem to believe that convection is a *sine qua non* condition for the presence of nonlinear effects in the light curves of pulsating stars (see, e.g., Wu 2001 or Montgomery 2005). Terms such as “convective harmonics” have been invoked to name, for example, the nonlinear features seen in the Fourier spectrum shown in our Figure 37.

These beliefs probably go back to the interesting papers of Brickhill (1992a, 1992b) who proposed a semi-analytic model to explain the nonlinear pulse shapes observed in large-amplitude ZZ Ceti stars. In his model, a sinusoidal pressure perturbation is applied at the base of a ZZ Ceti convection zone which acts as some sort of thermal buffer. The resulting temperature perturbation at the top of the convection zone (which lies in the atmo-

spheric layers) then assumes a nonsinusoidal behavior in this model. In essence, Brickhill (1992a, 1992b) has proposed a physical model to obtain a nonsinusoidal superficial temperature distribution, perhaps the missing recipe that we lamented above. However, in this approach, the presence of a convection zone is essential, and pulsating stars with radiative layers should not show highly nonlinear pulse shapes in their light curves if no other process than the nonlinear response of the convection zone comes in. This is contrary to observational evidence. Brickhill (1992a, 1992b) also linearized the flux perturbation, contrary to Brassard et al. (1995), and he could therefore not describe the nonlinear features coming from the energy transfer process across the atmosphere. Ultimately, the question is to ask if Brickhill’s model is able to reproduce, for example, the nonlinear structure in a star such as G117-B15A. Using the expressions computed by Wu (2001) who reexamined Brickhill’s model in more detail, we find that this is not possible. Indeed, from the amplitudes of the three independent modes observed in G117-B15A, and using the equations provided by Wu, it is impossible to account for the observed amplitudes of the eight nonlinear components seen in our Figure 37. This suggests to us that the pressure/temperature convective response model of Brickhill does not tell the full story for pulsating white dwarfs. In addition, as illustrated in our example for GD 154 in Figure 38, it is possible to reproduce quite well the pulse shape of a dominant mode in a large-amplitude ZZ Ceti star without invoking that specific model. Therefore, the fact that Montgomery (2005) was able to reproduce the pulse shape

of a large-amplitude mode in the ZZ Ceti G29–38 and another one in the V777 Her star PG 1351+489 on the sole basis of the Brickhill approach should not be considered as overwhelming evidence in favor of the validity of the approach. This is particularly true in the light of the fact that Montgomery (2005) has ignored completely the nonlinear response of the flux to temperature perturbations, a term that cannot be neglected in these two pulsators.

We do not suggest from the above discussion that the nonlinear response of the convection zone, when present, does not play a significant role in creating additional nonlinearities in the light curves of pulsating stars (those associated with nonsinusoidal temperature perturbations). We suggest instead that an improved physical model needs to be worked out, possibly on the basis of some of the seminal ideas first proposed by Brickhill or on some other original approach. We further suggest that a search for a mechanism able to produce nonsinusoidal temperature variations in radiative envelopes be carried out. We finally suggest that the nonlinear response of the emergent flux to temperature perturbations should *always* be included when modeling light curves of pulsating stars.

### 7.3. Rotational Splitting

Rotation destroys the spherical symmetry of a star and, in the case of a pulsating star, lifts the  $(2l + 1)$ -fold frequency (period) degeneracy of a pulsation mode specified by its radial order index  $k$  and its degree index  $l$ . In an ideal case, this leads to  $2l + 1$  detectable frequency components in the Fourier domain and thus, in principle, to the identification of the  $l$  and  $m$  angular indices of a mode. In practice, things are not that easy because the limited temporal resolution and the finite sensitivity of a given set of observations, combined with unfavorable viewing angles, may not reveal all of the components of a rotationally split frequency multiplet. In addition, although it is possible, again in principle, to infer the inclination angle  $i$  of the pulsation axis with respect to the line of sight by comparing the relative amplitudes of the  $m$  components within a multiplet (see, e.g., Fig. 1 of Brassard et al. 1995), this approach *never* works in practice because it requires the intrinsic amplitudes of all multiplet components to be the same, something that nature apparently does not like to provide. Still, rotational splitting is a phenomenon frequently observed in pulsating white dwarfs, and it has been very useful for identifying the angular indices of a large number of modes in many stars.

For the GW Vir pulsators, the observational study of the class prototype PG 1159–035 carried out by Winget et al. (1991) remains the classic reference and a model in the field. Rotational splitting was easily observed in a large number of modes through frequency triplets and quintuplets. Modes with values of  $l = 1$  and  $m = -1, 0, \text{ and } +1$  were formally identified in 20 cases, and quadrupole modes with their  $m$  components (a few of them missing sometimes) were identified in eight instances. The average frequency spacing between adjacent  $m$  components of

dipole modes was found to be  $4.22 \pm 0.04 \mu\text{Hz}$ , and that of quadrupole modes  $6.92 \pm 0.07 \mu\text{Hz}$ . This led to an estimate of the rotation period of  $1.38 \pm 0.01$  days. We note that, up to now, PG 1159–035 remains the pulsating white dwarf in which the largest number of pulsation modes has been found. To add a small item of triviality in this connection, PG 1159–035 was claimed in the past to be the pulsating star with the most detected modes after the Sun. It may now have lost this status following the discovery of a plethora of oscillations in the light curve of the pulsating sdB star PG 1605+072 (Kilkenny et al. 1999; Billères 2000).

Rotational splitting was also observed early on in the Fourier transform of the light curve of GD 358, the class prototype of the V777 Her pulsators (Winget et al. 1982b). Another outstanding data set, comparable in quality to that obtained earlier for PG 1159–035, was gathered several years later on GD 358, again through the Whole Earth Telescope (WET) as reported in Winget et al. (1994; also see Bradley & Winget 1994). All three of the  $m$  components of rotationally split dipole modes were formally identified in nine cases, and evidence for the presence of  $l = 2$  modes was also presented. In the latter case, the much lower observed amplitudes of the  $l = 2$  multiplet components prevented the formal identification in terms of the azimuthal index  $m$  ( $-2, -1, 0, +1, +2$ ), but there is little doubt that the identification of these frequency structures as rotationally split quadrupole modes is correct. Of great interest, it was also observed that the frequency spacing between adjacent  $m$  components in the triplet series increases with increasing radial order  $k$  from  $\sim 3.5$  to  $\sim 6.5 \mu\text{Hz}$ . Interpreted initially as the signature of very significant differential rotation between the core and the outer envelope of GD 358, this interpretation was found to be premature by Kawaler et al. (1999). In fact, it is very likely wrong,<sup>9</sup> and this interesting phenomenon has remained a puzzle, although Goupil et al. (1998) have proposed a possible solution in terms of nonlinear physics.

In the case of ZZ Ceti stars, but also in the more general context of pulsating white dwarfs, it would appear that the first suggestion for rotational splitting was made by McGraw & Robinson (1975) who commented on the even spacings observed between five frequency components in the Fourier spectrum of their light curve of G29–38. Since then, several other reports on rotational splitting in ZZ Ceti stars have been put forward. In this publication we provide an example of our

<sup>9</sup>There are a number of reasons to dispute this interpretation, but this is not the proper forum to discuss these. On more fundamental grounds, significant differential rotation is not expected in white dwarfs in general as argued convincingly by Tassoul & Tassoul (1983), but it would seem that this work has been largely ignored by many. An interesting counterexample, so to speak, is that of the ZZ Ceti star L19–2 (O’Donoghue & Warner 1982, 1987), which shows a rotationally split dipole mode with an asymmetry in frequency spacing about the central component that can be very well explained solely in terms of solid body rotation, but pushed to second order in the perturbation expansion (Brassard et al. 1989).

own, based on nearly 19 h of high sensitivity integrated light photometry of Ross 548 (ZZ Ceti itself) using the LAPOUNE/CFHT combination. Our choice of Ross 548 as an illustration is not innocent by any means, and we picked it because that star has often been depicted in the past as the prototypical case for a pulsating star undergoing *magnetic splitting*. As well explained in the theoretical paper of Jones et al. (1989), a large scale magnetic field of sufficient strength also destroys the spherical symmetry of a star and perturbs the pulsation periods. However, magnetic splitting of a mode with index  $l$  has its own specific signature, leading to  $l + 1$  frequency components in the Fourier domain as compared to  $2l + 1$  components for rotational splitting. Since the thesis work of McGraw (1977), it has been known that the light curve of Ross 548 is dominated by a pair of close pulsational doublets in the Fourier domain centered on 213 and 274 s, respectively. Hence, it has been very tempting to associate those doublets with dipole modes split by a magnetic field. A search for such a field was carried out by Schmidt & Grauer (1997) using spectropolarimetry, but none was detected and their upper observational limit was one order of magnitude below the minimum field strength required to produce substantial splitting.

There have been several explanations proposed to account for this small mystery, including the invocation of unusual field geometries, but the simplest of them all is that Ross 548 is not magnetic at all (at least at a level that would be significant to affect its global shape) and the famous frequency “doublets” are, in reality, triplets with a central component too small to have been detected from photometric runs on small telescopes. Our Figures 39 and 40 demonstrate vividly this point. For each multiplet structure, we show the prewhitening sequence in the Fourier domain, which leaves no doubt as to the existence of a central component. Note, in this context, the very low noise level in our CFHT observations. That level can be estimated from the lower curve in each figure and, compared to it, the amplitudes of the central frequency components are  $13\sigma$  detections. Hence, while the 213.133–212.768 s pair and the 274.251–274.775 s pair have been known for years, their smaller central components at 212.956 s and 274.528 s, respectively, have been missed in all previous observations. We thus propose that the 213 and 274 s structures observed in the light curve of Ross 548 are dipole modes split by rotation. The average frequency spacing between  $m$  components in the 213 s multiplet is  $4.0\ \mu\text{Hz}$ , while it is  $3.5\ \mu\text{Hz}$  in the 274 s multiplet. This immediately leads to an estimate of the rotation timescale of Ross 548 of the order of 37 h (a better estimate would, of course, require the computation of the rotation coefficient  $C_{kl}^r$  for each mode).

The finding that the 213 and 274 s “doublets” in Ross 548 are, in reality, rotationally split dipole modes with a smaller central component leads us to question the validity of applying the so-called  $O - C$  method to measure rates of period change when ignoring a component of a frequency multiplet. The  $O - C$  method works best if the signal is “monochromatic,” but if

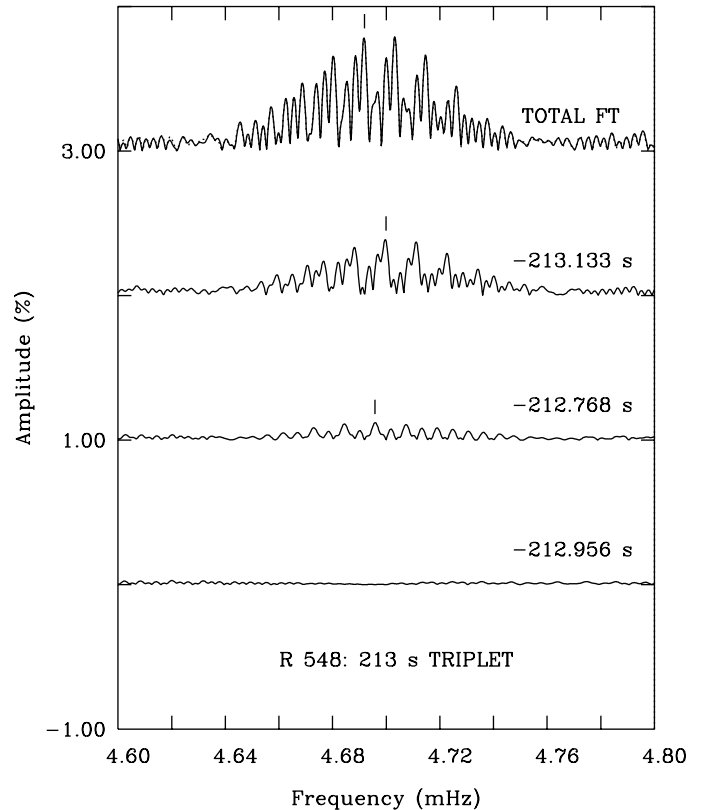


FIG. 39.—Fourier amplitude spectrum of the 213 s frequency complex observed in the light curve of the pulsating DA white dwarf Ross 548. The figure shows the prewhitening sequence that reveals a neat triplet structure, presumably a dipole mode split by rotation. The input light curves were obtained in white light using LAPOUNE attached to the CFHT. Nearly 19 h covering four consecutive nights were gathered.

one attempts to measure the times of arrivals of the pulses of a particular frequency component while ignoring the presence of a very nearby pulsation, a frequency modulation can result, completely skewing the value of the inferred rate of period change. This may explain the very puzzling results obtained by Mukadam et al. (2003) on precisely Ross 548. In that paper, the authors struggled with the difficulties of obtaining coherent values of the rates of period change  $dP/dt$  for each of the components of the 213 and 274 s “doublets.” In the end, they found an average rate for the 213 s complex in general agreement with the expectation of cooling theory, but the rate for the 274 s complex turned out, against all expectations, to be some 2 orders of magnitude higher. The authors proposed some possible explanations, but none appears very convincing in our view. We suggest instead to be particularly wary of these difficult measurements if the “purity” of the frequency investigated cannot be guaranteed. The same applies to the ZZ Ceti star G115–B15A (see Kepler et al. 1991, 2005b), and caution should be used when interpreting the derived  $O - C$  measurement because the 215.2 s pulsation mode that was monitored is

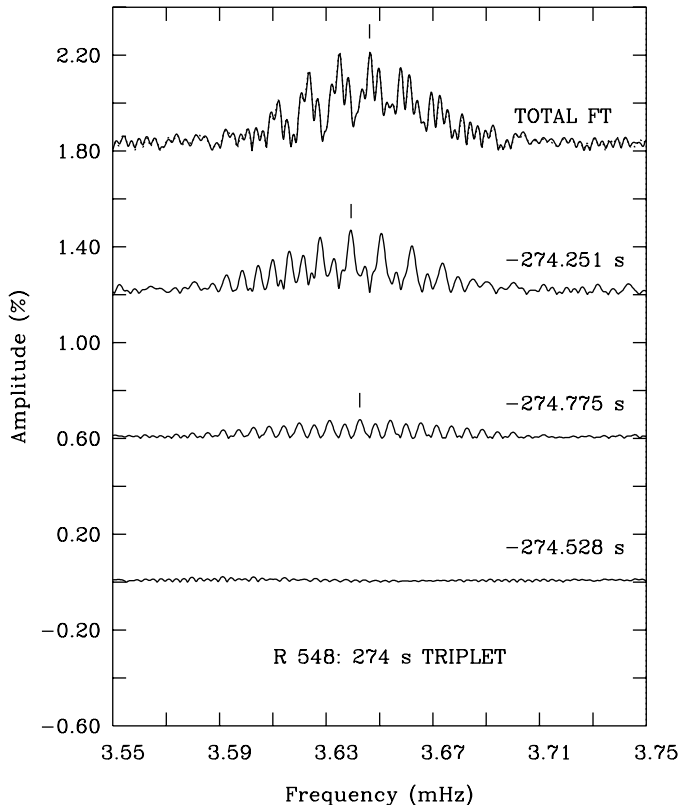


FIG. 40.—Similar to Fig. 39, but for the 274 s complex.

not a pure harmonic oscillation but, in reality, reveals itself as the central dominant component of a dipole mode (presumably) split by rotation when observed at very high sensitivity. We recall also that the  $O - C$  method failed in the case of the 516 s pulsation monitored for many years in PG 1159–035; it consistently gave the *wrong sign*. It was only when enough time had elapsed for the period to have increased sufficiently for the difference to be measured directly (see Costa et al. 1999) that the “correct” sign was recovered. Unfortunately, the direct method may remain out of reach for the pulsating DB and DA white dwarfs because they evolve much more slowly than GW Vir stars.

To end this discussion on rotational splitting, we find it interesting to point out that it leads, at least in principle, to the most convenient and reliable way for estimating rotation periods in white dwarfs in general, because pulsating white dwarfs are fully representative of the whole population (recall, for instance, that the ZZ Ceti instability strip is populated solely by pulsators). The reason for this state of affairs is that the classic method for inferring projected equatorial velocities in stars by measuring the rotational broadening of spectral lines does not work very well in white dwarfs. This is because the huge pressure broadening in the atmospheres of these stars simply masks the comparatively small contribution of rotational broad-

ening to the line profiles. To be fair, it is still possible to apply the classic spectroscopic method to the narrow NLTE cores of spectral lines in white dwarfs, but this requires very high resolution spectral observations and, therefore, has been limited to a handful of very bright white dwarfs.

There is also another way of inferring the rotation period of a white dwarf, and that is to measure its cyclic polarization state if the star, of course, has a magnetic field. However, it is not clear at all if magnetic white dwarfs (making up some 10% of isolated white dwarfs) are representative of the class, especially vis-à-vis the phenomenon of magnetic braking. In comparison, rotation periods (and not only  $V \sin i$ ) have so far been inferred from asteroseismology for some 14 white dwarfs, and efforts are ongoing. Table 4 presents a compilation of what can be found on the subject in the literature. We do not guarantee the reliability of all these values, but simply report what has been presented. The current results indicate that, as a class, isolated white dwarfs are extremely slow rotators and have lost essentially all of their angular momentum during previous evolutionary phases (likely to be associated with the mass loss episodes during the RG and AGB phases). Periods ranging from several hours (which is very slow from a dynamical point of view in a compact star such as a white dwarf) to days and more have been inferred.

## 8. ASTEROSEISMOLOGY

The study of pulsating stars is a fascinating topic in its own right. Indeed, one would certainly like to know why and how these stars do what they do. It can be argued, however, that asteroseismology has a more “practical” aspect and that its ultimate goal is the determination of the fundamental structural parameters of a star. In its most basic form, asteroseismology exploits the structural information contained in the periods of the pulsation modes extracted from light or radial velocity curves. Because linear pulsation theory in the adiabatic approximation can generally provide accurate estimates of the pulsation periods of stellar models, this approach is usually employed to calculate modes to be compared with given sets of observed periods. The goal is to find a model which has a theoretical period spectrum that matches a set of observed periods as closely as possible. If such a model is found, the hope is that the model provides a good representation of the physical properties of the real pulsating star. Of course, the level of confidence with which one can accept an asteroseismological solution is directly proportional to the quality (read realism) of the input stellar models and the care taken in the search for the optimal model in parameter space.

### 8.1. Period Spectra and Variations in Model Parameters

Before briefly reviewing the results of white dwarf asteroseismology, it is extremely instructive to examine how the periods of pulsating white dwarfs depend on the structural parameters of these stars. This issue has been examined

TABLE 4  
THE PULSATING WHITE DWARFS WITH INFERRED ROTATION PERIODS

Star	Type	$P_{\text{rot}}$ (h)	Reference
Ross 548 .....	ZZ Ceti	37	this work
HL Tau 76 .....	ZZ Ceti	53	Pech et al. 2006
GD 154 .....	ZZ Ceti	55	Pfeiffer et al. 1996
GD 165 .....	ZZ Ceti	50	Bergeron et al. 1993
L19–2 .....	ZZ Ceti	13	Bradley 2001
G226–29 .....	ZZ Ceti	9	Kepler et al. 2005a
G185–32 .....	ZZ Ceti	15	Pech & Vauclair 2006
GD 358 .....	V777 Her	29:	Winget et al. 1994
PG 0122+200 .....	GW Vir	37	Fu et al. 2007
NGC 1501 .....	GW Vir	28	Bond et al. 1996
PG 1159–035 .....	GW Vir	33	Winget et al. 1991
PG 1707+427 .....	GW Vir	16–31	Kawaler et al. 2004
PG 2131+066 .....	GW Vir	5	Kawaler et al. 1995
RXJ2117.1+3412 .....	GW Vir	28	Vauclair et al. 2002

thoroughly for DA stars in a series of papers by Brassard et al. (1991, 1992a, 1992b, 1992c), for DB stars by Bradley et al. (1993), and for PG 1159 stars by Kawaler & Bradley (1994, and see also Córscico & Althaus 2006 for a updated view), but there is still much to learn from addressing the question in the broader perspective of the three classes of stars. For white dwarfs, the pulsation periods are specified primarily by the total mass, the effective temperature, and the envelope layering. To illustrate the various dependencies of the pulsation periods on these model parameters for each type of pulsating white dwarfs in a uniform way we constructed a template model, computed its pulsation spectrum, and then varied the basic structural parameters and examined the effects on the periods in the same way.

To conduct this experiment properly, we first considered the full ranges of basic parameters in which pulsating white dwarfs are found. This is summarized in Table 5. For instance, we find that white dwarf pulsators have masses between  $0.5 M_{\odot}$  and  $1.1 M_{\odot}$ , corresponding to a range  $\Delta M = 0.6 M_{\odot}$ . Likewise, the fractional mass of the outer H layer in ZZ Ceti pulsators may vary from  $\log q(\text{H}) = -4$ , to  $\log q(\text{H}) = -14$ ., corresponding to a range  $\Delta \log q(\text{H}) = 10$ . dex; and so on. To be meaningful, our numerical experiment consists in varying each basic model

parameter by the *same relative amount*, thus producing the variations  $\delta$  listed in Table 5. We arbitrarily chose a relative variation of  $|16.7|\%$ . The question then is how varying the basic model parameters over the same relative intervals compared to the full ranges over which they are found affects the period spectrum.

We first considered a GW Vir star model that could be representative of a pulsator such as PG 0122+200 near the high-gravity red edge of the instability domain. We assumed a total mass of  $M = 0.6 M_{\odot}$ , an effective temperature of  $T_{\text{eff}} = 78,000$  K, and a He/C/O envelope on top of a C/O core containing a mass fraction  $\log q(\text{He}) = -2.0$ . We next computed the (adiabatic) period spectrum of that reference model for dipole modes in the range of periods from 50 to 1000 s. The lower limit of 50 s was sufficient to always include the shortest-period mode with  $k = 1$  in this and the other models considered. We then repeated the exercise for additional models in which (1) the mass was decreased to  $0.5 M_{\odot}$ , (2) the He/C/O envelope mass was decreased to  $\log q(\text{He}) = -2.33$ , and (3) the effective temperature was increased by 15,000 K (see Table 5). In all three cases, only one parameter was varied at a time, the others keeping their standard values defined by the reference model. In order to assess the impact of these variations, we finally computed for each pulsation mode—defined by its radial order  $k$ —the period difference between the period obtained for a “perturbed” model and that calculated for the reference model. For the V777 Her case, the reference model was defined by a total mass of  $M = 0.6 M_{\odot}$ , an effective temperature of  $T_{\text{eff}} = 24,000$  K, and a He envelope on top of a C/O core containing a mass fraction  $\log q(\text{He}) = -2.0$ . For the reference ZZ Ceti model the chosen parameters were  $M = 0.6 M_{\odot}$ ,  $T_{\text{eff}} = 11,800$  K,  $\log q(\text{He}) = -2.0$ , and  $\log q(\text{H}) = -6.0$ .

The results of this experiment for GW Vir models are shown in the upper part of Figure 41 where we plotted, for each of the three perturbed models, the period difference with respect to the period of the pulsation mode in the reference model. As can be seen clearly, the effects of varying the total mass largely dominate those of varying the mass of the outer He/C/O envelope or the effective temperature. Most interestingly, however, this dominance of the mass diminishes in importance when going down the cooling track in the HR diagram. Indeed, the middle

TABLE 5  
RANGES OF BASIC PARAMETERS FOR PULSATING WHITE DWARFS

Parameter	Type	Values	Range $\Delta$	Variation $\delta$ (16.7%)
mass ( $M_{\odot}$ ) .....	all	0.5–1.1	0.6	0.1
	ZZ Ceti	11,000, 13,000	2000	333
$T_{\text{eff}}$ (K) .....	V777 Her	23,000, 27,000	4000	667
	GW Vir	80,000, 170,000	90000	15000
	ZZ Ceti	–2., –12.	10.	1.67
$\log q(\text{He})$ (dex) .....	V777 Her	–2., –12.	10.	1.67
	GW Vir	–2., –4.	2.	0.33
$\log q(\text{H})$ (dex) .....	ZZ Ceti	–4., –14.	10.	1.67

part of Figure 41 shows the results of a similar experiment but, this time, using representative models of V777 Her stars. It is clear that the effects of varying the mass on the period spectrum are less important in V777 Her models than in GW Vir stars relatively speaking. This is even more pronounced for the even cooler ZZ Ceti stars as can be observed in the lower part of the figure. In that case, variations of the mass of the outer H layer even slightly dominate the variations of the total mass. We point out that the effects of varying the H-layer mass by a given amount are more important on the period spectrum than the effects of varying the He-layer mass by the same amount in a ZZ Ceti model because the contrast in mean molecular electronic weight  $\mu_e$  is larger between the H layer ( $\mu_e = 1$ ) and the He envelope ( $\mu_e = 2$ ) than between that envelope and the C/O core (also material with  $\mu_e = 2$ ). This directly affects the run of the

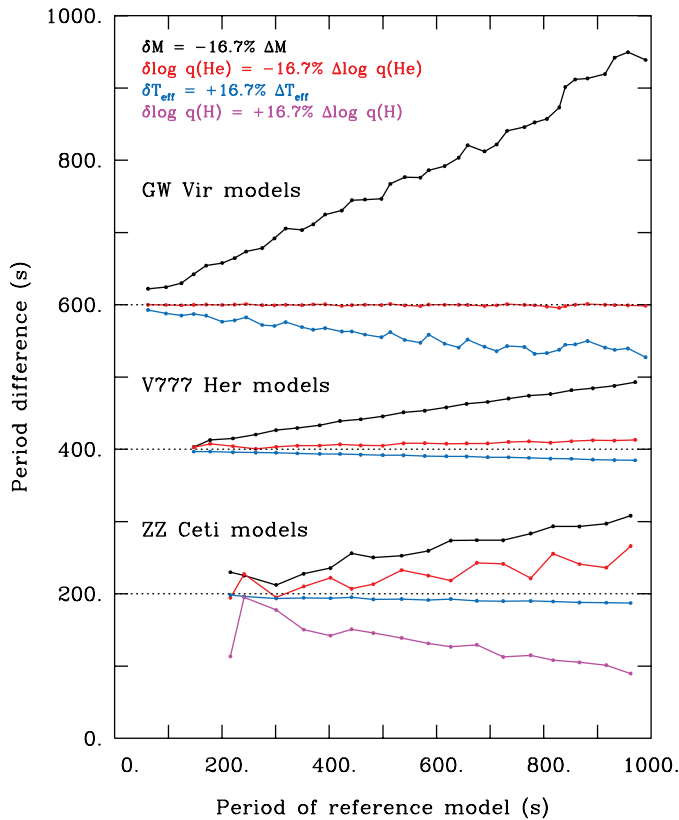


FIG. 41.—Differential effects of varying a number of model parameters on the theoretical  $g$ -mode period spectra of pulsating white dwarfs. For each type of pulsating white dwarfs, a representative reference model was built and its  $l = 1$  period distribution was computed for modes in the 50–1000 s interval. The black curves show the relative period spectra for models with a total mass decreased by the 16.7%  $\delta$  variation given in Table 5 ( $0.1 M_{\odot}$ ). The red curves refer to models with a He envelope mass decreased by the 16.7%  $\delta$  variation given in Table 5 (0.33, 1.67, and 1.67 dex for GW Vir, V777 Her, and ZZ Ceti models, respectively). The blue curves refer to models with an effective temperature increased by the 16.7%  $\delta$  variation again listed in Table 5 (15,000, 667, and 333 K for GW Vir, V777 Her, and ZZ Ceti models, respectively). The magenta curve refers to an increase of 1.67 dex of the H-layer mass in a ZZ Ceti model.

Brunt-Väisälä frequency and, therefore, the period distribution (for more details, see Brassard et al. 1992c).

Figure 41 demonstrates that, on a relative scale, the “information” that can be extracted from the pulsation periods of GW Vir stars primarily concerns the total mass. Hence, one can expect GW Vir adiabatic asteroseismology would lead to relatively accurate determinations of the total mass given proper equilibrium models, but at the expense of other parameters such as envelope layering and effective temperature. In contrast, for the ZZ Ceti stars, the information content is mostly shared between the total mass and the H and He envelope layering, meaning that these parameters could be inferred at a comparable level of accuracy, although it could be difficult in practice to untangle the individual effects of these various parameters. We note that the effective temperature derived from quantitative spectroscopy is less well constrained for GW Vir and V777 Her stars than for ZZ Ceti stars even on a relative scale, so this should be kept in mind in the context of the present discussion. We thus find that the three types of pulsating white dwarfs offer somewhat different asteroseismological potentials, and these differences are directly related to the outward migration of the  $g$ -mode formation zone resulting from the cooling process which produces ever increasing degenerate configurations from the GW Vir phase to the ZZ Ceti phase (recall our discussion around Fig. 8 above). In fact, in a GW Vir model, the so-called weight function of a mode is concentrated in the core (which contains some 99% of the total mass in our reference model above), meaning that the  $g$ -modes in such star probe the interior and not the outer envelope. That their periods are mostly sensitive to the total mass and not to the details of the outer envelope should not be surprising. In comparison, the region of period formation in a V777 Her model extends into the envelope from below, and the phenomenon is amplified in an even cooler ZZ Ceti star model. The periods then become sensitive to structural details there, such as envelope layering.

In this context, it is perhaps appropriate to point out that the fact that the three families of pulsating white dwarfs offer different asteroseismological capacities may not have been appreciated by some investigators in the past. We especially have in mind those who have tried to apply a method based on average period spacings to ZZ Ceti stars and used this to estimate the total mass. This method has, in fact, been developed for the GW Vir stars and only applies to those. Our results in Figure 41 clearly show that, for ZZ Ceti stars, periods and period spacings must depend strongly not only on the mass, but also on the H and He layering. The estimates of inferred masses for ZZ Ceti stars based on the average period spacing method are therefore of dubious value.

In the context of this section, we think it is highly instructive to push further and examine how the periods of pulsating white dwarfs may depend on other structural parameters beyond total mass, envelope layering, and effective temperature. In principle, and although this may be more difficult because their effects on

the periods are smaller, such extra parameters could also be measured in real pulsating stars through an application of the asteroseismological method. We carry out this illustrative exercise with the use of ZZ Ceti star models. Our approach is the same as in the previous discussion; i.e., we compute a reference model and then vary one parameter at a time to investigate the response of the  $g$ -mode period spectrum. We picked a standard ZZ Ceti model defined by  $T_{\text{eff}} = 11,800$  K,  $M = 0.6 M_{\odot}$ ,  $\log q(\text{He}) = -2.0$ , and  $\log q(\text{H}) = -5.0$ . In addition to these quantities, the model is further specified by the assumption of a pure C core, the use of the ML2 version of the mixing-length theory, and the supposition that the composition transition zones between the H and He layers and the He mantle and the core can be modeled within the framework of diffusive equilibrium.

Let us first focus on the group of curves distributed about a period difference of zero in Figure 42. The latter summarizes the results of our numerical experiment. The effects of He layering are again shown by the red curves, but for variations of  $\pm 0.5$  dex about the value of  $\log q(\text{He}) = -2.0$  in the reference model. Likewise, the magenta curves illustrate the important effects of varying the H-layer mass from  $\log q(\text{H}) = -4.0$  below the zero value to  $-6.0$ ,  $-7.0$ ,  $-8.0$ , and  $-9.0$ , from bottom to top above. These approximately cover the wide range of values that have been inferred in ZZ Ceti stars so far. The blue curves show the deviations for variations of  $\pm 350$  K in effective temperature about the reference value, and the black curves show the same for variations in mass corresponding to the spectroscopic uncertainties of  $\Delta \log g = \pm 0.05$  dex via the well-known mass-radius relationship.

The effects of varying the mass according to the spectroscopic uncertainties in  $\log g$  are reproduced (*black curves*) in the lower set of curves shown in Figure 42. These have been displaced vertically by an arbitrary amount to avoid total confusion with the first group of curves. The black curves encompass the effects on the period spectrum produced by varying the following other parameters. First, the effects of varying the core composition are shown by the three red curves. The one at the top corresponds to a model with a pure O core, while the one just under corresponds to a uniform C/O core mixture of 50/50 proportions in mass fraction. Clearly, the signature of the core composition on the period spectrum appears very weak for these models. However, the prospects for measuring the core composition through asteroseismology improve if the distribution of the C/O ratio in real stars is not uniform in the core. For example, Salaris et al. (1997) have evolved detailed models from the main sequence to the white dwarf stage and predict that the chemical composition in the C/O core of a white dwarf is generally not uniform (see, e.g., Figs. 6 and 7). Using one of their chemical profiles, we obtained the lower red curve showing a relatively small but quite significant signature on the period spectrum. The reason that this imprint is more important than in the uniform composition models is because the *variable* com-

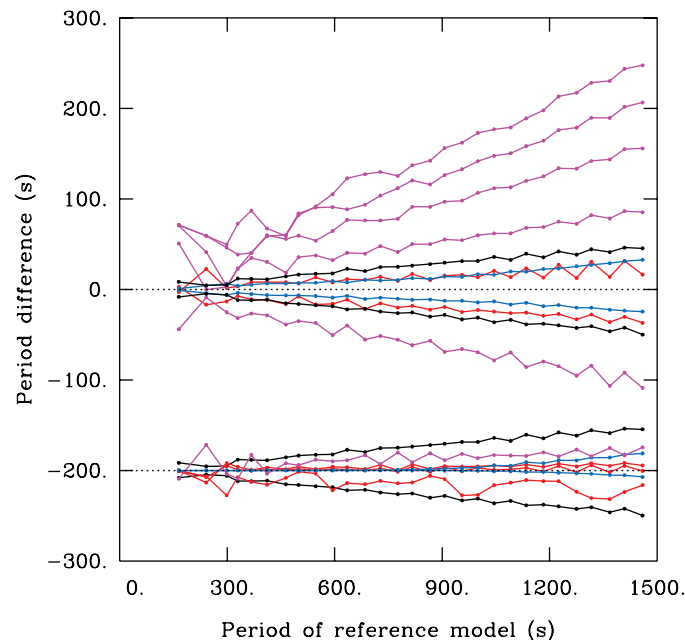


FIG. 42.—Differential effects of varying a number of model parameters on the theoretical  $g$ -mode period spectrum of a representative ZZ Ceti star model. All dipole modes in the 50–1500 s interval were computed. The first group of curves refers to variations of  $M$  (*black curves*),  $T_{\text{eff}}$  (*blue curves*),  $\log q(\text{He})$  (*red curves*), and  $\log q(\text{H})$  (*magenta curves*). The second group of curves in the lower half of the plot refers to variations of the total mass (*black curves*), core composition (*red curves*), convective efficiency (*blue curves*), and compositional transition zone profiles (*magenta curves*). See text for details.

position introduces an extra contribution to the local Brunt-Väisälä frequency and, hence, perturbs the period distribution (see, e.g., eq. [14] of Brassard et al. 1991). Second, the blue curves show the (small) effects of varying the parametrization of the mixing-length theory from ML1 (the negative values) to ML3 (the positive values). The general effect of increasing the convective efficiency is to increase the period of a mode, but only by a small amount, probably difficult to detect in practice. And third, the magenta curve shows the effects of relaxing the assumption of diffusive equilibrium in the computations of the compositional transition zone profiles. In our experiment, we arbitrarily increased the scale height of these zones by a factor of 2 to simulate the approach to diffusive equilibrium. As in the case of the nonuniform core chemical composition, diffusion produces small but not necessarily negligible effects on the period structure of a ZZ Ceti star. The importance of diffusion on the formation of the mechanical structure and, consequently, on the period structure of white dwarfs has been underlined by Fontaine & Brassard (2002) for V777 Her stars and by Córscico et al. (2002) for ZZ Ceti stars. Earlier considerations to this effect were also given by Dehner & Kawaler (1995). More recently, Brassard & Fontaine (2006) have presented evidence in favor of ongoing diffusion in the ZZ Ceti star GD 165 on the basis of their asteroseismological analysis of the star. Hence,

the potential for inferring other structural properties beyond the mass, the envelope layering, and the effective temperature does exist for pulsating white dwarfs. Whether this can be achieved in practice depends to a large degree on the particular star to be studied. A very important point in this connection is that the strongest signatures of the various parameters occur for low-order modes as can be seen in Figures 41 and 42, particularly for the ZZ Ceti stars. There is clearly more information content in the lowest-order modes, which show more complicated individual pulsation spectra, than in the high-order modes, which tend to show a fairly regular structure when approaching the asymptotic regime. Hence, the prospects for a successful asteroseismological exercise are generally better for a pulsating white dwarf showing the first few modes of its  $g$ -branch than for another object showing perhaps many more periods but corresponding to medium-order modes. To complement this brief study of the effects of varying the model parameters, we refer the reader to Fontaine & Brassard (1994b) who provided a detailed discussion of the reaction of the period spectrum of a representative ZZ Ceti model to variations in the constitutive physics (envelope and core equation of state, radiative opacity, conductive opacity, description of convection).

## 8.2. Current Asteroseismological Results

For the convenience of the reader, we have compiled all of the results claimed so far from white dwarf asteroseismology, hoping that we have not missed any significant one (and our apologies to the authors if we did). Tables 6 and 7 summarize this compilation. Column (1) of Table 6 (which refers to GW Vir and V777 Her stars) gives the name of the pulsating white dwarf, column (2) gives the inferred value of the total mass, and column (3) lists the inferred value of the fractional mass of the He or He-rich mantle. Note that in the case of GD 358, Fontaine & Brassard (2002) have emphasized the double-layered structure (a pure He envelope surrounds a mantle made of He/C/O, which itself surrounds a C/O core) that more realistic models of DB white dwarfs must feature when taking diffusion into account. In that case, there are two composition transition zones, and their respective fractional masses are indicated (the pure He envelope has a fractional mass of  $10^{-5.8}$ , and the He/C/O mantle has a fractional mass of  $10^{-3.0}$ ). The next columns indicate the inferred effective temperature, total luminosity, distance, and magnetic field strength. The next-to-last column lists other inferred properties as applicable, and the last one gives a reference to the analysis paper. In the case of the ZZ Ceti stars (Table 7), we eliminated the magnetic field column (since magnetic fields have not been quoted for these stars) and in the second column instead entered the primary quantity coming out of DA asteroseismology, i.e., the fractional mass of the outer H layer,  $\log q(\text{H})$ . Note that asteroseismological inferences have thus been made so far for 5 GW Vir, 2 V777 Her, and 10 ZZ Ceti stars. To these, we must

add NGC 1501 (Bond et al. 1996) for which a rotation period has been inferred as indicated in our Table 4.

We wish to point out that we compiled the results summarized in Tables 6 and 7 with some reluctance because the various claims do not all rest on the same solid uniform grounds as one would wish in an ideal situation. In fact, some of the claims, such as the detection of important differential rotation and the determination of a magnetic field of  $\sim 1300$  G in the pulsating DB star GD 358 (Winget et al. 1994), are unfounded in our opinion. Others, such as the determination of a high oxygen content in the core of GD 358 and its concomitant constraint on the rate of the  $^{12}\text{C}(\alpha, \gamma)^{16}\text{O}$  reaction rate (Metcalf et al. 2001), are, at best, premature (see Fontaine & Brassard 2002). Likewise, the claim that crystallization theory has been tested in the massive ZZ Ceti star BPM 37093 (Metcalf et al. 2004) and that more than 90% of that star is solidified has been challenged by us using more detailed and realistic models (Brassard & Fontaine 2005). We find instead, on the basis of the available period data for BPM 37093, that the likely value of the fraction of solidified matter in BPM 37093 is substantially less than 90% and, more importantly, cannot be pinned down with any reasonable accuracy.

Beyond these specific cases, the reliability of the various inferences listed in Tables 6 and 7 is clouded by issues such as the quality of the input equilibrium models used in past asteroseismological exercises, and how the “best” model was ultimately found. An example concerning the issue of the quality of the models is provided by the GW Vir stars that have been analyzed so far. Until very recently, all previous analyses had been based on the same equilibrium models (those computed by Kawaler & Bradley 1994 in their original study). However, our knowledge of the born-again, post-AGB evolutionary phases has, in the meantime, radically improved, thanks primarily to the pioneering work of Herwig et al. (1999) who were the first to be able to produce stellar descendants of these phases with the correct PG 1159 atmospheric chemical composition. Hence, there was an obvious need to redo the asteroseismological analyses of the available GW Vir period data sets in the light of these developments. In a remarkable effort, using updated and much more realistic post-AGB models than available previously, Córscico & Althaus (2006; see also Córscico et al. 2007) recently redefined the standard in the field, and their results have been reported in Table 6. We note that, despite their homogeneity, their results do remain sensitive to the details of their post-AGB calculations. For example, the evolutionary tracks produced in the detailed computations of Córscico & Althaus (2006) are significantly different from those obtained by Falk Herwig (for instance, the  $0.604 M_{\odot}$  track shown in Fig. 11; see also Fig. 2 of Werner & Herwig 2006) who developed the modern approach to post-AGB calculations involving late or very late thermal pulses. This question of the strong model dependence of the seismic results for GW Vir pulsators is an important issue. The derived masses, for instance, do depend

TABLE 6  
 ASTEROSEISMOLOGICAL INFERENCES FOR GW VIR AND V777 HER PULSATORS

Star (1)	$M$ ( $M_{\odot}$ ) (2)	$\log q(\text{He})$ (3)	$T_{\text{eff}}$ (4)	$\log(L/L_{\odot})$ (K) (5)	$d$ (pc) (6)	$B$ (G) (7)	Other (8)	Reference (9)
PG 1159–035	0.586	...	...	...	...	<6000	stratified	Winget et al. 1991
.....	$0.59 \pm 0.01$	–2.2	136,000	...	...	...	...	Kawaler & Bradley 1994
.....	0.56	–1.8	137,620	2.38	$482 \pm 44$	...	...	Córsico & Althaus 2006
PG 2131+066	$0.61 \pm 0.02$	–2.0	...	$1.0 \pm 0.2$	$470 \pm 150$	...	...	Kawaler et al. 1995
.....	0.60	–1.8	94,740	1.37	$716 \pm 166$	...	...	Córsico & Althaus 2006
PG 0122+200	$0.69 \pm 0.03$	...	...	...	...	...	...	O’Brien et al. 1998
.....	$0.59 \pm 0.02$	...	...	$1.3 \pm 0.5$	$700 \pm 600$	<4000	...	Fu et al. 2007
.....	0.64	–1.9	81,810	0.96	...	...	...	Córsico & Althaus 2006
PG 1707+427	0.57	...	...	...	...	...	...	Kawaler et al. 2004
.....	0.55	–1.8	87,585	1.31	$697 \pm 162$	...	...	Córsico & Althaus 2006
RXJ 2117.1 +3412	$0.56 \pm 0.03$	$-1.3 \pm 0.2$	...	$4.1 \pm 0.3$	$760 \pm 230$	...	...	Vauclair et al. 2002
.....	0.56–0.57	–1.2	163,400	3.36	452	...	...	Córsico et al. 2007
GD 358	$0.61 \pm 0.03$	$-5.7 \pm 0.3$	...	$-1.3 \pm 0.1$	$42 \pm 3$	1300	diff. rot.	Winget et al. 1994
.....	0.650	–2.74	22,600	...	...	...	$X_c(\text{O}) = 0.84$	Metcalfe et al. 2001
.....	$0.63 \pm 0.04$	$-5.8 \pm 0.4$ $-3.0 \pm 0.2$	$24,800 \pm 580$	$-1.3 \pm 0.1$ ...	$43 \pm 3$ ...	...	$X_c(\text{O})$ indeterminate	Fontaine & Brassard 2002
CBS 114	0.730	–6.66	21,000	...	...	...	$X_c(\text{O}) = 0.61$	Handler et al. 2002

sensitively on the details of the evolutionary calculations. In this context, Quirion et al. (2007a) have argued, against the widely accepted view, that the robustness of GW Vir asteroseismology rather rests with excitation physics and not with adiabatic seismology such as that discussed in this section.

Another issue with GW Vir asteroseismology has been the recurrent claim that the values of the “asteroseismological” masses could be tested independently with the help of “spectroscopic” masses. Such a comparison has been incorrectly interpreted as a valid and *independent* test of the consistency between asteroseismology and spectroscopy. In reality, both types of mass depend on a given set of evolutionary tracks: the seismic values are directly derived from the evolutionary models, while the spectroscopic values are simply interpolated from the tracks in the  $\log g - T_{\text{eff}}$  diagram given the derived values of  $\log g$  and  $T_{\text{eff}}$  from spectral analysis. Very clearly, the two types of derived mass *cannot* be considered independent measurements. Worse, in past comparisons, the asteroseismolo-

gical masses have often been inferred from a given set of evolutionary models, while the spectroscopic masses were obtained using different evolutionary tracks. Comparing the two types of mass in a coherent way is certainly worthwhile for checking the internal consistency of the analysis, but it does not provide additional independent information.

The question of finding the best model (or models) in parameter space is also of utmost importance in asteroseismology. Unfortunately, most of the white dwarf analyses reported in Tables 6 and 7 have relied on the trial-and-error method in which relatively few models are constructed. In this approach, there is no guarantee whatsoever that the optimal model found in the search (i.e., the one whose periods best match the observed periods) provides the best solution. The trial-and-error method is necessarily subjective, and does not lead to a guaranteed unique solution. Furthermore, it is extremely time consuming because it is not automated, and it pushes the limits of one’s patience. Meritorious efforts, such as those carried out by

TABLE 7  
 ASTEROSEISMOLOGICAL INFERENCE FOR ZZ CETI PULSATORS

Star	$\log q(\text{H})$	$M$ ( $M_{\odot}$ )	$\log q(\text{He})$	$T_{\text{eff}}$ (K)	$\log(L/L_{\odot})$	$d$	Other	Reference
G226–29 .....	–4.4, –6.6	...	...	...	...	...	...	Fontaine et al. 1992
GD 165 .....	–3.7, –6.4	...	...	...	...	...	...	Bergeron et al. 1993
	–3.8	0.65–0.68	–1.8	...	...	...	...	Bradley 2001
	–4.2	0.64	–1.7	11,980	–2.5	33	...	Brassard & Fontaine 2006
GD 154 .....	–9.7	...	...	...	...	...	...	Pfeiffer et al. 1996
G29–38 .....	–6.3	0.75	–2.0	...	...	...	...	Bradley & Kleinman 1997
G117-B15A .....	–4.0, –7.0	0.60	–2.0	...	...	...	...	Bradley 1998
Ross 548 .....	–4.0, –7.0	0.56	–2.0	...	...	...	...	Bradley 1998
L19–2 .....	–4.0	0.72	–2.0	...	...	...	...	Bradley 2001
BPM 37903 .....	–5.6	1.10	–2.2	11,500	...	...	90%	Metcalfe et al. 2004
	–5.5	1.10	–2.1	11,840	...	...	32–82%	Brassard & Fontaine 2005
G185–32 .....	–4.0, –6.0	0.60–0.65	...	...	...	...	...	Bradley 2006
	–3.7	0.64	–2.0	...	...	...	...	Pech & Vauclair 2006
HL Tau 76 .....	–3.6	0.58	–2.0	...	...	...	...	Pech et al. 2006

Paul A. Bradley for example, deserve to be commended in this connection. However, in the end, when several model parameters significantly and simultaneously affect the pulsation periods, there is no choice but to systematically and thoroughly explore parameter space even if it means computing tens of thousands, hundreds of thousands, or even millions of models.

Two groups have so far independently developed the numerical means to carry out such large-scale computations and to search automatically and objectively for the best-fitting model in parameter space in a white dwarf context. These calculations rely on adapted search algorithms that run on small clusters of dedicated PCs. On the one hand, Travis S. Metcalfe wrote a most interesting Ph.D. thesis at the University of Texas at Austin dedicated to this problem (Metcalfe 2001). On the other, we developed similar tools completely independently in Montréal and initially applied them to pulsating sdB stars (see, e.g., Brassard et al. 2001). These elaborated searches for the optimal model in parameter space have been carried out only for a few pulsating white dwarfs so far. From Tables 6 and 7, we identify the cases of GD 358 (Metcalfe et al. 2001; Fontaine & Brassard 2002), CBS 114 (Handler, Metcalfe & Wood 2002), GD 165 (Brassard & Fontaine 2006), and BPM 37093 (Metcalfe et al. 2004; Brassard & Fontaine 2005). (Note that the origin of our differences with Metcalfe et al. on GD 358 or BPM 37093, for example, is not at all related to their search technique in parameter space, but to the quality of their input models which, we claim, are not up to today’s standards.) Except for those cases and the GW Vir stars examined by Córscio & Althaus (2006) who explored some 3000 models, the results presented in Tables 6 and 7 must therefore be considered preliminary and uncertain.

It should be clear, in this context, that the period data for many stars listed in Tables 6 and 7 should be reexamined in the light of these relatively recent search strategies in parameter

space (which essentially boil down to sophisticated exercises in the forward method of asteroseismology). For these objects as well as other pulsating white dwarfs with reliable period data, there is indeed an obvious need for a systematic application of the search technique that we or our collaborator Stéphane Charpinet,<sup>10</sup> for example, have developed quite successfully for pulsating sdB stars (cf., Brassard et al. 2001; Charpinet et al. 2003, 2005a, 2005b; Randall et al. 2006; Fontaine et al. 2008b). This will best be done for ZZ Ceti pulsators which are more numerous than the other types. In the meantime, Table 8 gives an idea of the quality of the period-matching accuracy that we can currently reach with our technique for white dwarfs. Data are provided for the V777 Her prototype GD 358, as well as the ZZ Ceti pulsators BPM 37093 and GD 165. Note that, in each case, the individual mode identification was not fixed a priori (instead, it is a by-product of our search technique), except for the fact that only modes with  $l = 1$  or  $l = 2$  were allowed. In the specific approach used here, it is only a posteriori that the mode identification can be contrasted with the values or constraints derived from the methods described in § 7 above. For example, rotational splitting is clearly present for the largest amplitude modes at 120.36 and 192.68 s observed in the CFHT light curve of GD 165. It shows neat triplets for the two modes, consistent with our completely independent assignment of dipole modes in Table 8.

The case of BPM 37093 is unusual for a ZZ Ceti pulsator in that the mode assignment in Table 8 indicates quadrupole modes with what could be called medium-order values of  $k$ . A mixture of low-order dipole and quadrupole modes, such as that seen in

<sup>10</sup> As a spin-off of the Montréal approach, Stéphane Charpinet has developed his own independent search algorithms in Toulouse and has been applying them to sdB pulsators. Interesting performance comparisons between the two approaches are underway.

GD 165 for example, is more the norm. We cannot exclude the possibility that, in fact, *all* of the modes observed in BPM 37093 are  $l = 2$  modes, including the 613.5 s pulsation currently assigned by our search algorithm to a  $l = 1$  mode. Indeed, due to model imperfections, the period of that theoretical mode could quite possibly fall slightly closer to the observed value than that of its  $l = 2$  counterpart. In any case, BPM 37093 is that interesting object that is sufficiently massive (the only known pulsating white dwarf, in fact) to have part of its core in solidified form, and there has been a debate about the possibility of precisely inferring the crystallized mass fraction (Metcalf et al. 2004; Brassard & Fontaine 2005). The fact that the observed modes in BPM 37093 are medium-order and not low-order modes means, as discussed above around Figure 42, that the signature of the core composition on the observed periods is very weak. This unfortunately implies that the core composition of BPM 37093 remains unknown and that the crystallized mass fraction cannot be inferred with any degree of accuracy. If we consider only C/O cores, it must lie somewhere in the range from 32% (assuming a pure C core) to 82% (assuming a pure O core). This is the message we tried to convey in Brassard & Fontaine (2005).

TABLE 8

EXAMPLES OF FITS PROVIDED BY OUR PERIOD-MATCHING ALGORITHMS

Star	$l$	$k$	$P_{\text{theo}}$ (s)	$P_{\text{obs}}$ (s)	$ \Delta P $ (s)	$ \Delta P /P_{\text{obs}}$ (%)
GD 358 .....	1	8	422.39	423.30	0.91	0.21
	1	9	463.47	464.20	0.73	0.16
	1	10	502.48	501.60	0.88	0.18
	1	11	540.29	541.80	1.51	0.28
	1	12	575.91	576.80	0.89	0.15
	1	13	617.93	618.30	0.37	0.06
	1	14	657.56	658.40	0.84	0.13
	1	15	699.12	700.60	1.48	0.21
	1	16	734.17	734.30	0.13	0.02
	1	17	772.82	770.70	2.12	0.28
BPM 37093 .....	1	18	813.11	810.70	2.41	0.30
	2	28	511.52	511.7	0.18	0.04
	2	29	530.15	531.1	0.95	0.18
	2	30	547.99	548.4	0.41	0.08
	2	31	564.11	564.1	0.01	0.00
	2	32	582.48	582.0	0.48	0.08
	2	33	600.59	600.7	0.11	0.02
	1	19	614.11	613.5	0.61	0.10
GD 165 .....	2	35	635.49	635.1	0.39	0.06
	1	1	120.14	120.36	0.22	0.18
	1	2	192.71	192.68	0.03	0.02
	1	3	250.68	250.16	0.52	0.21
	2	2	113.98	114.24	0.26	0.22
	2	3	145.07	146.31	1.24	0.85
	2	4	168.69	168.19	0.50	0.30

### 8.3. Rates of Period Change

We cannot end a discussion of white dwarf asteroseismology without mentioning that rates of period change can also be exploited, at least potentially, to infer some structural parameters of a cooling white dwarf. Whether or not rates of period change can be measured with sufficient accuracy in pulsating white dwarfs is debatable in our opinion, but we wish to address mostly the principle of the approach in what follows.

We show, in Figure 43, the period spectrum of  $g$ -modes with  $l = 2$  as a function of effective temperature in a cooling DA white dwarf model defined by  $M = 0.6 M_{\odot}$ ,  $\log q(\text{H}) = -12$ , and  $\log q(\text{He}) = -2$ . The radial order of the mode varies from  $k = 1$  (*bottom curve*) to  $k = 22$  (*top curve*). The general behavior of the curves shown in the figure is representative of *all* of the ZZ Ceti stars: the period of a mode *always* increases with decreasing effective temperature, meaning that the rate of period change of a mode,  $dP/dt$ , must *always* be positive in these pulsators. The value of the rate of period change (related to the slope of the curves shown in Fig. 43) varies from one mode to another, however, and it bears the signature of the structure of the star. In particular, the curves shown in the figure bear the imprint of the envelope layering in this particular evolving stellar model.

In this context, the dotted part of the  $k = 13$  curve indicates that, at high values of  $T_{\text{eff}}$ , this particular mode is trapped above the H/He composition transition zone. Its amplitude below that zone is therefore quite small (see, e.g., Brassard et al. 1992a for a detailed discussion of trapping/confinement phenomena in ZZ Ceti star models), and it shows the smallest kinetic energy. Note that its immediate neighbors (the modes with  $k = 12$  and  $k = 14$ ) are also partially trapped above the H/He transition layer. With cooling, below  $T_{\text{eff}} \sim 13,000$  K, the most trapped mode eventually becomes the  $k = 12$  mode as indicated by

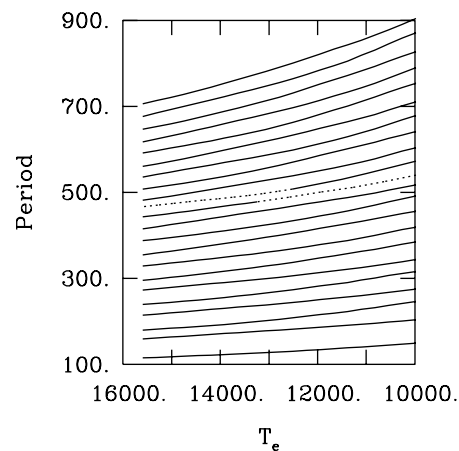


FIG. 43.—Evolution of the quadrupole period spectrum for a cooling model of a ZZ Ceti star defined by  $M = 0.6 M_{\odot}$ ,  $\log q(\text{H}) = -12$ , and  $\log q(\text{He}) = -2$ . The first 22 overtones ( $k$  values) are shown from bottom to top. The dotted part of two curves identifies the first trapped mode at the H/He interface.

the dotted part of the curve associated with that latter mode. This switch is sometimes referred to as an “avoided crossing” between modes. We mention this because it has been incorrectly claimed in the past that “trapped modes” in ZZ Ceti stars could show *negative* values of  $dP/dt$  under certain circumstances. In fact, the transition of the qualificative “trapped” (or, more precisely, “most trapped”) from one mode to another is quite a smooth process as can be seen in the figure. For a given value of  $k$ ,  $dP/dt$  is, again, *always* positive.

The dashed curves in Figure 44 show the actual computed values of  $dP/dt$  (in s/s) for three of the  $g$ -modes depicted in the previous figure: those with  $k = 1$ ,  $k = 10$ , and  $k = 20$ , from bottom to top. In comparison, the solid curves show similar results, but for a cooling model in which the H-layer mass has been increased to  $\log q(\text{H}) = -6$ . The extra structure in the  $k = 20$  solid curve corresponds to the onset of trapping for that overtone near  $T_{\text{eff}} \approx 14,500$  K, followed by the switch of trapping to the  $k = 19$  mode around  $T_{\text{eff}} \approx 12,300$  K. Clearly, this structure is not extreme enough for  $dP/dt$  to switch sign, and this is quite generally the case for all modes in ZZ Ceti star models. Neither is it nearly extreme enough to show orders of magnitude differences from modes that are not trapped as has also been claimed sometimes to account for widely different determinations of  $dP/dt$  values for the same pulsator.

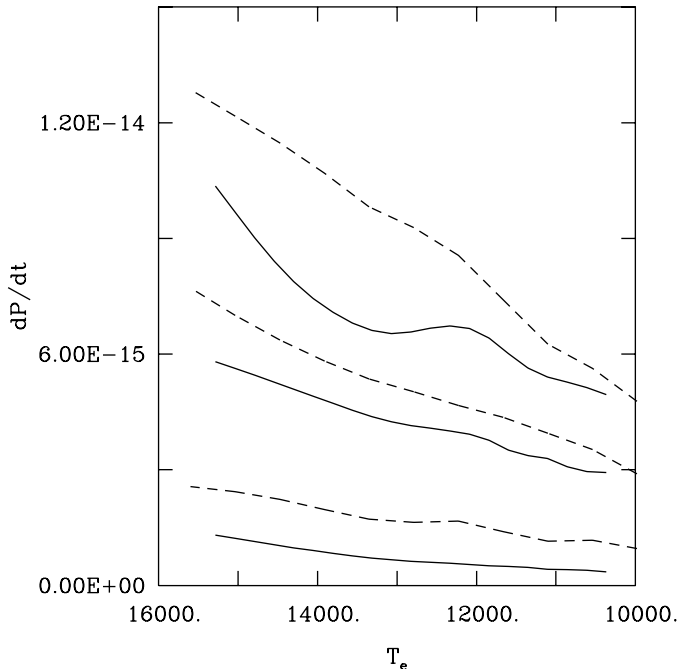


FIG. 44.—Rate of period change for quadrupole modes in evolving models of ZZ Ceti stars. The dashed curves are associated with a model defined by  $M = 0.6 M_{\odot}$ ,  $\log q(\text{H}) = -12$ , and  $\log q(\text{He}) = -2$ . The three curves correspond, respectively, to a  $l = 2$  mode with  $k = 20, 10$ , and  $1$ , from top to bottom. The solid curves are associated with the same modal overtones, but in a model with a thicker H layer  $\log q(\text{H}) = -6$ , the other parameters being the same.

The example shown in Figure 44 indicates values of  $dP/dt$  less than  $1.5 \times 10^{-14}$  s/s in a typical ZZ Ceti star. If such small values could be measured reliably for individual modes, then additional asteroseismological inferences could be obtained from the comparison between these values and theoretical rates of period change. In addition to the sensitivity to envelope layering illustrated in Figure 44,  $dP/dt$  also depends sensitively on the total mass, and on the core composition. The last item is particularly interesting because it may be difficult to infer the core composition of a pulsating white dwarf on the basis of period data alone (see § 8.1). On the other hand, in a rough first approximation, the cooling time of a white dwarf is inversely proportional to the mean atomic weight of the core material. This implies that reliable measurements of  $dP/dt$  could be extremely valuable for the independent determination of the core composition of a pulsating white dwarf because that composition very largely specifies the cooling rate. In our view, this is the most important and practical application of measurements of  $dP/dt$ . Unfortunately, as indicated above, these determinations are extremely difficult to carry out within a human timescale for V777 Her and ZZ Ceti pulsators.

Other potential applications of measurements of rates of period change in pulsating white dwarfs have been proposed. For instance, Winget et al. (2004) suggested that constraints on plasmon neutrino rates could be obtained from such measurements, given that neutrino cooling dominates over thermal cooling in the hot phases of white dwarf evolution. Likewise, Kim et al. (2006) have argued that constraints on the mass of the putative particles named axions may also be derived with the same technique, given the potential effect of axions on the cooling process. It is our view that, without knowing the envelope layering and the chemical composition of the core, these more exotic applications, as fascinating as they might appear, will remain out of reach. A more realistic application of  $dP/dt$  measurements, although of less interest here, is the search for planets around pulsating white dwarfs (see, e.g., Mullaly et al. 2007).

## 9. CONCLUDING REMARKS

In this article, we have tried to provide a broad overview of what is currently known about the three different categories of isolated pulsating white dwarfs, underlining their common features when possible, but, also, highlighting differences when appropriate. We have made a real effort to present the best updated view possible, including the results of the most recent developments, but we acknowledge that this view is necessarily the one seen through our own “spectacles.” In addition, we have attempted through numerous calculations and figures to illustrate the physical principles at work behind the various observed phenomena of interest in white dwarf seismology. Along the way, we have identified several areas for additional research which, according to us, should be given priority in the future. We recall the most important of these needed developments in the following subsection.

### 9.1. Suggestions for Future Progress

There is a need to build up statistics to better define the empirical boundaries of the instability domains in the  $\log g - T_{\text{eff}}$  diagram. This is within reach for the ZZ Ceti stars. However, the task is much more challenging for the V777 Her stars because of the relatively small number of known pulsators of that class and because of the effects of small invisible traces of H on the inferred atmospheric parameters. To progress on this front, we suggest that a systematic effort be carried out to determine as accurately as possible the atmospheric H abundance in all of the DB pulsators along with several nonpulsators located near the edges of the instability strip. The task of mapping the boundaries of the GW Vir instability strip in detail will also remain quite difficult because of intrinsic fuzziness and, again, because of small-number statistics.

Once these boundaries are well established, it will be possible to use the full potential of nonadiabatic asteroseismology. For the ZZ Ceti and V777 Her stars, an appropriate modeling of the blue edge of the strip will allow the calibration of the mixing-length theory at the base of the convection zone—in effect, a true measurement of the depth of that zone in evolving white dwarfs. From what we currently know of the ZZ Ceti stars, it would appear that DA white dwarf convection zones are characterized by a depth dependent efficiency, and we suggest that model atmospheres with a variable value of  $\alpha$  be developed to test the idea of reconciling the calibration found in the atmospheric layers (the so-called  $ML2/\alpha = 0.6$  parametrization of the mixing-length theory) with that to be found by matching the final empirical blue edge with the theoretical blue edge. The same should be attempted for DB pulsators, except that, as pointed out above, the boundaries of their instability domain may be intrinsically fuzzy, meaning that this task may be more complicated.

For the ZZ Ceti and V777 Her stars, both characterized by an important superficial convection zone, the modeling of the instability strip and, in particular, its red edge, is of paramount interest. For example, it will be extremely interesting to see if models can actually explain the phenomenon of “dying out amplitudes” that appears to characterize ZZ Ceti stars as they approach the red edge as observed in our Figure 20. A more convincing and working model of the interactions between convection and pulsations in these stars is needed beyond the semi-analytic approach developed by John Brickhill (and further developed by Yanqin Wu) in the past. This still remains a very interesting challenge for pulsation theorists. The same theorists should also quantitatively investigate the question of why  $p$ -mode pulsations have not been seen in pulsating DB and DA white dwarfs.

In the case of GW Vir stars, nonadiabatic calculations for individual pulsators should be redone in light of the availability of the new evolutionary tracks computed by Córscico & Althaus (2006). It will be interesting to see if the agreement between the observed and predicted period range in RXJ2117.1+3412 and

also NGC 246 (see our discussion around Fig. 26) can be improved. As indicated previously, with the blue edge being intrinsically fuzzy (due to a significant dispersion in the atmospheric chemical composition), it will remain difficult to exploit it for inferring class properties. On the other hand, once the empirical red edge is well pinned down, most interesting inferences about mass loss rates in PG 1159 stars could be obtained.

We further suggest that significant progress in the field of pulsating white dwarfs will be made by exploiting multicolor photometry, particularly optical photometry from the ground, in order to constrain the angular geometry of pulsation modes. What is needed compared to previous attempts is the gain in S/N that can be obtained on 4-m class telescopes. Equally exciting in this connection is the continuation of time-resolved low-resolution optical spectroscopic observations of pulsating white dwarfs carried out on 6–10-m class telescopes. While we are rapidly running out of sufficiently bright candidates, there are still a few that need to be investigated. Along with these efforts, we demonstrated that the angular geometry of a pulsation mode can also be derived by exploiting the nonlinearities observed in the light curves. This has been done correctly for only one star so far (G117-B15A), but there are several candidates with the appropriate data waiting to be modeled. In this connection, theorists are invited to think about an appropriate recipe that would give the nonlinear (read nonsinusoidal) temporal dependence of the temperature distribution in the atmospheric layers of a pulsating white dwarf.

At the most basic level of adiabatic asteroseismology, we are convinced that very important progress will materialize from the systematic reanalysis of all suitable period data sets via the automatic and objective search in parameter space described above. This is a major project requiring enormous computational resources, but the idea of deriving fundamental structural parameters of pulsating white dwarfs in a *homogeneous* way makes it entirely worthwhile. In conjunction with the independent constraints or inferences on modal angular geometry coming from the techniques mentioned in the previous paragraph, this project would allow, through feedback, the computation of white dwarf models at an unprecedented level of refinement. Above all, the systematic and homogeneous determination of the structural properties of many pulsating white dwarfs using an objective approach would meet what some refer to as the ultimate goal of asteroseismology.

There are already several suitable period data sets available in the literature for the above project to be carried out. A large number come from the WET collaboration, but others are also available. For example, over the years, we have accumulated very high-sensitivity light curves on a good dozen ZZ Ceti stars at the CFHT, and those should also be exploited systematically in the future. We also suggest that asteroseismological analyses of well-observed stars such as PG 1159–035 and GD 358 be redone but, this time, by considering *all* of the available periods,

including those associated with modes with  $l = 2$  and not only those referring to dipole modes as has been done in the past.

Finally, we point out that the intrinsic faintness of pulsating white dwarfs largely prevents their study with space experiments such as *MOST* and *COROT*, but the hope is that the launch of *Kepler* will partly remedy this unfortunate situation.

## 9.2. Some Philosophical Considerations

We felt that it would be appropriate to end this review on pulsating white dwarfs by raising a couple of issues related to the way our science has progressed in the past. We have been concerned with these issues for some time now and decided to take this opportunity to share our thoughts with the reader. We also hope that our remarks might lead to a frank and open debate in the community.

On the first account, we claim that, more often than not in the past, only rough and unsophisticated equilibrium models were used in asteroseismological exercises involving white dwarfs. We strongly suspect that this attitude goes back to an old saying made by a famous US astrophysicist who once joked, “Any fool can make a white dwarf!” We think that he should have qualified his statement in the following way: “Any fool can make a *crude* white dwarf!” This way of thinking has also impacted the field of cosmochronology, for instance, and we have heard the argument that white dwarf evolution is so “simple,” that age estimates based on it are much more reliable than those obtained from other methods (such as the main sequence turnoff approach, for example) countless times. By the same token, the implicit suggestion in white dwarf asteroseismology has often been that white dwarf models are so much simpler to build than main sequence models, say, that inferences from them must necessarily be more reliable. The truth of the matter is that the constitutive physics entering white dwarf model building—specifically the radiative opacity, the conductive opacity, the diffusion coefficients, and the equation of state of the envelope and that of the core—is much more uncertain than the equivalent for main sequence stars simply because the physical conditions in white dwarfs are much more extreme. The recent important contribution of Itoh et al. (2008) on the front of the conductive opacity is a perfect example that the constitutive physics under white dwarf conditions is far from being “settled.” In some cases, in particular for computing very cool models used in white dwarf cosmochronology, it is even necessary to *extrapolate* the radiative opacity into a regime where no data exists (and see Fontaine et al. 2001b for more on this issue). We disagree with this tendency to sweep under the rug, so to speak, the limitations of white dwarf physics and to be content with quickly built models. We strongly believe instead that, to be fully successful, white dwarf asteroseismology must be based on the most realistic models possible. Hence, we suggest that the ideal angle of attack for white dwarf seismology is to invest the necessary efforts, considerable as they may be, into building the

best possible models, and then use them to determine the basic structural properties of pulsators before anything else.

On the second account, we believe that the outstanding reputation currently enjoyed by white dwarf asteroseismology among the “pulsation community” is not fully deserved. We feel that the attention has been mostly attracted by some spectacular claims that have not been as properly scrutinized as they deserve. In particular, we point out that white dwarf asteroseismology has so far not “delivered” enough in terms of its most basic capacities, i.e., the reliable determination of the fundamental structural parameters of a pulsating star. However, it is absolutely essential that these parameters be known before trying to test some piece of exotic physics with white dwarf seismology. For instance, at the risk of being labeled as too “conservative,” we believe that it is futile to try to pin down the rate of plasmon-neutrino emission in a cooling white dwarf via its effect on the rate of period change of a pulsation mode if the total mass, the effective temperature, the core composition, and the envelope layering (all of which affect the value of  $dP/dt$ ) are not known to some degree of accuracy.

It is not our intention to be overly provocative, but we feel that the most spectacular claims that have come out of white dwarf seismology so far have not been challenged properly, if at all. Among those claims, we have singled out the following: (1) White dwarf asteroseismology has led to a measurement of differential rotation in a pulsating star of the kind, (2) White dwarf asteroseismology has led to a measurement of magnetic splitting in a pulsating star, (3) White dwarf asteroseismology has been used to constrain the rate of the  $^{12}\text{C}(\alpha, \gamma)^{16}\text{O}$  thermonuclear reaction in stars, (4) White dwarf asteroseismology has been used to test crystallization physics in dense stellar plasmas, (5) White dwarf asteroseismology has revealed the existence of “convection harmonics,” (6) White dwarf asteroseismology can provide interesting constraints on the rate of plasmon-neutrino emission, (7) White dwarf asteroseismology can currently lead to measurements of the masses of axions and other exotic particles, and (8) G117-B15A is the most stable optical clock there is.

These are all extremely interesting possibilities, and because of that, they deserve to be closely examined. After all, as is well known, extraordinary claims deserve extraordinary scrutiny. It is our view that this fundamental effort of critical examination has not been done so far, except in a couple of instances by ourselves as it turns out (see, e.g., Fontaine & Brassard 2002; Brassard & Fontaine 2005). We blame “consensus science” which seems to dominate in the very small white dwarf asteroseismological community for this state of affairs. We end with a friendly plea for self-discipline about exaggerated claims in the white dwarf field. We collectively owe it to ourselves and to our science.

We wish to thank the following collaborators for their interest in this paper: Pierre Bergeron, Stéphane Charpinet, Pierre Chayer, Patrick Dufour, Alex Gianninas, Betsy Green, Jim Liebert,

Pierre-Olivier Quirion, Suzanna Randall, Valérie Van Grootel, and François Wesemael. We are particularly grateful to Suzanna Randall for her invaluable help in making this a much better manuscript. G. F. also wishes to acknowledge the essential influence of John McGraw (observations) and Don Winget (theory) who got

him interested in pulsating white dwarfs some 30 years ago now. This work was supported in part by the Natural Sciences and Engineering Research Council of Canada. G. F. acknowledges in addition the contribution of the Canada Research Chair Program.

## APPENDIX

### A NEW TYPE OF PULSATING WHITE DWARF

After the bulk of this paper was completed, a new exciting development came on the scene of white dwarf asteroseismology. This followed from the unexpected discovery of a new type of white dwarfs, those with carbon-dominated atmospheres, also known as Hot DQ stars (Dufour et al. 2007). These are very rare, and Dufour et al. (2007) reported the discovery of nine of those, out of a total of about 10,000 white dwarfs identified spectroscopically. The Hot DQ stars were uncovered within the framework of the SDSS project. Among other characteristics, they all bunch together in a narrow range of effective temperature centered around 20,000 K (Dufour et al. 2008a).

It has been known for quite some time (see, e.g., Fontaine & Van Horn 1976) that models of carbon-atmosphere white dwarfs in this temperature range possess superficial convection zones that bear strong similarities with those found in H- and He-atmosphere stars. Given that the newly found C-atmosphere white dwarfs are sandwiched between the V777 Her and ZZ Ceti instability strips, and given that convection plays a key role in the excitation of pulsation modes in these pulsators, it follows that the prospects of finding unstable models of Hot DQ stars looked good at the outset.

We therefore carried out an exploratory stability survey of models of C-atmosphere white dwarfs using a full nonadiabatic approach (Fontaine et al. 2008a). Our theoretical survey has revealed that  $g$ -modes can indeed be driven in models of Hot DQ stars. However, we found that only those stars with a sufficiently large amount of He ( $X(\text{He}) > 0.25$ ) in their C-rich envelope mixture could pulsate *in the range of effective temperature where the real C-atmosphere white dwarfs are found*.

In this connection, Figure 45 displays some revealing results. It depicts the locations of theoretical instability strips for evolving  $0.6 M_{\odot}$  white dwarf models with different envelope compositions. For the reasons given above, the red edge of each of these strips is cooler than it should be, but the blue edge is secure. Along with the usual V777 Her (pure He) and ZZ Ceti (pure H) instability strips, one can recognize the red edge of the pulsating pure C envelope white dwarf models. In fact, the pure C instability strip extends all the way up to the GW Vir regime as described at length in Quirion et al. (2007a; see also Fig. 12 above). Given that the true red edge is hotter than the  $\sim 28,000$  K value found in our survey, it follows that pure C-atmosphere white dwarfs cannot pulsate in the range of effective temperature where the Hot DQ stars congregate.

On the other hand, models with a mixed He and C envelope composition can also pulsate, but in different temperature intervals. For instance, Figure 45 illustrates a new instability strip between the V777 Her and the ZZ Ceti domains associated with white dwarf models with a mixed envelope composition specified by  $X(\text{He}) = X(\text{C}) = 0.5$ . Naively, one could have expected to find such a strip in between the pure C and pure He strips, but structural differences in the mixed envelope composition models explain why this is not so (see Fontaine et al. 2008a for more detailed explanations). In brief, the survey of Fontaine et al. (2008a) revealed that some Hot DQ white dwarfs can indeed undergo low-order, low-degree  $g$ -mode pulsational instabilities, provided that the surface gravity is larger than average and a substantial amount of He is present in the C-rich envelope mixture.

In parallel with our theoretical investigations, but totally independently, Montgomery et al. (2008) carried out an

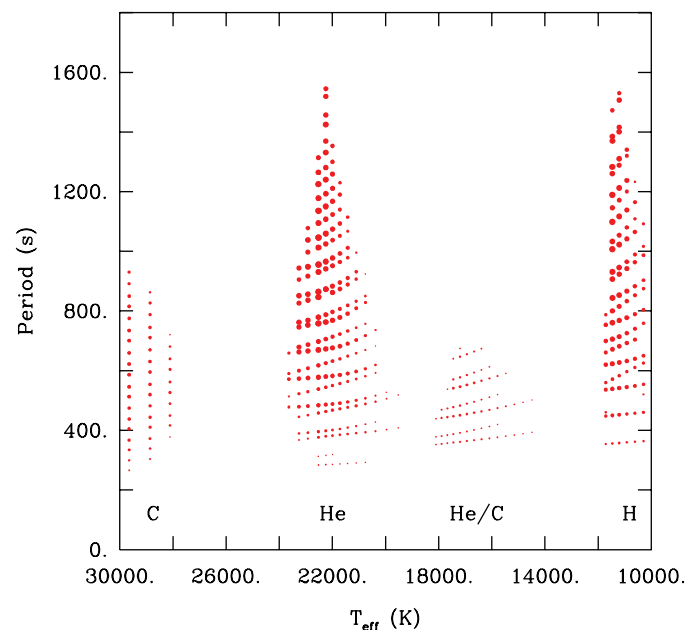


FIG. 45.—Predicted spectra of excited  $g$ -modes computed from four distinct evolutionary sequences, each characterized by a total mass of  $0.6 M_{\odot}$ , but with a different envelope composition: pure C, pure He,  $X(\text{He}) = X(\text{C}) = 0.5$ , and pure H, from left to right. The format is the same as in Fig. 12. The so-called ML  $2/\alpha = 0.6$  version of the mixing-length theory was used in these calculations.

observational search for luminosity variations in six Hot DQ stars accessible to observations in the winter of 2008. They were able to report the very exciting discovery that SDSS J1426+5752, one of the Hot DQ's found by Dufour et al. (2007), pulsates in, at least, one mode with a period of 417 s, thus establishing the existence of a fourth type of pulsating white dwarf. Full credit should be given to Montgomery et al. (2008) for this important breakthrough. In addition, they reported that no luminosity variations were found, to the limit of detection, in the five other stars in their sample.

Following this discovery, E. M. Green, G. Fontaine, & P. Dufour (2008, in preparation) undertook follow-up wide band photometric observations of SDSS J1426+5752 at the Steward Observatory 1.6 m telescope on Mount Bigelow with the help of the new Montréal 4K  $\times$  4K CCD camera (Mont4K), a joint venture between the University of Arizona and the Université de Montréal. Some 106 h of observations were obtained on this rather faint star ( $g = 19.2$ ). Figure 46 illustrates one of the nightly light curves obtained by Green et al., leaving no doubt as to the variability of SDSS J1426+5752. Figure 47 shows the final Fourier amplitude spectrum for the full data set and the prewhitening sequence where three significant peaks are removed. These results confirm the presence of a dominant pulsation with a period of 417 s and of its first harmonic (*top curve* in Fig. 47) as first reported by Montgomery et al. (2008). In addition, they also reveal the likely presence of an additional pulsation with a period of 319 s at the  $4.9 \sigma$  level (*middle curve* in Fig. 47). Hence, with at least two independent periodicities un-

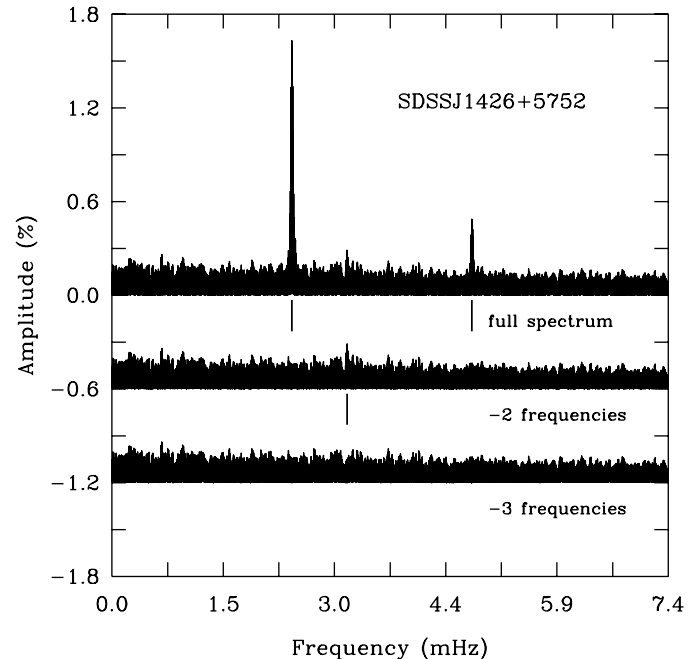


FIG. 47.—Fourier amplitude spectrum and prewhitening sequence for the full set of 106 h of data on SDSS J1426+5752.

covered, SDSS J1426+5752 can be considered as a multiperiodic pulsator like the other types of pulsating white dwarfs.

In view of the rather poor SDSS spectrum available for SDSS J1426+5752, follow-up spectroscopic observations were

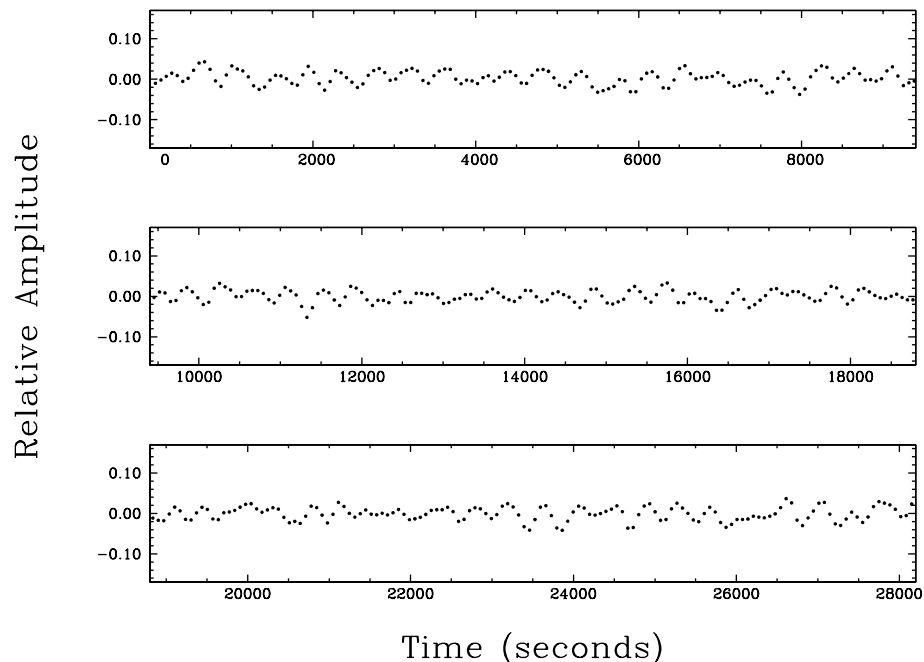


FIG. 46.—Sample broadband light curve of SDSS J1426+5752 obtained with the Mont4K/Bigelow combination 2008 May 1. Each plotted point corresponds to an effective sampling time of 67 s.

pursued by Dufour et al. (2008b) using both the MMT and one of the Keck telescopes. The objective was, first, to obtain a sufficiently good spectrum for detailed atmospheric modeling and, second, to search for the presence of He required to account for the observed pulsational instabilities according to the nonadiabatic calculations of Fontaine et al. (2008a). The spectral analysis of the improved spectra readily revealed the presence of a substantial amount of helium in the atmosphere of SDSS J1426+5752, an abundance comparable to that of carbon by mass fraction. This is in line with the expectations of nonadiabatic pulsation theory which require an important He “pollution” in the atmosphere/envelope of SDSS J1426+5752 for it to pulsate at its current effective temperature.

To add to this small success, an unexpected surprise came out of the follow-up spectroscopic observations of Dufour et al. (2008b). It was found that the strong carbon lines seen in the spectrum of SDSS J1426+5752 feature Zeeman splitting, a structure that could not be seen in the original noisy SDSS spectrum.

The observed splitting between the  $\pi$  and  $\sigma$  components implies a large scale magnetic field of about 1.2 MG. Hence, SDSS J1426+5752 is both a pulsating and a magnetic white dwarf. As there is no sign of binarity in either the light curve or the optical spectrum (although the phase coverage has been quite limited), SDSS J1426+5752 is most likely the first example of an isolated pulsating white dwarf with a large detectable magnetic field. As such, it is the white dwarf equivalent of an roAp star.

It remains to be seen if other stars similar to SDSS J1426+5752 will be found or if it will remain an isolated “freak.” If we adopt a conservative point of view, it takes at least *two* members to define a “class,” so we should perhaps refrain from referring to it as the prototype of a class for the time being. Nevertheless, SDSS J1426+5752 is certainly different from the other kinds of pulsating white dwarfs discussed in this paper. Please stay tuned, as further data releases from the SDSS project might reveal siblings of this unique star.

## REFERENCES

- Allard, N. F., Koester, D., Feautrier, N., & Spielfiedel, A. 1994, *A&AS*, 108, 417
- Arras, P., Townsley, D. M., & Bildsten, L. 2006, *ApJ*, 643, L119
- Beauchamp, A. 1995, Ph.D. thesis, Université de Montréal
- Beauchamp, A., Wesemael, F., Bergeron, P., Fontaine, G., Saffer, R. A., Liebert, J., & Brassard, P. 1999, *ApJ*, 516, 887
- Bergeron, P., Fontaine, G., Billères, M., Boudreault, S., & Green, E. M. 2004, *ApJ*, 600, 404 (zz20)
- Bergeron, P., & McGraw, J. T. 1990, *ApJ*, 352, L45 (zz24)
- Bergeron, P., Wesemael, F., Lamontagne, R., Fontaine, G., Saffer, R. A., & Allard, N. 1995, *ApJ*, 449, 258
- Bergeron, P. et al. 1993, *AJ*, 106, 1987
- Billères, M. 2000, Ph.D. thesis, Université de Montréal
- Bond, H. E., & Ciardullo, R. 1993, in *White Dwarfs: Advances in Observations and Theory*, NATO ASI Series, ed. M. A. Barstow (Dordrecht: Kluwer), 491 (gw5)
- Bond, H. E., & Grauer, A. D. 1987, *ApJ*, 321, L123 (gw2)
- Bond, H. E., Grauer, A. D., Green, R. F., & Liebert, J. 1984, *ApJ*, 279, 751 (gw10)
- Bond, H. E., & Meakes, M. G. 1990, *AJ*, 100, 788 (gw3)
- Bond, H. E. et al. 1996, *AJ*, 112, 2699
- Bradley, P. A. 1998, *ApJS*, 116, 307
- . 2001, *ApJ*, 552, 326
- . 2006, *Mem. Soc. Astron. Italiana*, 77, 437
- Bradley, P. A., & Kleinman, S. J. 1997, in *White Dwarfs*, ed. J. Isern, M. Hernanz, & E. Garcia-Berro (Dordrecht: Kluwer), 445
- Bradley, P. A., & Winget, D. E. 1994, *ApJ*, 421, 236
- Bradley, P. A., Winget, D. E., & Wood, M. A. 1993, *ApJ*, 406, 661
- Brassard, P., & Fontaine, G. 1997, in *White Dwarfs*, ed. J. Isern, M. Hernanz, & E. Garcia-Berro (Dordrecht: Kluwer), 451
- . 1999, in *ASP Conf. Ser. 173, Theory and Tests of Convection in Stellar Structure*, ed. A. Gimenez, E. F. Guinan, & B. Montesinos (San Francisco: ASP), 329
- . 2005, *ApJ*, 622, 572
- . 2006, *Mem. Soc. Astron. Italiana*, 77, 439
- Brassard, P., Fontaine, G., Billères, M., Charpinet, S., Liebert, J., & Saffer, R. A. 2001, *ApJ*, 563, 1013
- Brassard, P., Fontaine, G., & Wesemael, F. 1995, *ApJS*, 96, 545
- Brassard, P., Fontaine, G., Wesemael, F., & Hansen, C. J. 1992a, *ApJS*, 80, 369
- Brassard, P., Fontaine, G., Wesemael, F., Kawaler, S. D., & Tassoul, M. 1991, *ApJ*, 367, 601
- Brassard, P., Fontaine, G., Wesemael, F., & Talon, A. 1993, in *White Dwarfs: Advances in Observations and Theory*, NATO ASI Series, ed. M. A. Barstow (Dordrecht: Kluwer), 485
- Brassard, P., Fontaine, G., Wesemael, F., & Tassoul, M. 1992c, *ApJS*, 81, 747
- Brassard, P., Pelletier, C., Fontaine, G., & Wesemael, F. 1992b, *ApJS*, 80, 725
- Brassard, P., Wesemael, F., & Fontaine, G. 1989, in *IAU Colloq. 114, White Dwarfs*, ed. G. Wegner (Berlin: Springer), 258
- Brickhill, A. J. 1983, *MNRAS*, 204, 537
- . 1990, *MNRAS*, 246, 510
- . 1991a, *MNRAS*, 251, 673
- . 1991b, *MNRAS*, 252, 334
- . 1992a, *MNRAS*, 259, 519
- . 1992b, *MNRAS*, 259, 529
- Castanheira, B. G., et al. 2006, *A&A*, 450, 227
- . 2007, *A&A*, 462, 989
- Chanmugan, G. 1972, *Nature*, 236, 83
- Charpinet, S., Fontaine, G., & Brassard, P. 2003, in *White Dwarfs, Proc. 13th European Workshop on White Dwarfs*, ed. D. de Martino, R. Silvotti, J.-E. Solheim, & R. Kalytis (NATO Sci. Ser. II, 105; Dordrecht: Kluwer), 69
- Charpinet, S., Fontaine, G., Brassard, P., Billères, M., Green, E. M., & Chayer, P. 2005b, *A&A*, 443, 251
- Charpinet, S., Fontaine, G., Brassard, P., Chayer, P., Rogers, F. J., Iglesias, C. A., & B., Dorman 1997b, *ApJ*, 483, L123
- Charpinet, S., Fontaine, G., Brassard, P., & Dorman, B. 1997a, *ApJ*, 489, L149

- Charpinet, S., Fontaine, G., Brassard, P., Green, E. M., & Chayer, P. 2005a, *A&A*, 437, 575
- Ciardullo, R., & Bond, H. E. 1996, *AJ*, 111, 2332 (gw1)
- Clemens, J. C., van Kerkwijk, M. H., & Wu, Y. 2000, *MNRAS*, 314, 220
- Córsico, A. H., & Althaus, L. G. 2006, *A&A*, 454, 863
- Córsico, A. H., Althaus, L. G., & Miller Bertolami, M. M. 2006, *A&A*, 458, 259
- Córsico, A. H., Althaus, L. G., Miller Bertolami, M. M., & Werner, K. 2007, *A&A*, 461, 1095
- Córsico, A. H., Benvenuto, O. G., Althaus, L. G., & Serenelli, A. M. 2002, *MNRAS*, 332, 392
- Costa, J. E. S., Kepler, S. O., & Winget, D. E. 1999, *ApJ*, 522, 973
- Cugier, H., & Daszyńska, J. 2001, *A&A*, 377, 113
- Dehner, B. T., & Kawaler, S. D. 1995, *ApJ*, 445, L141
- Dolez, N., & Vauclair, G. 1981, *A&A*, 102, 375
- Dolez, N., Vauclair, G., & Chevreton, M. 1983, *A&A*, 121, L23 (zz11)
- Dreizler, S., Werner, K., & Stahn, T. 2005, in *ASP Conf. Ser. 334, fourteenth European Workshop on White Dwarfs*, ed. D. Koester, & S. Moehler (San Francisco: ASP), 512
- Dufour, P., Fontaine, G., Liebert, J., Schmidt, G. D., & Behara, N. 2008a, *ApJ*, 683, 978
- Dufour, P., Fontaine, G., Liebert, J., Williams, K., & Lai, D. K. 2008b, *ApJL*, 683, L167
- Dufour, P., Liebert, J., Fontaine, G., & Behara, N. 2007, *Nature*, 450, 522
- Dziembowski, W., & Koester, D. 1981, *A&A*, 97, 16
- Fontaine, G., Bergeron, P., Billères, M., & Charpinet, S. 2003, *ApJ*, 591, 1184 (zz4)
- Fontaine, G., Bergeron, P., Brassard, P., Billères, M., & Charpinet, S. 2001a, *ApJ*, 557, 792 (zz5)
- Fontaine, G., Bergeron, P., Vauclair, G., Brassard, P., Wesemael, F., Kawaler, S. D., Grauer, A. D., & Winget, D. E. 1991, *ApJ*, 378, L49 (gw7)
- Fontaine, G., & Brassard, P. 1994a, in *ASP Conf. Ser. 57, Stellar and Circumstellar Astrophysics*, ed. G. Wallerstein, & A. Noriega-Crespo (San Francisco: ASP), 195
- . 1994b, in *IAU Colloq. 147, The Equation of State in Astrophysics*, ed. G. Chabrier, & E. Schatzman (Cambridge: Cambridge University Press), 347
- . 2002, *ApJ*, 581, L33
- Fontaine, G., Brassard, P., & Bergeron, P. 2001b, *PASP*, 113, 409
- Fontaine, G., Brassard, P., Bergeron, P., & Wesemael, F. 1992, *ApJ*, 399, L91
- . 1996, *ApJ*, 469, 320
- Fontaine, G., Brassard, P., Charpinet, S., Green, E. M., Chayer, P., Randall, S., & Dorman, B. 2006, in *Proc. SOHO18/GONG2006/HELASI, Beyond the Spherical Sun (ESA SP-624; Noordwijk: ESA)*, 32
- Fontaine, G., Brassard, P., & Dufour, P. 2008a, *A&A*, 483, L1
- Fontaine, G., & Chayer, P. 2006, in *ASP Conf. Ser. 348, Astrophysics in the Far Ultraviolet*, ed. G. Sonneborn, H. W. Moos, & B.-G. Andersson (San Francisco: ASP), 181
- Fontaine, G., McGraw, J. T., Coleman, L., Lacombe, P., Patterson, J., & Vauclair, G. 1980, *ApJ*, 239, 898 (zz30)
- Fontaine, G., McGraw, J. T., Dearborn, D. S. P., Gustafson, J., & Lacombe, P. 1982, *ApJ*, 258, 651 (zz27)
- Fontaine, G., & Van Horn, H. M. 1976, *ApJS*, 31, 467
- Fontaine, G., & Wesemael, F. 1984, *AJ*, 89, 1728 (zz22)
- Fontaine, G., et al., 2008b, in *ASP Conf. Series 392, Hot Subdwarf Stars and Related Objects*, ed. U. Heber, S. Jeffery, & R. Napiwotzki (San Francisco: ASP), 231
- Fu, J.-N., et al. 2007, *A&A*, 467, 237
- Gautschy, A. 1997, *A&A*, 320, 811
- Gianninas, A., Bergeron, P., & Fontaine, G. 2005, *ApJ*, 631, 1100 (zz31)
- . 2006, *AJ*, 132, 831 (zz1)
- . 2007, in *ASP Conf. Ser. 372, Proc. 15th European Workshop on White Dwarfs*, ed. R. Napiwotzki, & M. Burleigh (San Francisco: ASP), 577
- Giovannini, O., Kepler, S. O., Kanaan, A., Costa, A. F. M., & Koester, D. 1998, *A&A*, 329, L13 (zz28)
- Goupil, M. J., Dziembowski, W. A., & Fontaine, G. 1998, *Baltic Astronomy*, 7, 21
- Grauer, A. D., & Bond, H. E. 1984, *ApJ*, 277, 211 (gw9)
- Grauer, A. D., Bond, H. E., Green, R. F., & Liebert, J. 1988, *AJ*, 95, 879 (vh4)
- . 1989, *AJ*, 98, 2221 (vh1)
- Green, E. M., et al. 2003, *ApJ*, 583, L31
- Handler, G. 1998, *A&A*, 339, 170
- . 2001, *MNRAS*, 323, L43 (vh7)
- Handler, G., Metcalfe, T. S., & Wood, M. A. 2002, *MNRAS*, 335, 698
- Herald, J. E., & Bianchi, L. 2004, *ApJ*, 609, 378
- Herwig, F., Blöcker, T., Langer, N., & Driebe, T. 1999, *A&A*, 349, L5
- Hesser, J. E., Lasker, B. M., & Neupert, H. E. 1976, *ApJ*, 209, 853 (zz2)
- Itoh, N., et al. 2008, *ApJ*, 677, 495
- Jones, P. W., Pesnell, W. D., Hansen, C. J., & Kawaler, S. D. 1989, *ApJ*, 336, 403
- Jordan, S., Koester, D., Vauclair, G., Dolez, N., Heber, U., Hagen, H.-J., Reimers, D., Chevreton, M., & Dreizler, S. 1998, *A&A*, 330, 277 (zz10)
- Kanaan, A., Kepler, S. O., Giovannini, O., & Diaz, M. 1992, *ApJ*, 390, L89 (zz19)
- Kawaler, S. D., & Bradley, P. A. 1994, *ApJ*, 427, 415
- Kawaler, S. D., Sekii, T., & Gough, D. 1999, *ApJ*, 516, 349
- Kawaler, S. D., et al. 1995, *ApJ*, 450, 350
- . 2004, *A&A*, 428, 969
- Kepler, S. O., Robinson, E. L., Koester, D., Clemens, J. C., Nather, R. N., & Jiang, X. J. 2000, *ApJ*, 539, 379
- Kepler, S. O., et al. 1991, *ApJ*, 378, L45
- . 2005a, *A&A*, 442, 629
- . 2005b, *ApJ*, 634, 1311
- Kilkenny, D., Koen, C., O'Donoghue, D., & Stobie, R. S. 1997, *MNRAS*, 285, 640
- Kilkenny, D., et al. 1999, *MNRAS*, 303, 525
- Kim, A., Montgomery, M. H., & Winget, D. E. 2006, in *ASP Conf. Ser. 352, New Horizons in Astronomy: Frank N. Bash Symposium*, ed. S. J. Kannappan, S. Redfield, J. E. Kossler-Silacci, M. Landriau, & N. Drory (San Francisco: ASP), 253
- Koen, C., O'Donoghue, D., Stobie, R. S., Kilkenny, D., & Ashley, R. 1995, *MNRAS*, 277, 913
- Koesterke, L., Dreizler, S., & Rauch, T. 1998, *A&A*, 330, 1041
- Koesterke, L., & Werner, K. 1998, *ApJ*, 500, L55
- Landolt, A. U. 1968, *ApJ*, 153, 151 (zz7)

- Lasker, B. M., & Hesser, J. E. 1971, *ApJ*, 163, L89 (zz3)
- Ludwig, H.-G., Jordan, S., & Steffen, M. 1994, *A&A*, 284, 105
- McCook, G. P., & Sion, E. M. 1999, *ApJS*, 121, 1
- McGraw, J. T. 1976, *ApJ*, 210, L35 (zz6)
- . 1977, Ph.D. thesis, University of Texas at Austin
- . 1977, *ApJ*, 214, L123 (zz25)
- . 1979, *ApJ*, 229, 203
- . 1980, *Space Sci. Rev.*, 27, 601
- McGraw, J. T., Fontaine, G., Dearborn, D. S. P., Gustafson, J., Lacombe, P., & Starrfield, S. G. 1981, *ApJ*, 250, 349 (zz9)
- McGraw, J. T., & Robinson, E. L. 1975, *ApJ*, 200, L89 (zz8)
- McGraw, J. T., & Robinson, E. L. 1976, *ApJ*, 205, L55 (zz13)
- McGraw, J. T., Starrfield, S. G., Liebert, J., & Green, R. F. 1979, in *IAU Colloquium 53, White Dwarfs and Variable Degenerate Dwarfs*, ed. H. M. Van Horn, & V. Weidemann (Rochester, NY: Univ. Rochester Press), 377 (gw4)
- Metcalfe, T. S. 2001, Ph.D. thesis, University of Texas at Austin
- Metcalfe, T. S., Montgomery, M. H., & Kanaan, A. 2004, *ApJ*, 605, L133
- Metcalfe, T. S., Winget, D. E., & Charbonneau, P. 2001, *ApJ*, 557, 1021
- Montgomery, M. H. 2005, *ApJ*, 633, 1142
- Montgomery, M. H., Williams, K. A., Winget, D. E., Dufour, P., DeGennaro, S., & Liebert, J. 2008, *ApJ*, 678, L51
- Mukadam, A. S., Kepler, S. O., Winget, D. E., & Bergeron, P. 2002, *ApJ*, 580, 429 (zz34)
- Mukadam, A. S., et al. 2003, *ApJ*, 594, 961
- . 2004, *ApJ*, 607, 982
- . 2006, *ApJ*, 640, 956
- Mullally, F., Thompson, S. E., Castenheira, B., Winget, D. E., Kepler, S. O., Eisenstein, D. J., Kleinman, S. J., & Nitta, A. 2005, *ApJ*, 625, 966
- Mullally, F., Winget, D. E., Kepler, S. O. 2007, in *ASP Conf. Ser. 372, Proc. 15th European Workshop on White Dwarfs*, ed. R. Napiwotzki, & M. Burleigh (San Francisco: ASP), 363
- Nagel, T., & Werner, K. 2004, *A&A*, 426, L45 (gw6)
- Nitta, A., et al. 2007, *Commun. Astroseismology*, 150, 249
- O'Brien, M. S., et al. 1998, *ApJ*, 495, 458
- O'Donoghue, D., & Warner, B. 1982, *MNRAS*, 136, 293
- . 1987, *MNRAS*, 228, 949
- Pech, D., & Vauclair, G. 2006, *A&A*, 453, 219
- Pech, D., Vauclair, G., & Dolez, N. 2006, *A&A*, 446, 223
- Pesnell, W. D. 1987, *ApJ*, 314, 598
- Pfeiffer, B., et al. 1996, *A&A*, 314, 182
- Quirion, P.-O., Fontaine, G., & Brassard, P. 2004, *ApJ*, 610, 436
- . 2005, *A&A*, 441, 231
- . 2007a, *ApJS*, 171, 219
- . 2007b, in *ASP Conf. Ser. 372, Proc. 15th European Workshop on White Dwarfs*, ed. R. Napiwotzki, & M. Burleigh (San Francisco: ASP), 649
- Randall, S. K., Fontaine, G., Brassard, P., & Bergeron, P. 2005, *ApJS*, 161, 456
- Randall, S. K., Fontaine, G., Charpinet, S., Lynas-Gray, A. E., Lopes, I. P., O'Toole, S. J., & Brassard, P. 2006, *ApJ*, 648, 637
- Richer, H. B., & Ulrych, T. J. 1974, *ApJ*, 192, 719 (zz14)
- Robinson, E. L. 1979, in *IAU Colloquium 53, White Dwarfs and Variable Degenerate Dwarfs*, ed. H. M. Van Horn, & V. Weidemann (Rochester, NY: U. Rochester Press), 343
- Robinson, E. L., Kepler, S. O., & Nather, R. N. 1982, *ApJ*, 259, 219
- Robinson, E. L., & McGraw, J. T. 1976, *ApJ*, 207, L37 (zz29)
- Robinson, E. L., Stover, R. J., Nather, R. E., & McGraw, J. T. 1978, *ApJ*, 220, 614 (zz21)
- Robinson, E. L., et al. 1995, *ApJ*, 438, 908
- Saio, H. 1996, in *ASP Conf. Ser. 96, Hydrogen-Deficient Stars*, ed. C. S. Jeffery, U. Heber, & S. Moehler (San Francisco: ASP), 361
- Saio, H., Winget, D. E., & Robinson, E. L. 1983, *ApJ*, 265, 982
- Salaris, M., Dominguez, I., Garcia-Berro, E., Hernanz, M., Isern, J., & Mochkovitch, R. 1997, *ApJ*, 486, 413
- Sauvenier-Goffin, E. 1949, *Ann. d'Astrophys.*, 12, 39
- Schmidt, G. D., & Grauer, A. D. 1997, *ApJ*, 488, 827
- Schulov, O. S., & Kopatskaya, E. N. 1973, *Astrofizika*, 10, 117 (zz33)
- Silvotti, R. 1996, *A&A*, 309, L23 (gw13)
- Silvotti, R., Fontaine, G., Pavlov, M., Marsh, T., Dhillon, V., & Littlefair, S. 2007, in *ASP Conf. Ser. 372, Proc. 15th European Workshop on White Dwarfs*, ed. R. Napiwotzki, & M. Burleigh (San Francisco: ASP), 593
- Silvotti, R., Pavlov, M., Fontaine, G., Marsh, T., & Dhillon, V. 2006, *Mem. Soc. Astron. Italiana*, 77, 486 (zz16)
- Silvotti, R., Voss, B., Bruni, I., Koester, D., Reimers, D., Napiwotzki, R., & Homeier, D. 2005, *A&A*, 443, 195 (zz15)
- Stahn, T., Dreizler, S., & Werner, K. 2005, in *ASP Conf. Ser. 334, 14th European Workshop on White Dwarfs*, ed. D. Koester, & S. Moehler (San Francisco: ASP), 545
- Starrfield, S., Cox, A. N., Hodson, S. W., & Pesnell, W. D. 1982, in *Pulsations in Classical and Cataclysmic Variables*, ed. J. P. Cox, & C. J. Hansen (Boulder: Univ. Colorado), 78
- . 1983, *ApJ*, 268, L27
- Starrfield, S., Cox, A. N., Kidman, R. B., & Pesnell, W. D. 1984, *ApJ*, 281, 800
- . 1985, *ApJ*, 293, L23
- Solheim, J.-E., Vauclair, G., Mukadam, A. S., Janulis, R., & Dobrovolskas, V. 2007, *A&A*, 468, 1057 (gw11)
- Stobie, R. S., Chen, A., O'Donoghue, D., & Kilkenny, D. 1993, *MNRAS*, 263, L13 (zz35)
- Stobie, R. S., O'Donoghue, D., Ashley, R., Koen, C., Chen, A., & Kilkenny, D. 1995, *MNRAS*, 272, L21 (zz23)
- Tassoul, M. 1980, *ApJS*, 43, 469
- Tassoul, M., Fontaine, G., & Winget, D. E. 1990, *ApJS*, 72, 335
- Tassoul, M., & Tassoul, J.-L. 1983, *ApJ*, 267, 334
- Thompson, S. E. 2004, Ph.D. thesis, University of North Carolina at Chapel Hill
- Townsend, R. H. D. 2002, *MNRAS*, 330, 855
- van Zyl, L., Warner, B., O'Donoghue, D., Sullivan, D., Pritchard, J., & Kemp, J. 2000, *Baltic Astron.*, 9, 231
- van Kerkwijk, M. H., Clemens, J. C., & Wu, Y. 2000, *MNRAS*, 314, 209
- Vauclair, G., Belmonte, J. A., Pfeiffer, B., Chevreton, M., Dolez, N., Motch, C., Werner, K., & Pakull, M. W. 1993, *A&A*, 267, L35 (gw12)
- Vauclair, G., Chevreton, M., & Dolez, N. 1987, *A&A*, 175, L13 (zz32)
- Vauclair, G., Dolez, N., & Chevreton, M. 1981, *A&A*, 103, L17 (zz18)
- Vauclair, G., Dolez, N., Fu, J. N., & Chevreton, M. 1997, *A&A*, 322, 155 (zz12)
- Vauclair, G., Dolez, N., Fu, J. N., Homeier, D., Roques, S., Chevreton, M., & Koester, D. 2000, *A&A*, 355, 291 (zz26)

- Vauclair, G., Solheim, J.-E., & Ostensen, R. H. 2005, *A&A*, 433, 1097 (gw8)
- Vauclair, G., et al. 2002, *A&A*, 381, 122
- Voss, B., Koester, D., Ostensen, R., Kepler, S. O., Napiwotzki, R., Homeier, D., & Reimers, D. 2006, *A&A*, 450, 1061 (zz17)
- Voss, B., Koester, D., Ostensen, R., Napiwotzki, R., Homeier, D., & Reimers, D. 2007, in *ASP Conf. Ser. 372, Proc. 15th European Workshop on White Dwarfs*, ed. R. Napiwotzki, & M. Burleigh (San Francisco: ASP), 583
- Warner, B., & Robinson, E. L. 1972, *Nature*, 239, 2
- Werner, K. 2001, in *Encyclopedia of Astronomy and Astrophysics* (London: IPP), 1992
- Werner, K., & Herwig, F. 2006, *PASP*, 118, 183
- Winget, D. E. 1981, Ph.D. thesis, University of Rochester
- Winget, D. E., & Claver, C. F. 1988, *IAU Circ.*, 4594 (vh2)
- Winget, D. E., & Fontaine, G. 1982, in *Pulsations in Classical and Cataclysmic Variables*, ed. Cox, & C. J. Hansen (Boulder: Univ. Colorado), 142
- Winget, D. E., Nather, R. E., & Hill, A. J. 1987, *ApJ*, 316, 305 (vh3)
- Winget, D. E., Robinson, E. L., Nather, R. E., & Balachandran, S. 1984, *ApJ*, 279, L15 (vh6)
- Winget, D. E., Robinson, E. L., Nather, R. E., & Fontaine, G. 1982b, *ApJ*, 262, L11 (vh5)
- Winget, D. E., Sullivan, D. J., Metcalfe, T. S., Kawaler, S. D., & Montgomery, M. H. 2004, *ApJ*, 602, L109
- Winget, D. E., Van Horn, H. M., Hansen, C. J., Fontaine, G., & Tassoul, M. 1982a, *ApJ*, 253, L29
- Winget, D. E., Van Horn, H. M., Tassoul, M., Hansen, C. J., Fontaine, G. 1983, *ApJ*, 268, L33
- Winget, D. E., et al. 1991, *ApJ*, 378, 326
- . 1994, *ApJ*, 430, 839
- Wu, Y. 2001, *MNRAS*, 323, 248
- Wu, Y., & Goldreich, P. 1999, *ApJ*, 519, 783